The Institute of Paper Chemistry

Appleton, Wisconsin

Doctor's Dissertation

Longitudinal Compression of Individual Pulp Fibers

David P. Dumbleton

June, 1971

LONGITUDINAL COMPRESSION OF INDIVIDUAL PULP FIBERS

A thesis submitted by

David P. Dumbleton

B.A. 1964, Northwestern University

B.S. 1966, University of Wisconsin

M.S. 1968, Lawrence University

in partial fulfillment of the requirements
of The Institute of Paper Chemistry
for the degree of Doctor of Philosophy
from Lawrence, University,
Appleton, Wisconsin

June, 1971

TABLE OF CONTENTS

SUMMARY

Individual pulp fibers have been found to come under longitudinal tensile and compressive stresses in many commercial processes. It has been demonstrated by other workers that drying pulp fibers under tensile loads increased the Young's modulus, tensile strength, rupture energy, and crystallite orientation of the fibers, and decreased their ultimate elongation. Little was known, however, about the effects which longitudinal compression had upon the mechanical properties of fibers. It was the purpose of this study to observe changes which such compression caused and to examine alterations in fiber structure which accompanied these changes.

Experimental work was carried out on springwood and summerwood fibers of a longleaf pine holocellulose pulp and with summerwood fibers of a longleaf pine kraft pulp. Drying these fibers under longitudinal compression resulted in large decreases in tensile strength, initial modulus and crystallite orientation and increases in ultimate elongation and rupture energy. The strength losses were found to be permanent and could not be recovered by rewetting the fibers. Rewetting caused large decreases in the elongation properties of springwood, and smaller decreases in summerwood.

Load-elongation properties of the fibers were drastically altered by drying under longitudinal compression. Load-unload cycling showed that these fibers were very inelastic, demonstrating a large secondary creep effect. Large increases in initial modulus were observed for each successive load-unload cycle of compressed fibers. This effect was also observed in the concave upward appearance of the load-elongation curves for the longitudinally compressed fibers.

Analysis of Laue x-ray patterns showed large decreases in crystallite orientation due to drying under longitudinal compression. The effect in summerwood fibers was greater than that in springwood fibers, probably because the summerwood fibers were better oriented initially. Small changes were also observed in the relative crystallinity of the summerwood fibers, but this was an orientation related effect, and probably not physically significant. Changes in orientation were not sufficient on the basis of uniform change in helix angle to account for the large decreases in fiber length during compression drying.

Polarized light microscopy and electron microscopy were used to show that structural disorder in the fibers resulted from the application of longitudinal compressive strains. This disordering consisted of multiple misaligned zones distributed along the fiber length. Comparison of the microphotographic evidence with that of other investigators revealed that the structural damage observed in this study was very similar to that obtained in other mechanical processes. However, a careful examination of the fibers demonstrated that structural misalignment was most severe in the direction perpendicular to the surface of the flattened fiber ribbon. This had been alluded to by other workers, but the connection between the appearance of misalignments as observed from different directions had not been made previously.

The results indicated that the reduction in fiber strength was primarily due to the misaligned zones. Stress concentrations within the zones and delamination, which hinder the redistribution of stress, are the primary mechanisms by which strength is decreased. Results from the x-ray diffraction analysis led to the conclusion that a large fraction of the crystalline

material of the fiber becomes partially or completely disoriented during longitudinal compression.

It is likely that the effects outlined in this study are a significant factor in causing different paper mechanical properties to be observed in the cross-machine direction from those in the machine direction. Similarly, the implications of this study are of practical importance to any sheet in which fiber strength is a limiting factor. In the case of the so-called extensible papers, these effects are undoubtedly of predominating importance.

INTRODUCTION AND OBJECTIVES

Structural damage to individual pulp fibers during processing has received considerable attention in recent years. Very little is known, however, about what effect this structural damage, particularly that caused by longitudinal compression, has upon the tensile mechanical properties of the fibers.

A knowledge of the changes to be expected in the mechanical properties of such fibers is of considerable importance to the many theories relating the stress/strain behavior of the paper sheet to the stress/strain behavior of the component fibers. As longitudinal compressive forces occur in the fibers of all machine-made papers, their effect on fiber mechanical properties assumes considerable importance in any attempt to understand the fundamentals of stress/strain behavior of such papers. These longitudinally compressed fibers must also be of importance to studies attempting to evaluate the distribution of energy within a sheet of paper during straining due to their drastically altered structure.

The objectives of this thesis are to determine the mechanical property and structural changes in individual pulp fibers associated with drying them under longitudinal compression.

HISTORICAL REVIEW

Many investigations concerned with structural and mechanical properties of cellulosic fibers are available, and several excellent summaries have been compiled. While a complete discussion of fiber structure and mechanical properties is beyond the scope of this study, it will be necessary to discuss those areas which are considered most important and to refer the reader to more detailed analyses on occasion. Nor will the reasons for studying individual fiber properties be considered here, but the reader is referred to the works of Van den Akker, et al. (1), Helle (2), Bergman and Rennel (3), and Duncker and Nordman (4) for good discussions of the importance of the properties of the individual fibers to the properties of the resultant sheet.

The purposes of this review are: (1) to outline the structural features of the wood pulp fiber considered important to this work, (2) to outline how changes in the structure of the fiber may occur, (3) to discuss some of the factors known to affect the tensile mechanical properties of fibers, and (4) to discuss what has been shown to date about the phenomenon of longitudinal compression of pulp fibers. Excellent reviews have been presented by Ott and Spurlin (5), Dunning (6), and Ebeling (7).

STRUCTURE OF WOOD FIBERS

MOLECULAR ORGANIZATION

It is only at the molecular level and at the most macroscopic levels that there is general agreement about what structural elements constitute the fiber wall. At the molecular level the wood fiber is composed of three principal constituents with a fourth category containing other minor components.

The three major components are cellulose, hemicellulose, and lignin. The fourth consists of a number of pectinaceous and inorganic materials.

Cellulose is a linear polymer of glucose molecules linked by β-1,4 glycosidic bonds. The number of glucose residues per weight average cellulose molecule in the native state is generally in the region of 1 to 3 thousand (8). These linear molecules tend to aggregate into highly ordered crystalline structures due to the flatness of the glucose rings, the polar hydroxyl groups which permit inter- and intramolecular hydrogen bonding, and the relative rigidity of the cellulose chain.

The generally accepted unit cell for this crystalline structure was proposed by Meyer and Misch (9). It is the basic crystalline element in all naturally occurring cellulosic fibers and is designated Cellulose I. A monoclinic unit cell, it has the following dimensions: b = 10.3 A. and lies in the direction of the cellulose chain, a = 8.35 A., lies in the direction of the plane of the glucose ring, and c = 7.9 A. lies perpendicular to the glucose ring. The angle between the a and c axes is 84° in Cellulose I. Although the details of the Meyer and Misch model have been criticized, the essential aspects (i.e., unit cell dimensions and directions of the unit cell axes) are still considered correct. It is these portions of the model which are of importance to later sections of this thesis.

The polycrystalline nature of cellulose leads directly to a consideration of the next level of organization into structural elements. It is generally accepted that there are regions of relatively high order (crystalline) and regions of relatively low order (amorphous) within the cell wall, with zones of gradual transition between these regions. The original idea of crystalline

micelles within an amorphous matrix was conceived by Naegli (10) long before the advent of x-ray crystallographic analysis. From this original concept have grown the many detailed models attempting to explain the connection between polycrystalline and amorphous cellulose within the cell wall. Such models attempt to describe the geometric arrangement of the polymer chains, the size and shape of the crystalline regions, their spatial distribution and the physical nature of the amorphous regions. A good discussion of the various sides to this question is given by Ebeling (7) and detailed considerations may be found in the comprehensive works of Hearle (11), Côté (12), and Frey-Wyssling and Mühlethaler (13).

In lieu of a repetition of this many-sided argument, the following summary will provide a generalized conceptual model which has proven workable in the investigation of the overall effects of structural changes on the mechanical properties of fibers.

The cellulosic material of the cell wall may be considered to be organized into elementary fibrils whose long dimension is not well defined. The length of the elementary fibril consists of ordered and less-ordered regions. The length of the fibril does not seem to be related to the length of the polymeric chains, but the b crystallite axis parallels the long axis of the elementary fibril. The width of the fibrils is probably on the order of 50-100 A. with degree of order in the lateral dimension varying from that of the highly ordered fibrillar core to that of the amorphous interfibrillar matrix. The crystalline regions may be considered to have relatively high energy hydrogen bonds. The amorphous region is also highly hydrogen bonded on the basis of conclusions reached with infrared spectroscopic studies (14,15), but the distribution of the energies of these hydrogen bonds is relatively wide, indicating

a state of dynamic equilibrium, with bonds being continually broken and reformed, within the amorphous matrix.

There are two primary reasons for this discussion of the conceptual model for the cell wall ultrastructure. The first is to demonstrate the impossibility of assigning a value for "percent crystallinity" to a fiber. Because the boundaries between crystalline and amorphous material are poorly defined and because there are considerable quantities of material having intermediate degrees of order, such a designation is meaningless. Thus, structures can only be compared on the basis of a relative degree of order since no absolute basis for comparison is available. This concept is important to a discussion of the x-ray data presented later in the thesis. The second reason for the discussion involves the relative position of the b crystallite axes within the fibril. The directions of the b crystallite axes are very important to later determination of the structural orientation of the fibrils within the macroscopic fiber structure. The x-ray determination of the fibril orientation is dependent on the assumption that the b crystallite axes lie parallel to the microfibrillar axes, making the fundamental conceptual model of the elementary fibril germane to later interpretations.

Before leaving the discussion of the molecular make-up of the fiber wall, the role of its other two principal constituents must be briefly presented. The general distribution of these two constituents, as well as of cellulose, is shown schematically in Fig. 1.

Although the lignin was almost entirely removed from the fibers of this study, it is an important factor in that its removal leaves interstices within the fiber structure. How intimately associated the lignin is with the other cell wall components is not known exactly, but it is generally considered to

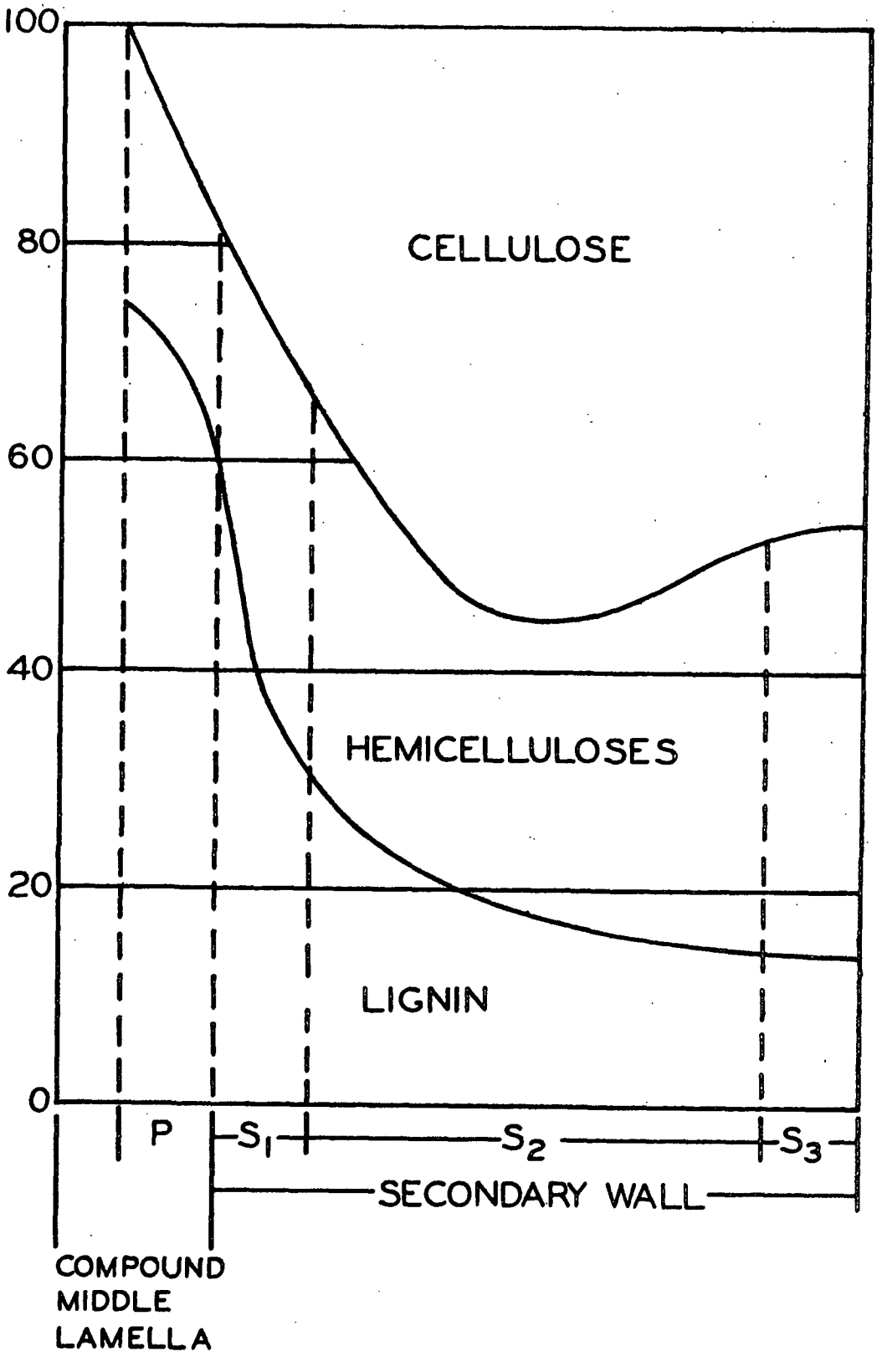

Figure 1. Distribution of Tracheid Chemical Components. From Panshin, et al. (16)

exist as a matrix along with the hemicelluloses (8). Because it is distributed to some extent throughout the entire cell wall, its removal is certain to affect the fiber porosity and the ability of water to penetrate the structure.

The hemicelluloses are also distributed throughout the fiber wall, and are probably in quite intimate contact with the cellulose. It has been shown, in fact, that xylan is oriented parallel with the cellulose in wood (17). It has been postulated that xylan can crystallize in the spaces between the cellulosic microfibrils (18,19). Spiegelberg (20) has also hypothesized that the hemicelluloses are located within the microstructure of the fiber. Due to the more highly branched nature of the hemicelluloses, their primary location must be within the less-ordered regions of the cell wall, though apparently in close proximity to the elementary fibrils.

MICROSCOPIC ORGANIZATION

In the preceding section the organization of the cell wall was discussed at the molecular level — up to the aggregation of the cellulose molecules into elementary fibrils. That these elementary fibrils are further combined into fibrils of yet larger dimensions seems quite likely. Unfortunately, there is very little agreement concerning the size of these bundles of elementary fibrils, nor is there any consensus about the number of levels of organization between that of the elementary fibrils and that of the macrofibrils which are visible with the light microscope.

Most attempts to elucidate the sizes of the various fibrillar aggregations of the cell wall have used cotton fibers rather than wood fibers. Frey-Wyssling (21) assigned three levels of aggregation, calling them elementary fibrils, microfibrils, and macrofibrils, and tried to establish the magnitude

of the cross-sectional areas of these levels of organization. In Table I, results of the type presented by Frey-Wyssling are shown, but they have been slightly modified by the more recent work of Dolmetsch and Dolmetsch (22). It must be emphasized that such values are only useful for order-of-magnitude comparisons of the levels of structural organization. There does not appear to be any common structural element which is well defined and uniform in size for any of the cellulosic materials studied.

TABLE I

LATERAL DIMENSIONS OF FIBRILLAR ELEMENTS

	Area of Cross Section	Number of Cellulose Chains in Cross Section
Tracheid	350 $\mu m.^2$	1,000,000,000
Macrofibril	$(0.2\ \mu m.)^2 = 0.04\ \mu m.^2$	125,000
Microfibril	$(250\ A.)^2 = 62{,}500\ A.^2$	2,000
Elementary fibril	$(30\ A. \times 40\ A.) = 1200\ A.^2$	40
Cellulose molecule	$(4\ A. \times 8\ A.) = 32\ A.^2$	1

The fibrillar material is further organized into four distinctly different concentric layers which make up the cell wall. These layers are shown in Fig. 2 and consist of (1) the primary wall or P layer, (2) the outer secondary wall or S_1 layer, (3) the middle secondary wall, the S_2 layer, and (4) the inner secondary wall or S_3 layer. Chemical and mechanical treatment of the fiber can break down each of these layers into additional readily distinguishable lamellae (23,24).

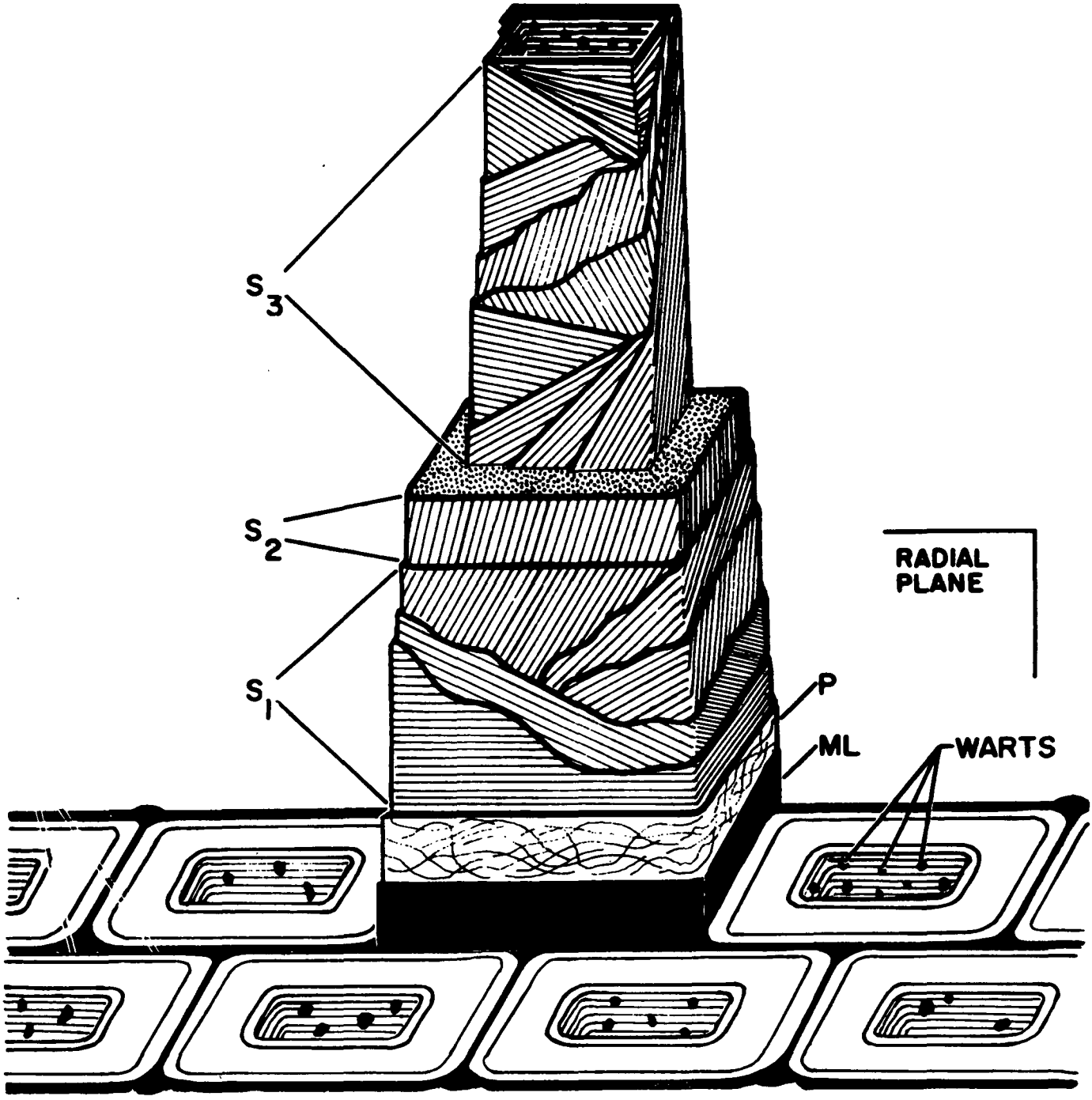

Figure 2. Schematic Diagram of the Layered Structure of a Softwood Tracheid. From Dunning (6)

Figure 2 also indicates the variation in the way that the fibrillar material is oriented within these layers. In the primary wall the fibrils are intertwined and randomly oriented with perhaps some preference toward orientation in a direction transverse to the fiber longitudinal axis. The fibrils of all the remaining layers are helically wound around the long axis of the fiber.

The S_1 layer consists of several lamellae, the predominant helix angle being about 60-65° in longleaf pine (6). However, the S_1 lamellae apparently alternate between a right- and a left-hand helical orientation of the fibrils about the fiber axis. The boundaries between the P and S_1 layers are not clearly defined due to the presence of transition lamellae. Actually, the definition of what constitutes the primary layer is an ontogenetic one, depending on a knowledge of the growth processes occurring in the early stages of cell development, as yet not clearly understood (13). Thus, there seems to be a gradual transition between the randomly ordered primary layer and the well-oriented S_1 with its alternating transverse helices.

The S_2 layer, which makes up approximately 80% of the cell wall, also consists of well-oriented helical arrangements of fibrils, but in the S_2 the helices are all right handed, having angles of 10-20° from the fiber axis. The boundary between the S_1 and S_2 layers is, like that between the P and S_1 layers, not well defined. Dunning (6) found what he interpreted to be numerous transition lamellae between the S_1 and S_2 layers with fibril orientations of succeeding lamellae progressing from the nearly transverse orientation of the S_1 to the nearly longitudinal orientation of the S_2. However, the S_1 and S_2 layers tend to separate from one another under chemical and/or mechanical action, indicating a definite weakness in the transition region (25).

The lamellae of the S_3 were observed to continue the stepwise transition seen between the S_1 and S_2. The numerous S_3 lamellae show progressively different orientations from the transition region with the S_2 all the way to the fiber lumen. On the average, the S_3 shows a somewhat higher component of longitudinally aligned fibrils than does the S_1 (6). Bucher (26) has given an average helix angle of 65-90° for the S_3 of tracheids indicating its similarity to the S_1. In Dunning's work (6), the S_3 lamellae were found to have a wide range of angles.

It should be emphasized that although no well-defined structural element can be described, all of the above-mentioned layers of the tracheid were defined in terms of fibril orientation. This is based on the generally accepted assumption that the elementary fibrils are oriented parallel to one another within any single micro- or macrofibril. In turn, these larger aggregates are oriented generally parallel to one another, at least within any particular lamella of the fiber wall. Thus, any change in average fibrillar orientation can be used as an important parameter for indicating changes in the cell wall structure. This is important to later interpretations of x-ray diffraction data.

MORPHOLOGICAL VARIATIONS IN CELL WALL STRUCTURE

Even within a single tree, the fibers are not uniform, but show a distribution in their basic properties. Seasonal variations in growth pattern result in the distinctly different springwood and summerwood fiber types, the former having relatively thin walls and the latter relatively thick ones. In addition, there are large numbers of fibers showing transitional properties somewhere between the two extremes. The difference in fiber wall thickness is mainly due to

the amount of S_2 layer present: summerwood is approximately 88% S_2 and springwood about 78% S_2 in spruce tracheids (27).

Springwood and summerwood fibers show differences in several other properties. Size of lumen and diameter of the summerwood fiber are both smaller than in springwood. Springwood fibers are somewhat shorter in length than summerwood fibers. The average microfibril orientation relative to the fiber axis is always larger in springwood then in summerwood fibers (28). Correlations have been made between average microfibrillar orientation angle and fiber length (29) and thickness of fiber wall (30).

Variations in properties of the fibers also depend on the age of the tree at the time the fiber was formed. It has been found that for softwood tracheids there is considerable variation in the fibers of each successive year up to the age of 10-15 (16). Beyond this juvenile wood portion of the tree, the fiber properties become much more uniform from growth ring to growth ring.

CHANGES IN FIBER STRUCTURE DUE TO LONGITUDINAL COMPRESSION

DISORDERING IN COMPRESSED WOOD

Probably the earliest evidence of the localized failure of fibers under compressive loads parallel to their long axes was from the microscopic examination of wood which had been compressed in the direction of its grain. As early as 1920, Robinson (31) described diagonal striations, disturbances in the parallel order of the internal structure of the fiber, occurring in wood blocks compressed in this way. These were termed slip planes through an incorrect analogy with slip planes in metals and other crystalline materials which have a similar appearance. Robinson was able to increase the microscopic visibility

of these striations by using polarized light with polarizer and analyzer at 90° from one another.

This initial work was followed by similar investigations whose various contributions were summarized in 1947 by Wardrop and Dadswell (32). These workers separated the observed changes in cell wall structure into two categories. The first group were called "slip planes" as before, and were noted to be contiguous from one cell to the next in wood blocks. The second group were termed "minute compression failures" and were seen as dislocations in the walls of many fibers, but were not contiguous from one fiber to another as were the "slip planes." This had been recognized earlier by Ambronn (33) and Bienfait (34). The latter investigator thought that the "minute compression failures" represented the points of origin for more macroscopic compression failure. He also stated that such "initial compressions" increased the bending and shock resisting abilities of lumber. Ambronn's model for the two types of dislocation is shown in Fig. 3.

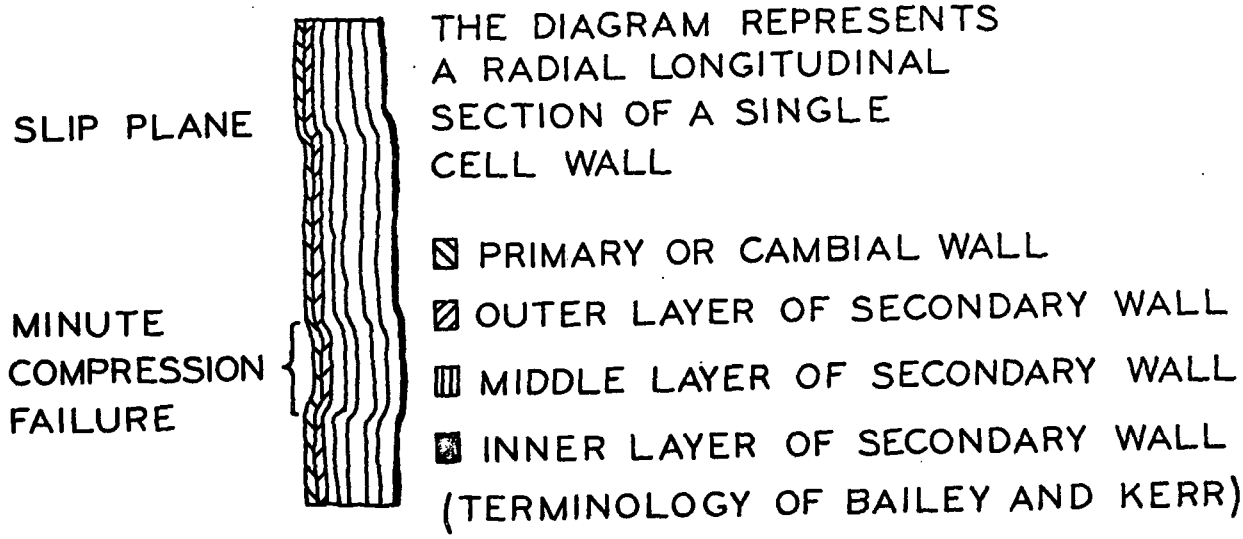

Figure 3. Model of Compression Failures in Wood Fibers. From Ambronn (33)

Wardrop and Dadswell (32) expanded on the work of the earlier investigators to show how the lines of compression failure might propagate themselves from one fiber to the next. A model for this behavior is shown in Fig. 4.

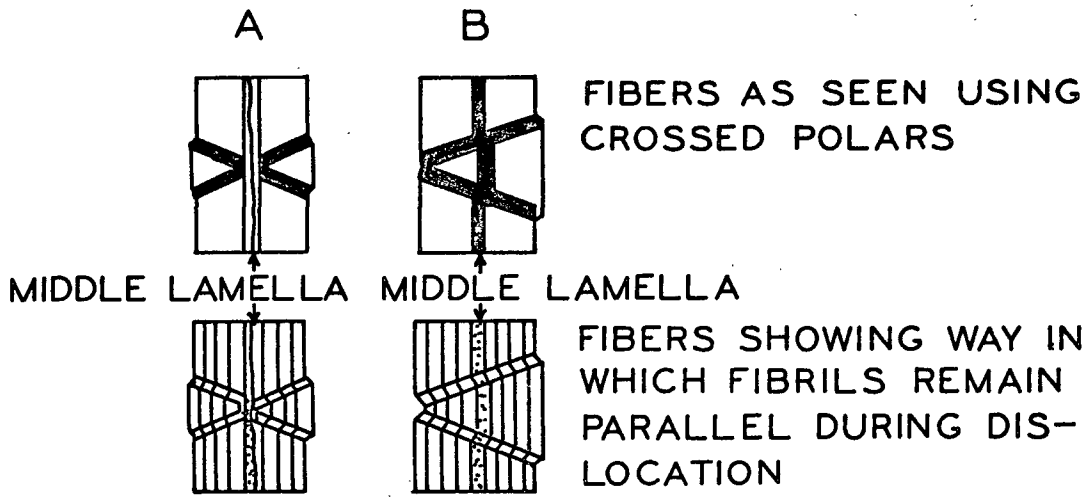

Figure 4. Model for the Propagation of "Slip Planes" Through Fibers in a Wood Block. From Wardrop and Dadswell (32)

They stated that most trees contain many such dislocations in their natural state. They also attempted to produce "minute compression failures" by compression loading of beams, but were unsuccessful except when the beams were loaded for long periods of time (months). They did discover that during the steam bending of wood many such failures occurred in fibers located in the concave (compressed) portions of the bends.

One other feature of this early work is of interest. Wardrop and Dadswell hypothesized after Frey-Wyssling (35) that the lignin's role in the fiber wall was to strengthen the fiber against compression failure by a cementing action, thus holding the internal fibrils together to prevent buckling. They also discovered that compressionwood cells, which have thick walls and are heavily

lignified, did not show any "minute compression failures." They used this to substantiate their theory. However, Green and Yorston (36) had taken a different approach to this same problem. They discovered that wood blocks which had been subjected to longitudinal compression (which presumably would show compression failure of the cell walls) were much more susceptible to attack by acid pulping than were normal wood blocks. They also noted that such "susceptible wood" was associated with compressionwood in trees in the natural state. From this, one can infer a difference in the conclusions regarding the presence or absence of microscopic compression failures in compressionwood.

Kisser and Steininger (37) attempted to characterize the development of the lines of compression failure in terms of the compressive stress applied to the wood. They defined three quantities for this characterization. $\underline{P}_{mst}$ was defined as the stress at which the first narrow lines of failure could be observed within the single cell walls. $\underline{P}_{Mst}$ was defined as the stress at which more macroscopic failure lines passing through many fibers could be seen. $\underline{P}_{B}$ was the stress at which the wood block failed under compression. Using three different wood species (Larix, Abies, and Picea) these workers found that these three quantities retained a remarkably constant ratio of $\underline{P}_{mst}:\underline{P}_{Mst}:\underline{P}_{B} = 1:1.52:1.9$ at all moisture levels except at complete saturation. Thus, the microscopically visible failure lines appear at about 50% of the ultimate buckling load. This study was carried out by stressing individual blocks to different levels for a period of two hours and then comparing them.

This work may be compared with the later investigation of Dinwoodie (38) who examined the structural changes in thin wood sections under longitudinal compression, using a cinematographic technique in order to get a continuous picture of the changes which occurred. Dinwoodie found that small "compression

creases" occurred at levels below 25% of the ultimate buckling strength of the wood. He also concluded that since this microscopic crinkling occurred at low levels of compressive stress, it must be of primary responsibility in the plastic deformation of wood. He characterized the sequential development of the sites of dislocations in the following way:

> The stress or thrust line develops into the slip plane, many of which develop progressively and horizontally into small and then successively larger creases up to failure, where considerable buckling and delamination within the cell wall occur.

Finally, he determined that the angle of propagation which the failure lines made with the long axes of the fibers was about 62°. This compares with angles of from 60 to 70° found by other workers (31,37,39). To this author's knowledge, no connection has been made as yet between the microfibrillar angle of the S_1 layer and the angle of propagation of the compressive lines.

Several different terms have been used above to describe the lines of compression failure.

Recently Hartler (40) unified the terminology of these treatments and called them by the general name of "misaligned zones." This term will be used from here on to describe all observable compression failures in tracheids with the addition of more specific designations where required. Although "slip plane" is still used by many writers, it is an essentially incorrect term, as has been pointed out by Frey-Wyssling (41,41A).

Hartler and Le Mon (42) and Dinwoodie (43) also carefully investigated the various sectioning parameters. These are extremely important in obtaining artifact-free wood sections. Misaligned zones are, in fact, very easily created by incorrect sectioning technique. Though this was known to other workers

(31,32,34,37), the sectioning technique was not carefully described by any of them. Thus, the earlier literature concerning the presence of misaligned zones in the cell walls of undamaged wood must be treated with some skepticism.

Compression damage to wood has also been shown to have a considerable effect on the reaction with pulping chemicals, as mentioned earlier. One of the earliest studies, that of Green and Yorston (36), has been described earlier in this section. More recently Stone and Nickerson (44,45) considered this problem in more detail. They crushed wood chips both parallel to and across the grain, and found that the latter had little effect on the degradation by pulping chemicals. They found, however, that crushing parallel to the grain resulted in an increase in the rate of cellulose degradation during sulfite cooking and a drop in the leveling-off degree of polymerization. In their findings, crushing did not affect the rate of pulping or the final chemical composition of the pulp. By using progressively higher increments of compressive deformation (5, 10, 20, 35, and 50%) they obtained correspondingly more severe degradation with each increment. They discovered that the fibers were uniformly damaged throughout the blocks, even at the 5% level, and that the damage was related only to the percentage deformation, and not to the energy input.

Hartler and Sundberg (46) and Hartler (47) extended this type of investigation to sulfate pulping. They found that a 10% compressional deformation parallel to the grain resulted in a 35% reduction in fiber strength after kraft pulping. They compared this with a 33% loss following sulfite pulping. It was discovered that the leveling-off degree of polymerization was somewhat reduced for the kraft pulp and even more reduced for the sulfite pulp when compared with pulp from undamaged wood. Rånby (48) and Hartler (49)

attributed these differences to localized disordering of the hydrogen bonds in transition regions between the crystalline and amorphous substance of the fiber.

Preferential staining has also been used to demonstrate changes in structure at the misaligned zones. Ambron (33) first showed that pleochroic dyes, such as Congo Red, which tend to orient themselves within the fiber structure, helped to accentuate the misaligned zones under polarized light. Green (50) used Herzberg stain, an iodine-iodide salt complex which stains tracheids different colors, depending on the availability of lignin and other noncellulosic material, to show that these are distributed differently in the misaligned zones. Certain Cibacron* dyes which are known to react with free hydroxyl groups were also strongly attracted and retained in compression-damaged tracheids. Such evidence suggests that changes occur in the fiber structure even at the submicroscopic and molecular levels.

DISORDERING DURING CHIPPING, PULPING, AND REFINING

Compression of wood blocks parallel to the grain is not the only way of introducing misaligned zones into fibers. Unintentional damage during chipping, when the chipper knives are dull or poorly aligned, often leads to misaligned zones identical to those already described. Green and Yorston (36,51) first brought attention to this type of damage in their investigation into the effects of damaged fibers on pulp produced by the sulfite process. They found that elimination of the misaligned zones caused by chipping resulted in a 35% improvement in the tensile strength of the sheets made from the pulp. More recently, Bausch and Hartler (52) came to a similar conclusion in a more detailed study.

*Widmer, W., Ciba Rev. 120:4-6(1957).

In his discussion of wood damage and its influence on pulp quality, Stone (53) concluded that "latent damage" to the wood, particularly during chipping, was developed into pulp weakness by acid pulping but not by kraft pulping. However, Hartler and Sundberg (46) and Hartler (47) showed that such damage causes equal weakening in the fibers of both sulfite and kraft pulps. Hartler (40) resolved this apparent discrepancy by pointing out that Stone measured sheet strength not fiber strength. Since, as Hartler has pointed out, fiber strength is a controlling factor in sulfite but not in kraft paper, the effect of fiber damage is not apparent in sheets made from kraft pulp.

Forgacs (54) and Forgacs and Mason (55) also investigated misaligned zones, calling them "nodes." Forgacs (54) observed that the number of such misaligned zones increased steadily as the pulp yield decreased. However, he also discovered that the misalignments were caused by the mechanical defibration which was used after pulping. The pulping only affected the ease with which misaligned zones were formed. Alexander, Martin, and McGovern (56) reached different conclusions regarding the effect of pulp yield on formation of misaligned zones. For them, more such zones were visible in pulps of higher yield. Ebeling (7) felt this was because Forgacs observed only the easily visible, larger bends as "nodes," whereas Alexander and coworkers carefully observed all microscopic cracks and striations.

The well-developed misaligned zones which Forgacs (54) observed, occurred at remarkably regular intervals of about 0.2-0.4 mm. Emerton (57) also mentioned this. Forgacs noted that the misalignments appeared to be preferentially located in the area of ray crossings. This was supported by the later work of Iwasaki and coworkers (58).

Several studies have shown that the formation of misaligned zones is one of the significant effects of the beating process. Iwasaki, Lindberg, and Meyer (58) used ultrasonic beating to obtain misaligned zones having the same appearance as those in the fibers of compressed wood. The interval at which the misalignments occurred had no correlation with the wavelength of the ultrasonic vibration applied. They further found that the formation of misaligned zones was only a first step in the beating process and was followed by the removal of the S_1 layer, swelling of the fiber and, finally, fibrillation. Summerwood fibers were found to be much more difficult to beat than springwood fibers, as were kraft fibers when compared with holocellulose or sulfite fibers. Samuelsson (59) used the same kind of treatment and found that the stiffness of the fibers was drastically reduced.

More recently, Alexander, Martin, and McGovern (56) used PFI milling to treat kraft fibers. They distinguished between the appearance of the misalignments in the various fibers studied. In flexible fibers such as low-yield springwood, they found that the misalignments took the form of a soft pleat. In stiffer fibers the folds were more sharp-edged, resembling cracks. They used moisture regain and x-ray techniques to conclude that beating caused a reduction in the internal order of the pulp fibers. They also tested the tensile properties of the fibers, but could only conclude that the summerwood fibers were stronger than the springwood fibers.

Less commonly used, but of considerable importance to this discussion, is the refining of pulp at high consistencies; that is consistencies above 10%. By reviewing the literature concerned with this type of refining, Page (60) came to several interesting conclusions. He found that regardless of the type of beater used, for a given development of tensile strength, the higher the

refining consistency, the higher was the stretch-to-rupture of the sheet. He concluded that this increase was due to the increasing interaction between pulp fibers at higher consistencies resulting in axial compressive forces on the fibers. Such compressed fibers could then be expected to show increased stretchability in the dried sheet.

Furthermore, by microscopic examination of these fibers in polarized light, he was able to demonstrate the presence of many misaligned zones. Higher consistencies produced larger numbers of misaligned zones. Finally, by photographing a few stained fibers before and after PFI milling at 20% consistency he showed length reductions of up to 6%.

DISORDERING DURING CONSOLIDATION OF THE PAPER WEB

During the final drying of a sheet of paper, many forces come into play to make the fiber conform to its neighbors, and to make the fibers adhere to one another. Van den Akker (61) demonstrated how axial compressive forces might come into play at the points of fiber-to-fiber bonding. These forces would originate because of anisotropy of the fiber shrinkage during water removal. Fibers normally shrink only a few percent longitudinally, but in the lateral dimension shrinkages of 30% and more are normal. As a result, cross-bonded fibers will exert forces on one another in the manner shown in Fig. 5, if the bonds should form before the shrinkage occurs. The necking down in the area around the bond is exaggerated for emphasis. Indeed, Page and Tydeman (62) showed, using direct observation under the microscope, that optical contact at fiber bond sites is reached, and presumably bonding forces take over, at solids contents of 40-50%. These same researchers (63) also showed that the major portion of the shrinkage of the sheet occurs after the fibers are well bonded.

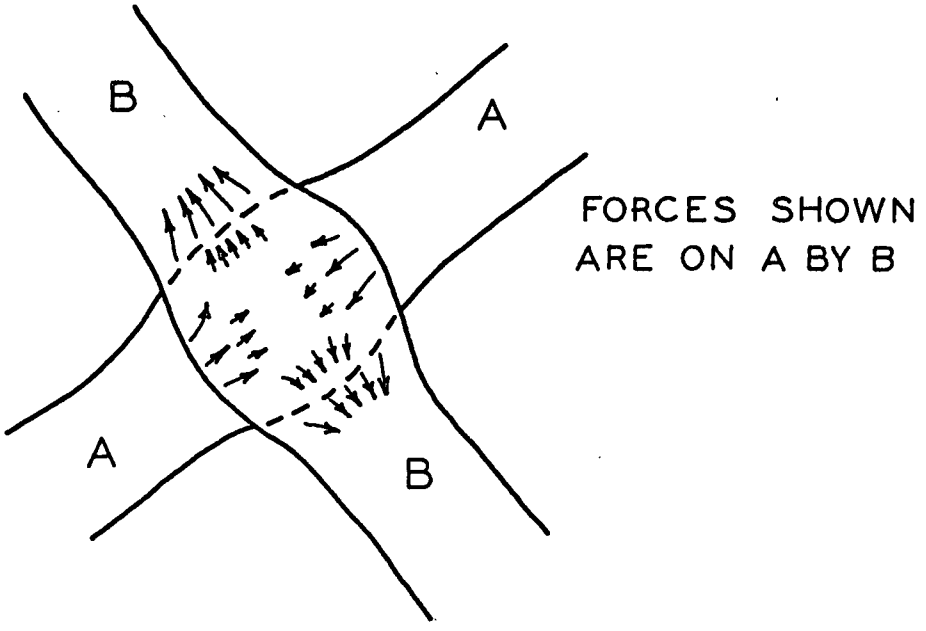

Figure 5. Longitudinal Compression at a Fiber-Fiber Bond

Van den Akker (61) theorized that in a sheet of paper under uniaxial tension, all fibers lying at an angle of about 0°-30° or 150°-180°, with respect to the line at 90° from the tension axis, will come under net axial compressive loads. Were the fibers not able to withstand some of this compression, in fact, paper would show a considerably higher Poisson contraction than it normally does.

In their investigation into the shrinkage of paper, Page and Tydeman (63) discovered that the shrinkage of bonded crossings of fibers causes longitudinal shortening of the fibers to maintain the same relative positions within the structure. Microscopic examination of the fibers in these areas showed the presence of very small misaligned zones which these investigators termed "micro-compressions." These findings are illustrated in Fig. 6.

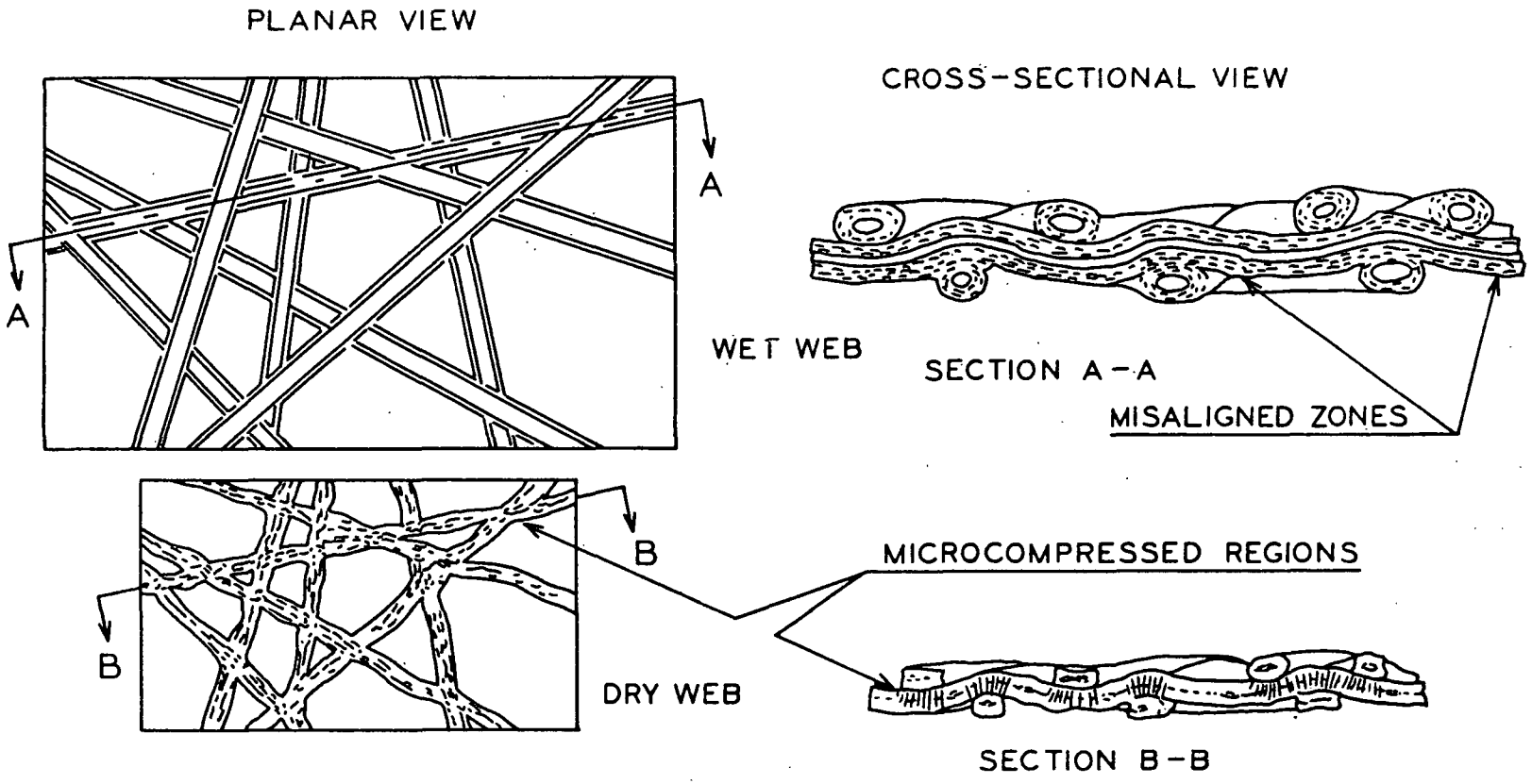

Figure 6. Schematic of Paper Shrinkage During Free Drying. From Page and Tydeman (63)

Actually, the drying forces needed to cause axial compression in the fiber do not seem to be very large. Hartler (64) found that simple unrestricted drying of a completely uninjured pulp fiber resulted in the formation of a few misaligned zones, demonstrating that even internal drying forces occurring between the fiber lamellae are sufficient to cause this type of damage. In another study, McIntosh and Leopold (65) demonstrated that a single wet fiber would adhere so well to a sheet of swollen cellulose film that when the film was allowed to shrink, the fiber shrank longitudinally an equivalent amount with simultaneous formation of an abundance of misaligned zones.

DISORDERING IN EXTENSIBLE PAPERS

Closely related to the experimental technique for obtaining longitudinally compressed individual fibers described in this thesis is the Clupak process which is used to produce so-called extensible papers. This process was discussed by Diaz (66) and Schoudy (67), upon whose work the following description is based. The essentials of the process are as follows: An elastic rubber blanket is longitudinally prestretched. A moist web of paper is brought into contact with the stretched blanket and then tightly pressed against a smooth metal drum. The rubber is then allowed to contract back to its original dimensions, causing the web to shrink with it and slip across the surface of the metal roll. A certain moisture content is required in order for the paper web to conform properly to the rubber blanket. The resultant shrinkage is then dried into the sheet.

Such paper has load-elongation properties considerably different from those of normal paper. For a 50-lb. basis weight kraft bag paper, the stress-strain properties in the machine direction are altered as shown in Fig. 7.

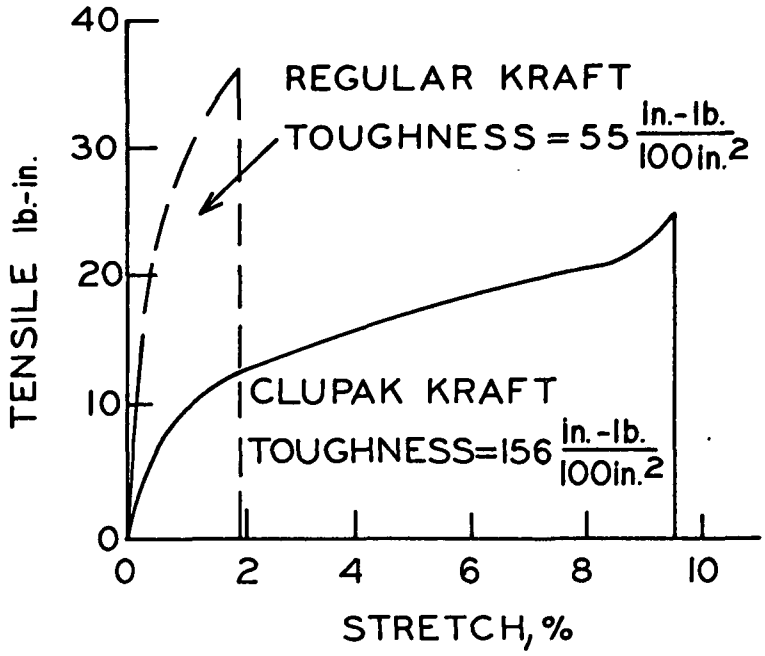

Figure 7. Machine Direction Stress-Strain Behavior of 50-Lb. Basis Weight Kraft Bag Papers. From Schoudy (67)

Note that the extensibility has been increased by about 500% with about a 25% loss in tensile strength. Most important is the quantity which Schoudy called toughness. This is the energy which the sheet is able to absorb before rupturing. It is this property which is most significant to the ultimate usefulness of the bag, because this high-rupture energy gives the paper high impact resistance. An additional result of the process is that the Clupak sheet is much softer and more flexible than the normal stiff bag paper. The process also alters the cross-machine direction properties as shown in Fig. 8, although not as drastically as in the machine direction.

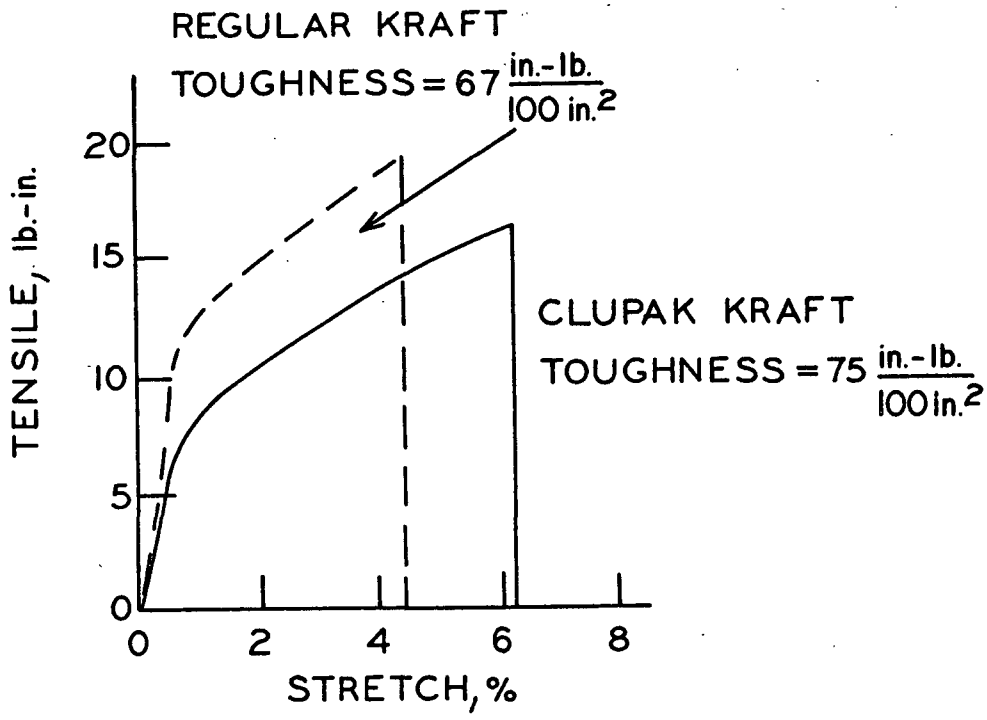

Figure 8. Cross-Machine Direction Stress-Strain Behavior of 50-Lb. Basis Weight Kraft Bag Papers. From Schoudy (67)

In a more comprehensive study, Welsh (68) compared Clupak papers with creped papers. Creping might also be expected to cause longitudinal compressive forces in the fibers. However, the buckling in creped paper results in considerably more macroscopic dislocations in the paper structure which influence the appearance of the sheet. On the other hand, the Clupak sheet looks about the same as an uncompacted sheet to the unaided eye.

Ihrman and Öhrn (69) studied the microscopic details of compacted sheets in some detail. They compared ordinary flat kraft bag paper with wet-creped kraft, blanket compacted Clupak type kraft, and a compacted kraft produced by using a rubber roll instead of the rubber blanket. They found that the blanket-compacted

sheet was almost of the same appearance as the uncompacted kraft and had only barely perceptible, very fine wrinkles in the surface. The double roll compacted kraft had somewhat more visible wrinkles and the creped kraft had very macroscopic wrinkles. They also microscopically examined cross sections of compacted and uncompacted sheets. Their results were very similar to those shown in Fig. 9 and 10, obtained from Schneider (70). Note the extensive bending and kinking of the fibers in the compacted sheet.

GENERALIZATIONS ABOUT DISORDERING

All of the treatments described above result in some type of longitudinal disorder. In fact, the major difference between any of these misaligned zones appears to be one of size. All of them have common origin in some type of longitudinal compressive force applied to the fiber. Their dimensions seem to vary in magnitude from a fraction of a fiber diameter to "microcompressions" at bonding sites up to more macroscopic kinks having dimensions of a fiber diameter or more in the fibers of sheets treated by the Clupak process.

Similarly, their frequency of appearance varies from one or two "nodes" or misaligned zones per fiber up to hundreds of misalignments appearing uniformly every few micrometers. It is apparent that the frequency of the misalignments is related to the length and severity of the mechanical treatment applied. It is probable, therefore, that any frequency and size of misalignments could be obtained by carefully controlling the compressive load and strain on the fiber.

Some mention should also be made of the fact that some delamination of the fibers' internal lamellae probably accompanies the formation of misaligned zones, particularly in the experimental technique of this study where shear forces as well as longitudinal compressive forces are applied. The occurrence

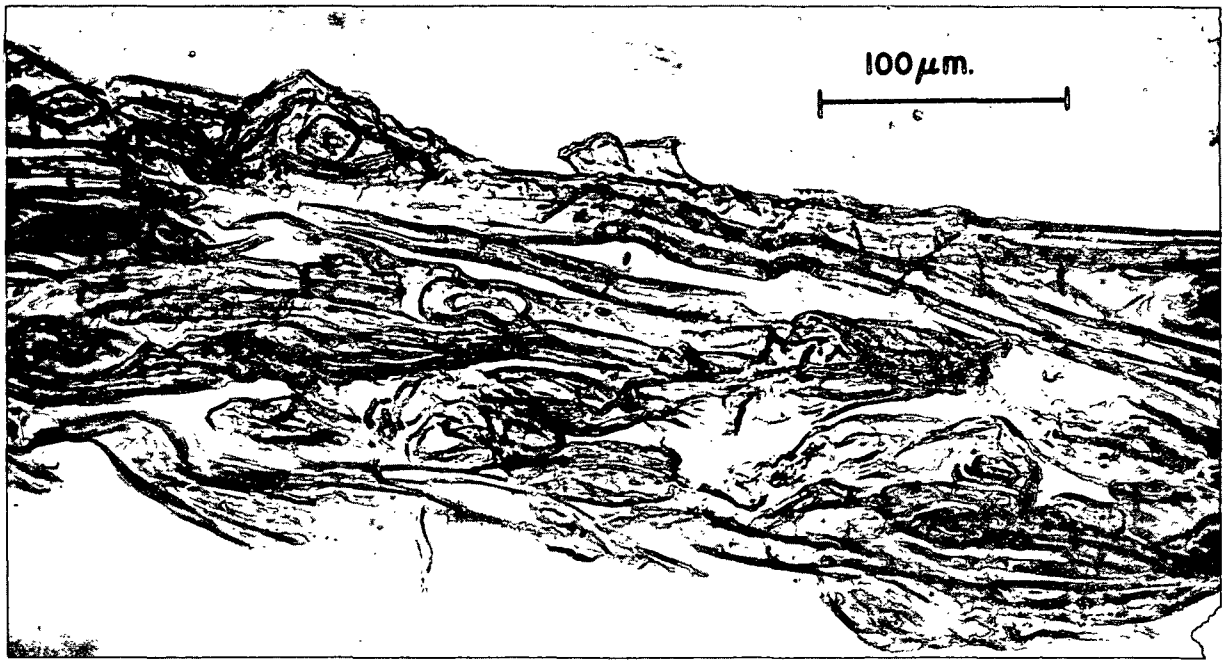

Figure 9. Machine Direction Cross Section of a 50-Lb. Conventional Kraft Paper X325. From Schneider (70)

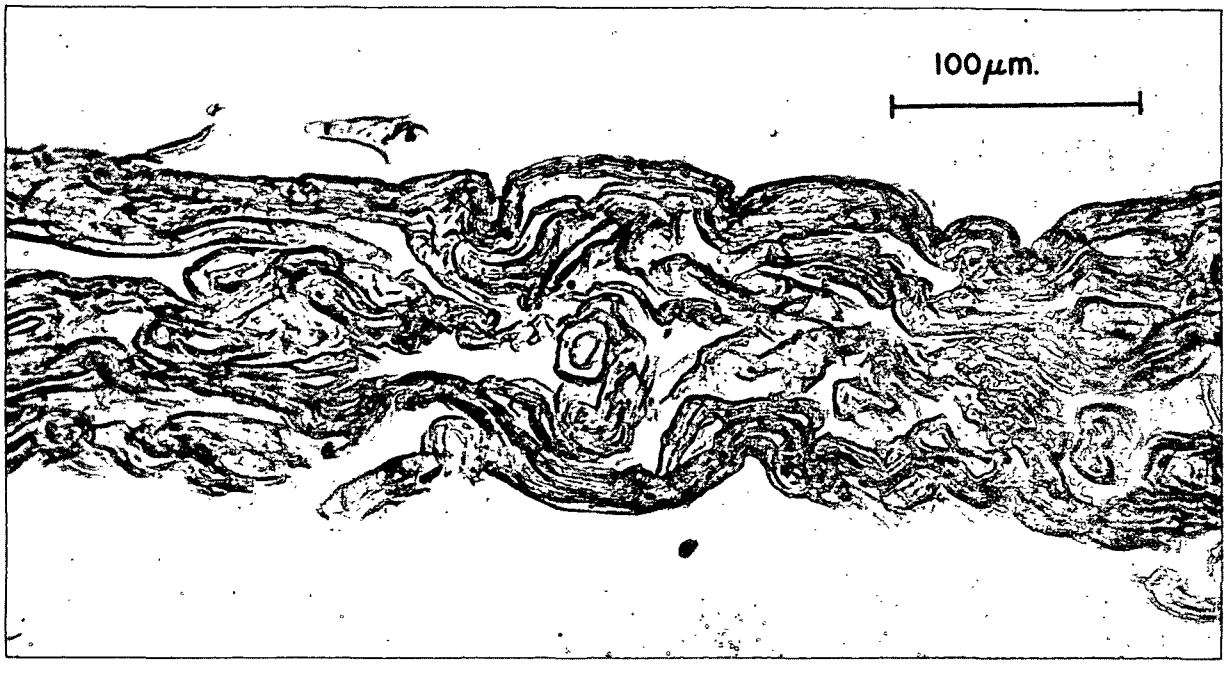

Figure 10. Machine Direction Cross Section of a 50-Lb. Clupak Kraft Paper X325. From Schneider (70)

of cell wall delamination has been adequately summarized by Ebeling (7). Only a few of the most pertinent investigations will be mentioned here.

As has been mentioned by Emerton (25), there is a decided looseness between the S_1 and S_2 layers. In addition to this, however, it appears that mechanical action on the fiber can cause delamination between the individual lamellae of the S_2. Page and DeGrace (24) brought attention to this delamination caused by beating and refining. They noted that it did not appear to occur in groundwood or high-yield pulps, but manifested itself at lower yields. They attributed delamination to the flexing of the lamellate cell wall, causing interlamellar separation at planes weakened by pulping. They could not conclude whether equal weakening effects occurred at all interlamellar planes. The number of concentric lamellae observed (about 10 for sulfite fibers and 4 for sulfate fibers) was an order of magnitude lower than the numbers of elementary lamellae which Stone and Scallan (71) have proposed for the average cell walls of wood fibers.

Although Page and DeGrace did not find delaminations in the fibers of high-yield pulps, Dinwoodie (72) found that multiple delamination did occur in the fibers of wood blocks at compression stresses above perhaps 50% of buckling stress. Emerton (57) concluded that coaxial delamination of the cell wall is a general phenomenon occurring during beating, and that it was the cause of increases in fiber flexibility.

Dolmetsch (73) also reached the conclusion that the bonding between interlamellar planes was weakened at the misaligned zones. He demonstrated that preferential splitting took place between the lamellae at the misaligned zones when such fibers were swollen in an alkaline medium. A generalized model, representing the different kinds of misalignments, is presented in Fig. 11; it includes the Dolmetsch concept of interlamellar separation at a misaligned zone.

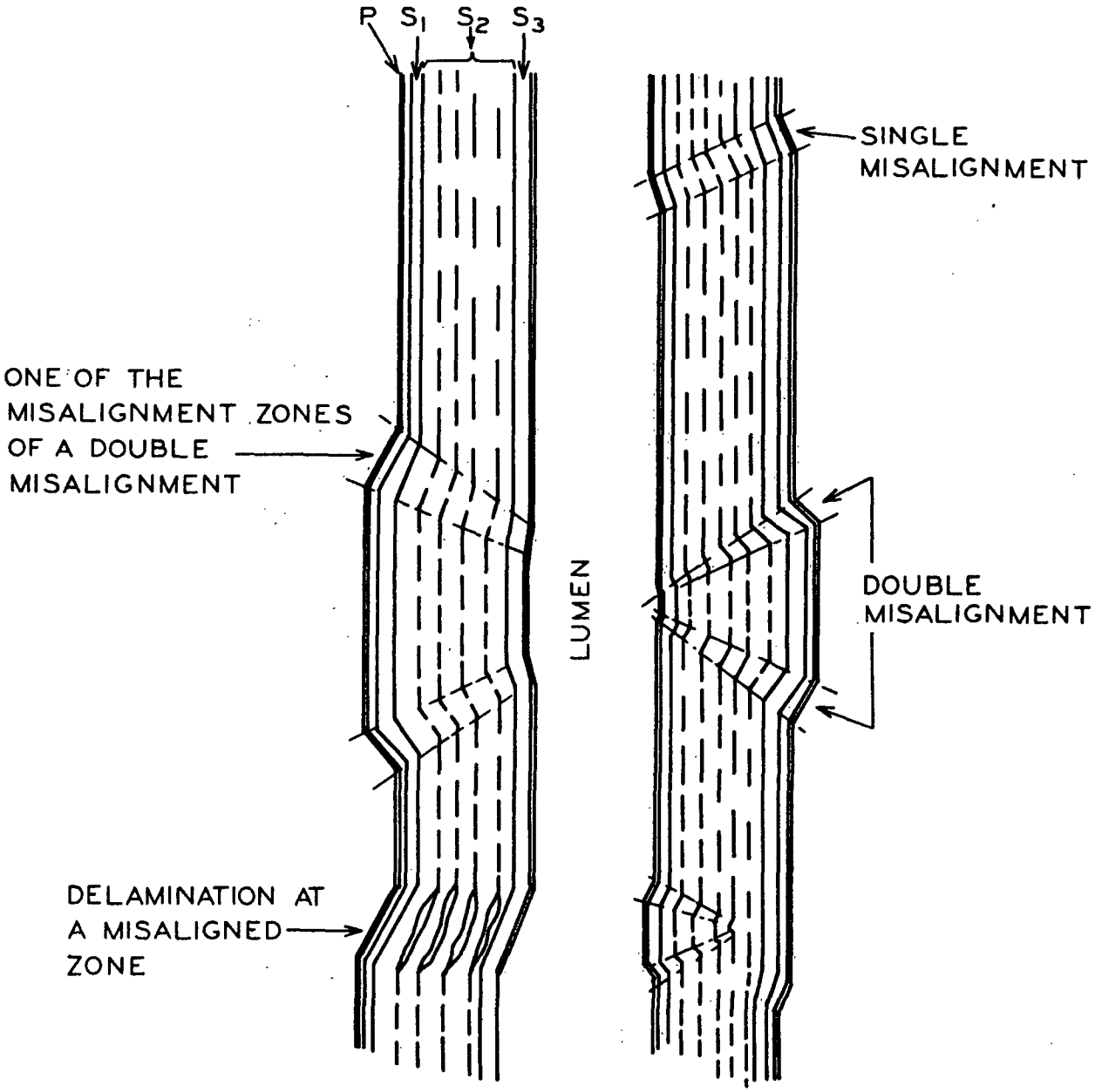

Figure 11. Generalized Model for Different Types of Misaligned Zones. From Hartler (40) and Dolmetsch (73). Drawing After Ebeling (7)

FACTORS IMPORTANT TO THE TENSILE PROPERTIES OF FIBERS

Many mechanical properties such as flexibility, torsion strength, and compression resistance are important to the ultimate use characteristics of cellulosic fibers. It is the tensile load-elongation properties which have been most extensively studied, however, due to the relative ease with which they may be determined. Several comprehensive reviews dealing with the mechanical properties of fibers have considered in detail the factors which determine tensile properties. Among these are the works of Wakeham (74), Morton and Hearle (75), and Meredith (76). The following discussion will be taken primarily from these authors, and will attempt a brief summary of some of the more significant factors upon which tensile properties of pulp fibers depend.

Wood pulp fibers are viscoelastic materials and as a result display load-elongation behavior typical of such substances. When tensile stress is introduced, the initial response of the fiber is essentially elastic. If the loading is of short duration and is not greater than the yield point, the elongation is largely recoverable. If the load is sufficient to reach the region of plastic deformation, however, the elongation will be only partially recoverable. Loadings of longer duration will also cause the time-dependent creep phenomenon to become important. Creep is defined as having two components: primary creep which is recoverable, and secondary creep which is not.

Load-unload cycling is a fast method for obtaining information about the recovery properties of the fiber. Depending on the nature of the particular fiber, "work hardening" may result in changes of fiber properties observed in successive cycles. Thus, a fiber which has been loaded and unloaded several times would be found to have appreciably different properties from those it originally had. The elastic recovery for each cycle may be defined as the

ratio of the elongation which was recovered on unloading the fiber to the total elongation which took place on loading the fiber. The amount of elongation which is not recovered is considered to be the "permanent set," although, as in all viscoelastic materials, some strain recovery would take place over a period of hours. As secondary creep becomes more important at higher loads, the "permanent set" increases with increases in applied stress, and when the cycling is carried further into the plastic regime, only a small fraction of the elongation is recovered.

The rate at which the fiber is strained has an effect on the form of the load-elongation curve. Rates of loading are intimately related to the phenomenon of creep although creep effects are minimized by more rapid rates of loading. Meredith (76) found that over a range of six orders of magnitude in the rate of elongation, the strength and Young's modulus differed by about 50% although the ultimate elongation remained about the same.

Initial span may also have an effect on observed mechanical properties. Pierce (77) formulated a theory based on the statistical distribution of weak links along the fiber length to account for the span effect. Hartler, Kull, and Stockman (78) found that the observed tensile strength of wood pulp fibers decreased with increasing span. Hardacker (79), however, found the effect to be small or nonexistent for certain classes of pulp fibers and large for others.

Changes in the relative proportion of crystalline material or the size of the crystallites within the cell wall probably have an effect on fiber mechanical properties, but the measurement of these quantities is difficult.

Howsmon and Sisson (80) and Wakeham (74) have discussed this problem. Their qualitative conclusions were that tensile strength and Young's modulus increase, but ultimate elongation, work-to-rupture, and flexibility decrease with increasing crystallinity, but these authors made no mention of how crystallinity was determined. Howsmon and Sisson (80) mentioned that it is not known exactly what is determined by many measurements of so-called "crystallinity." Indeed, the measured values of crystallinity are generally directly related to orientation and their effects are difficult to separate. Fibril or crystallite orientation is a more readily determined quantity, and as a result, many workers have correlated orientation with mechanical properties. The many methods available for determining fibril orientation have been summarized by Page (81). Howsmon and Sisson (80) examined the work of a number of investigators to reach some generalizations about the effect of orientation on the mechanical properties of cotton and viscose fibers. They concluded that an increase in fibril orientation resulted in increased strength and Young's modulus and decreased ultimate elongation.

Because pulp fibers are hygroscopic, the humidity at which their properties are tested is very important. As relative humidity increases, the tensile strength and elongation increase, and the elastic modulus decreases in natural fibers. When moisture enters the fiber structure, it is generally accepted that the crystalline regions remain unchanged, but that the less-ordered regions sorb water. This decreases secondary bonding and leads to lower resistance to deformation. Water may be considered to be somewhat like a lubricant which allows some internal slippage for accommodating a strain. This also helps to explain how internal stresses can be made more uniform to increase the tensile strength.

Drying fibers under axial tensile stress has also been investigated in connection with the effect on fiber mechanical properties. Many such investigations have been carried out on textile fibers, but the work of Jentzen (82) was the first study concerned with the effects on pulp fibers. He found that drying under load results in increases in tensile strength, Young's modulus and work-to-rupture, and a decrease in ultimate elongation. Such changes were reversed by rewetting the fiber. He tried to relate these mechanical property changes to changes in crystallinity and crystallite orientation. He found no changes in the crystallinity or in the orientation of the summerwood, but observed that the springwood orientation did decrease due to drying under load. The fact that he failed to find any change in the summerwood orientation can probably be attributed to experimental limitations and the fact that the summerwood fibers were very highly oriented before the load was applied, making small changes difficult to detect.

In order to make mathematical predictions about its mechanical properties, several models of the structure of the fiber have been attempted. The theories of Hearle (83), Cowdrey and Preston (84), and Mark (85), though undoubtedly heuristic, are of limited applicability and depend on oversimplifications and assumptions regarding uniformity of the fiber structure. These theories do, however, go a step beyond the spring and dashpot models which have been used to model viscoelastic behavior in that all try to take into account the known helical arrangement of the fibrils within the cell wall. Hearle (83) assumed that all resistance to stretching of the fiber was due to resistance to radial compression of the layers of microfibrils. Cowdrey and Preston (84) criticized this approach, but assumed instead that the fiber wall consists of fibrillar helices of common orientation angle with fibrils which can move freely past one

another (i.e., no lateral bonding between fibrils). Mark (85) also made such assumptions as, for example: (1) Layers of the cell wall are completely elastic. (2) Cell wall layers are completely homogeneous. (3) Applied stress creates a condition of plane stress and strain within the walls. Thus, it is obvious that all of these attempts at describing mechanical properties of fibers are not only limited, but do not account for the true state of variation within the cell wall. Of particular significance is the fact that none of these theories can be applied to fibers having discontinuities in their structure, and it is just such fibers that this study is concerned with.

EXPERIMENTAL APPROACH

Other investigators have found that drying fibers under various tensile stresses or strains results in large changes in mechanical properties. Longitudinal compressive stresses or strains during drying could likewise be expected to result in mechanical property changes. The literature review also indicated that such compression would result in longitudinal structural discontinuities in the fiber wall.

It was necessary to devise a method for obtaining uniform longitudinal compressive strains in individual fibers while simultaneously drying them. The strain which was dried into the fibers was determined by measuring the lengths of the fibers before and after treatment for comparison with the known applied strain. Due to the experimental problems involved in applying a known longitudinal compressive load, strain was chosen as the independent variable.

Tensile load-elongation characteristics were the mechanical properties studied. These properties were compared for several levels of applied strain. Load-unload cycles were used to obtain some information about relaxation properties. Some fibers were then rewet and redried following strain-drying to determine if the mechanical property changes were recoverable.

Changes in fiber structure were also determined. Polarized light microscopy was used to demonstrate structural discontinuity caused by longitudinal compression. Electron microscopy was useful for obtaining a more detailed picture of the structural changes which occurred. Finally, Laue x-ray diffraction patterns were used to determine changes in the average relative crystallinity and average crystallite orientation of bundles of fibers.

Springwood and summerwood fibers were separately treated and tested throughout the study. The majority of the work was carried out on holocellulose summerwood fibers. Some work was also done with kraft summerwood fibers. Each of these samples was carefully prepared to provide uniform populations of fibers. This was necessary in order to reduce the statistical spread of the data.

EXPERIMENTAL

HOLOCELLULOSE PULP PREPARATION

Longleaf pine (Pinus palustris) was chosen as the wood species to be used in this thesis because it had already been the subject of intensive investigation by Jentzen (82), Spiegelberg (20), and Dunning (6). These works could then be used for comparison and for additional information on fiber structure. A 25-cm. diameter, 20-cm. thick bolt of a freshly cut longleaf pine was obtained from the Woodlands Research Department of Union-Camp Corporation, Savannah, Georgia. This bolt was received in a plastic bag approximately one week after cutting and was still very wet.

Several 2-cm. thick disks were cut from the bolt and were divided into thin, pie-shaped wedges. The tree was found to be 26 years old. In order to avoid using any fibers from the juvenile-wood portion of the tree, the growth rings corresponding to ages 0-17 years were cut from the wedges and discarded. The remainder of each wedge was then cut transversely at each division line between springwood and summerwood, and the two fiber types were placed in separate beakers of water. Each chip was then examined under a hand lens, and a razor was used to separate any springwood adhering to summerwood chips or vice versa. Any such adhering material or other fibers appearing to be transitional between summerwood and springwood were cut away and discarded. The final chip dimensions were about 0.2 cm. x 1.5 cm. x 2.0 cm.

Each complement of chips was treated in the same manner by the method now outlined. The wet chips were drained and immersed in methanol. They were allowed to soak in methanol for about 8 days, transferring to fresh solvent every second day. This soaking was intended to remove all of the

water before treatment with the extracting solvent. The chips were next extracted for three weeks with 1:1-chloroform:methanol solution, changing the solvent weekly. Vacuum was applied periodically to remove air trapped in the wood. The chips were then placed in each of the following solvents for two days with vacuum applied periodically: 100% methanol, 50% methanol, 25% methanol, and distilled water. Several previously weighed and marked chips were removed at this point to determine the amount of water and extractives present in the original wood.

The extracted chips were then delignified using, in slightly modified form, the room temperature acid chlorite process described by Thompson and Kaustinen (86). The chips were placed in a solution containing 100 grams per liter of sodium chlorite and enough acetic acid to lower the pH to 6.8. The liquor-to-wood ratio was 7.5:1. Fresh sodium chlorite was added to the solution whenever chlorine dioxide gas ceased evolving. Completion of pulping was arbitrarily determined by observing the softness of the chips. Pulping was judged complete after 40 days for the springwood and after 44 days for the summerwood. The pH of the pulping solutions was monitored daily (Appendix I).

After removal of the cooking liquor the chips were thoroughly washed with distilled water. This was followed by seven days of soaking in distilled water with fresh water applied daily. After treatment, the chips still maintained their integrity, although they were quite soft. At this point several previously weighed chips were removed for a yield determination. Finally the chips were immersed in distilled water containing (0.01%) phenyl mercuric acetate (PMA) and stored at 40°F.

A nonmechanical method was selected for defibration of the sample chips to obtain fibers for testing. This was necessary because Dunning (6) found that even the mild mechanical defibration used by Spiegelberg (20) caused extensive damage to the fibers. In order to obtain fiber populations of maximum uniformity, a single chip of each fiber type was selected. Each chip was placed in a beaker of 0.1N potassium hydroxide through which nitrogen was continuously bubbled to help in mixing, to prevent further oxidation and to provide a shear field to aid in defibration. This treatment was continued for two hours followed by filtration and washing with 1% acetic acid solution and then distilled water. After filtering, the fibers were finally dispersed in distilled water containing 0.01% PMA and stored at 40°F.

PREPARATION OF KRAFT PULP

A disk from the longleaf pine bolt described in the last section was used to prepare a kraft pulp. The disk was cut into matchstick-sized chips after elimination of the juvenile wood as before. Summerwood and springwood were not segregated in this preparation. The pulp was prepared in a small cylindrical bomb which was heated in an oil bath. The cooking liquor had a sulfidity of 33% and NaOH content of 40 grams per liter as NaOH. The bomb was completely filled with chips and liquor was used to fill all the remaining void space, resulting in a liquor-to-wood ratio of 4.3:1. The digester temperature was raised from 70°C. to 172°C. in 90 minutes and was maintained at 172°C. for 90 minutes. This was followed by quenching.

The pulp was thoroughly washed, soaked, and filtered. It was then placed in a 10% sodium chlorite solution (acidified to pH 6.8) sufficient to give a 7.5:1 liquor-to-wood ratio. This mild bleaching was allowed to proceed for one week. The fibers were then washed, filtered, and covered with distilled

water containing 0.01% PMA and stored at 40°F. No additional defibration was required as the fibers were very well dispersed after this procedure.

DRYING FIBERS UNDER LONGITUDINAL COMPRESSION

APPARATUS

It was necessary to devise an apparatus to dry never-dried fibers under longitudinal compression. Because fibers are much longer than they are wide, it was apparent that the device would have to distribute the longitudinal compressive forces along the length of the fiber in some manner. In addition, the fiber could not be so enclosed that drying was prohibited. The device which was used to fulfill these requirements is shown in Fig. 12 and 13.

This device works on the same general principle as the commercial processes for producing extensible papers. Two rubber blankets are prestrained, the wet fibers are aligned between the blankets in the direction of the strain, the blankets are brought into intimate contact and held together by air pressure, and the strain is reduced simultaneously in both blankets. The result is a longitudinal compressive strain on the fibers.

The apparatus consists of two nearly identical halves which are joined together by the pivot rod (A). Each half contains a line clamp (B), two carrier rolls (C), a take-up roll (D) which can be turned by means of a thumbscrew (E), and a rubber blanket (F). Each rubber blanket is gripped at one end by a line clamp (B). The blanket then passes over the two carrier rolls (C). The carrier rolls orient the blankets into two planes which are parallel and in intimate contact when the apparatus is closed, as in Fig. 13. Finally, the blankets are attached to the take-up rolls (D) which are used to

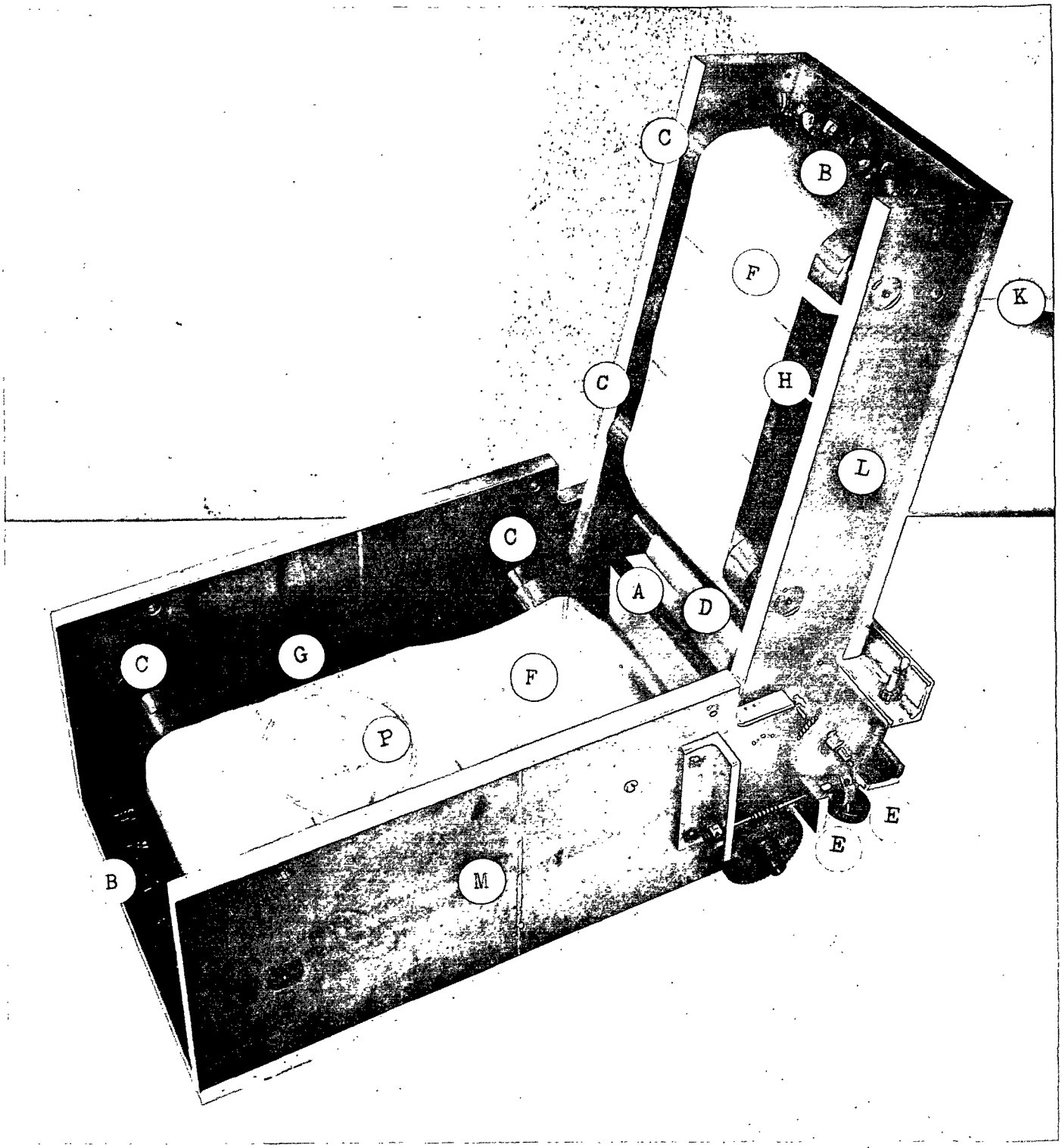

Figure 12. Apparatus for Drying Fibers Under Longitudinal Compression. In Open Position

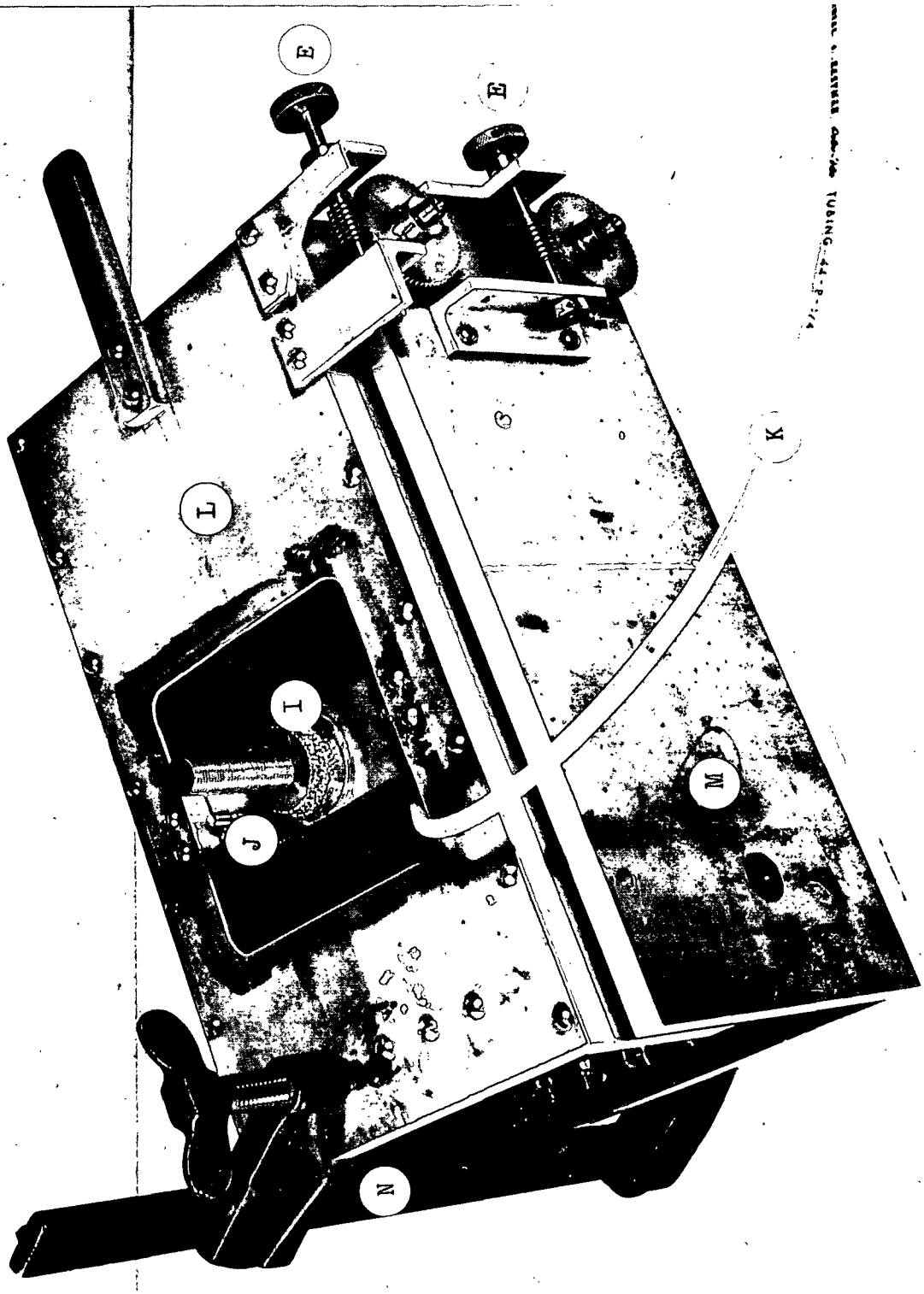

Figure 13. Apparatus for Drying Fibers Under Longitudinal Compression. In Closed Position

adjust the strain in the blankets. The take-up roll in the lower half of the apparatus is not clearly shown in Fig. 12, but it is contiguous with the lower gear.

The two halves of the apparatus differ somewhat in one respect. The lower half is fitted with a very smooth plate set on a post which is adjusted so that the plate is in intimate planar contact with the lower rubber blanket. The outline of this plate is visible (G) as a rectangular plate beneath the lower rubber blanket. The upper half of the apparatus, however, is fitted with a pressure cup (H) the outline of which is visible beneather the upper blanket. This cup is not fixed, but can be adjusted up or down using the nut (I). The cup is kept parallel to the plane of the upper blanket by a pair of guides (J), one of which is visible. The pressure cup is attached to an air pressure source by the line (K).

The upper support frame (L) was built to fit inside the lower support frame (M) when the apparatus is closed, as in Fig. 13. This brings the rubber blankets into intimate contact. The clamp (N) is used to hold the two halves tightly together so that when the air pressure is applied the rubber mats are held tightly in contact with each other. The pivoting arrangement allows easy access to the area where the fibers are located (P).

The properties of the rubber blankets are critical to the success of this apparatus. These blankets were obtained from Davol, Inc. of Providence, Rhode Island. They are made of vulcanized natural rubber approximately 0.25 mm. in thickness. This rubber is permeable to water vapor because of its porosity and because of absorption of water and subsequent transmission to the exterior surface. As received, the rubber surface was covered with talc which served as a surface-release agent. The talc was removed as completely as possible

before the rubber was used. This particular rubber sheeting is commonly known as dental dam, and has the elastic properties of normal natural rubber.

Calibration was carried out with the rubber blankets mounted in the apparatus. Fiducial marks were placed on the surfaces of the blankets which were then stretched to a level sufficient to increase the distance between the fiducial marks about 25%. This distance was then carefully measured. The blankets were then relaxed in intervals and the decrease in distance between fiducial marks was recorded along with the number of turns of the thumbscrew required to reach that level of contraction. The blanket contraction was calculated as the percentage decrease relative to the original extended distance between fiducial marks. These data were then used to plot calibration curves for the two blankets which are presented in Fig. 14. Note that the curves are not the same but are parallel. This difference was found to be an apparatus characteristic and was unaffected when the rubber blankets were changed. The slight lag noted for the lower blanket may have been due to contact with the metal plate (G). Both curves were very reproducible even after a considerable number of use cycles.

When the rubber blankets are allowed to contract, the result is not only a longitudinal compression of the fibers, but also a lateral tension, due to the Poisson effect. A longitudinal contraction of 20% in the rubber blankets is accompanied by a lateral expansion of up to 10%. The presence of this effect should be kept in mind. However, because of lateral shrinkages of fibers during drying of as much as 50%, it is felt that differences in the Poisson effect at various negative strain levels are of little significance.

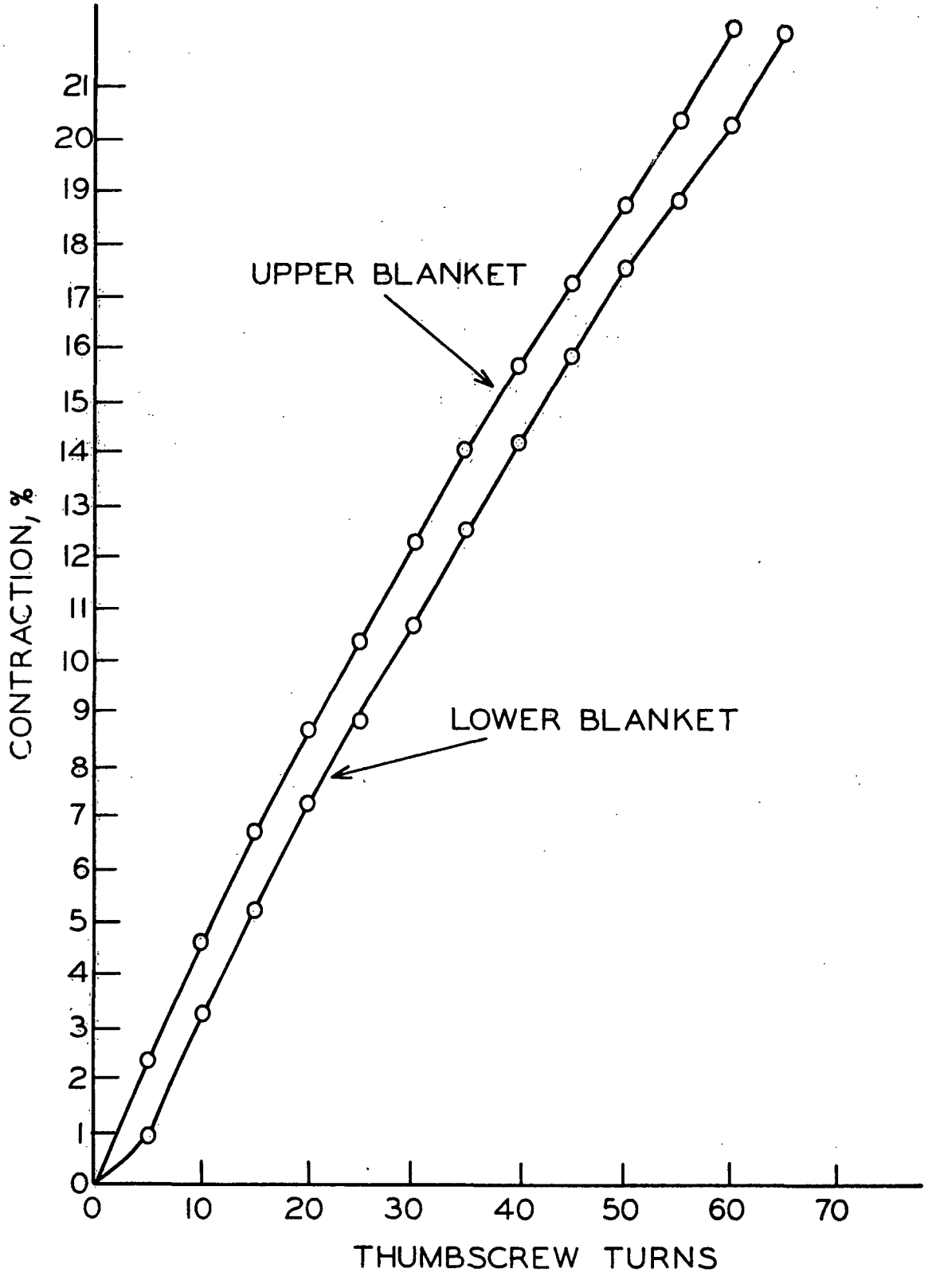

Figure 14. Calibration Curves for Rubber Blankets

PROCEDURE

Several fibers could be treated at one time in the apparatus, and when some proficiency had been gained, the number was usually about twenty. These fibers were separated from a slurry and placed in individual sample cups of water. The lengths of the wet fibers were measured by the method outlined in the next section.

Next, the rubber blankets were strained to the level which had been predetermined during calibration. Thin strips of water were then scribed onto the blankets in the area (P). A binocular microscope mounted on a cantilever was placed over this area and focused on the water strips. The fibers were then placed in these strips of water and carefully aligned in the direction of the blanket strain with the aid of the microscope. After removal of the microscope, the apparatus was closed, clamped shut, the pressure cup adjusted downward to obtain firm contact, and air pressure was then applied. The rubber blankets were then allowed to contract the required number of thumbscrew turns. However, the tight contact between the pressure cup and the smooth plate prohibited the rubber blankets from contracting in the area where the fibers were located. Contraction in this area was accomplished by moving the pressure cup upward very slightly, permitting air leakage around the smooth lip of the cup. When this was done, the rubber blankets were free to contract while still maintaining smooth contact between them. The pressure cup was so adjusted that this contraction took approximately 30 seconds. The cup was then tightened down again to stop the leakage of air.

Drying was accomplished in approximately six hours, but normally the fibers were left in the apparatus under pressure for about twelve hours.

After the air was turned off, the apparatus was opened and the fibers could be removed from the surface of the blanket. Removal was easily accomplished with minimal manipulation of the fibers. The entire procedure was carried out in a room controlled at 73°F. and 50% R.H.

DETERMINATION OF COMPRESSIVE STRAIN

In order to determine if the fibers were indeed being longitudinally compressed, it was necessary to measure the length of each fiber before and after compression. A Bausch and Lomb student microscope was fitted with a prism arrangement with camera attached which permitted the examination of the specimen without removing the camera. A wet fiber was placed in a drop of water on a glass reticle having one millimeter divisions. A cover glass was located over the fiber and water was placed in a well around the interface between the reticle and cover glass to keep the fiber from drying out. This arrangement is shown in Fig. 15. The fiber was then aligned under the microscope and photographed at 2.5 magnification with 35 mm. Kodak Plus-X film using transmitted light. Because the fiber and the reticle divisions were in nearly the same focal plane, the reticle divisions were also imposed on each photograph for use as reference dimensions. The fiber was then removed for treatment as outlined in the preceding section.

After removal from the compression apparatus, the fibers were photographed again. The procedure was the same except that no water was used with the dry fibers, and reflected light was found to give better image definition in this case. Figures 16-19 demonstrate the types of photographs obtained.

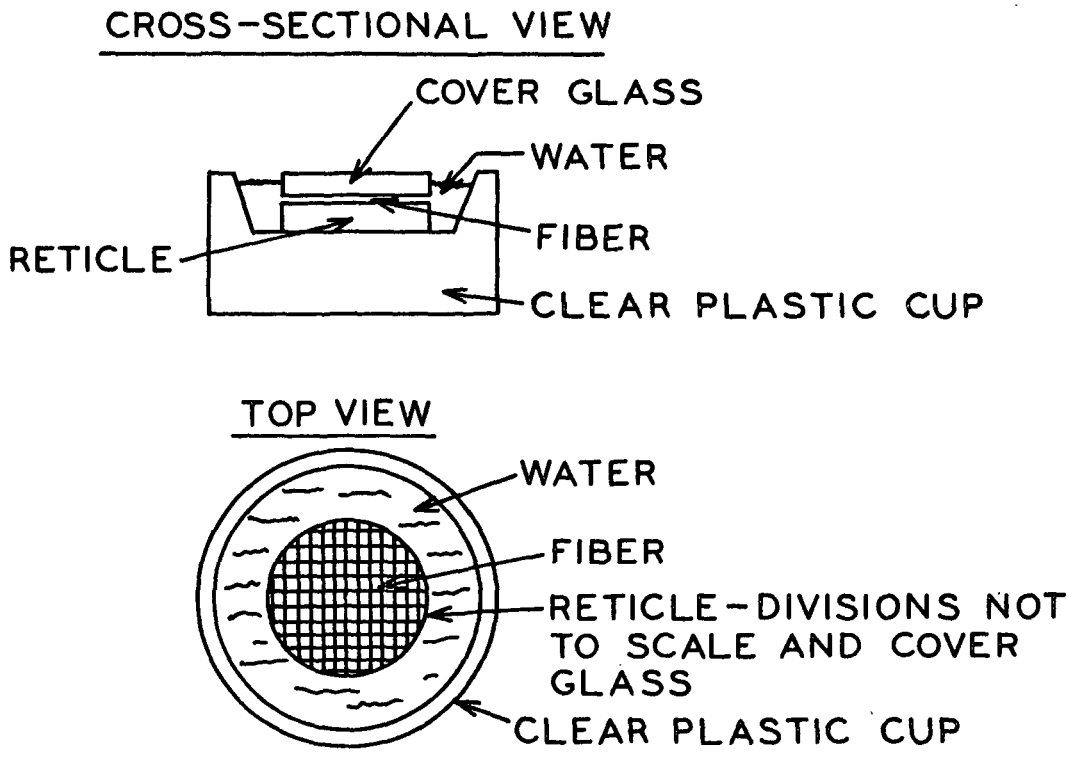

Figure 15. Wet Fiber Mounted for Photographing

Figure 16. Wet Holocellulose Summerwood Fiber on Grid Reticle

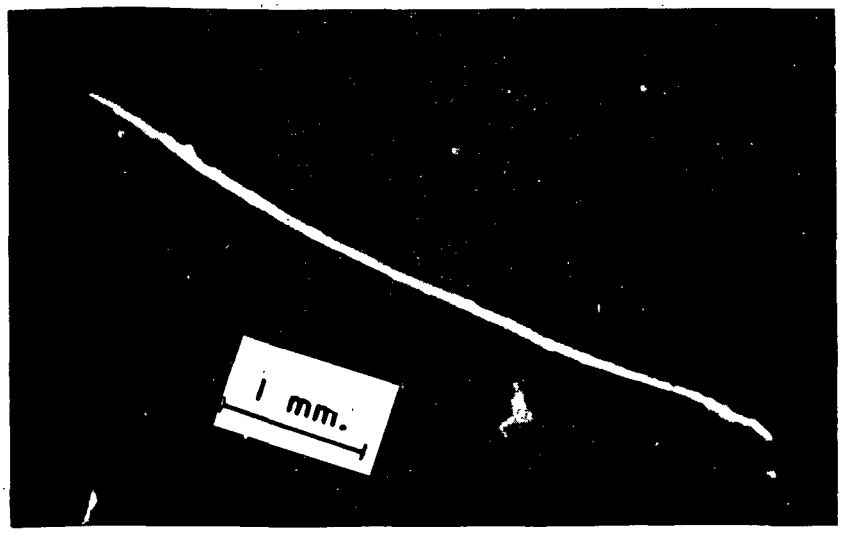

Figure 17. Same Fiber as Fig. 16 Dried Under 10% Longitudinal Compressive Strain

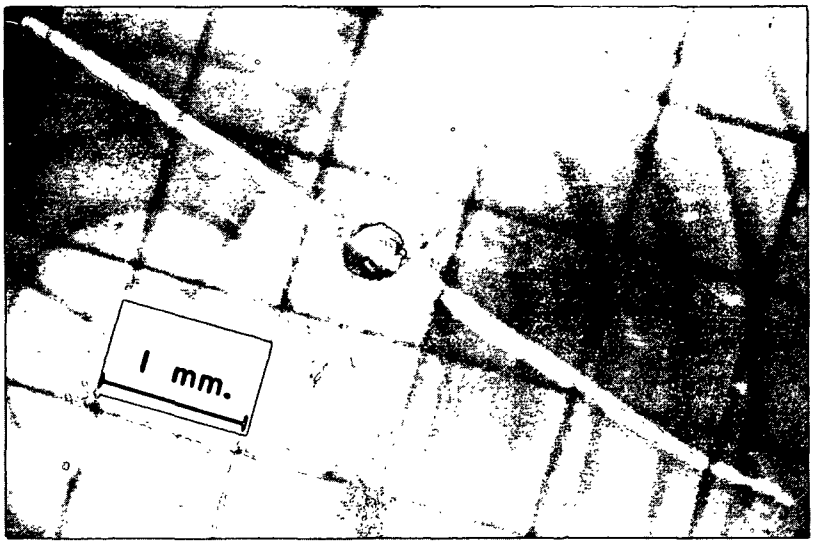

Figure 18. Wet Holocellulose Summerwood Fiber on Grid Reticle

Figure 19. Same Fiber as Fig. 18 Dried Under 20% Longitudinal Compressive Strain

The fiber lengths before and after straining were obtained from the photographs by means of an x-y digital comparator developed by Hardacker (87). This comparator operated in the following way: The photograph was positioned in a frame whose motion and position in the x and y directions was controlled and recorded digitally. The digital readout of x and y coordinates could be recorded on computer cards at any point desired by use of an interlock system connecting the comparator to a card punch. The fiber photograph was enlarged onto a screen fitted with crosshairs which defined the point recorded by the digital readout. The length of the fiber was determined by recording the coordinates of one end of the fiber and then taking numerous coordinates along the fiber length and finishing with the opposite end of the fiber. By following any directional changes in the fiber's center line, an accurate trace could be made of the entire fiber. The fiber length was determined as the sum of the distances between each point recorded and its neighbor.

This sum was divided by the previously recorded distance between the division lines of the grid reticle to give the fiber length in millimeters. The fibers were usually quite straight, which limited the number of points required to define the fiber's length to an average of around ten. The accuracy of this method was judged superior to other methods available for determining fiber length because simpler methods generally measure only end-to-end distance without taking bends into account.

Two terms were devised for use in describing the longitudinal compressive strains induced in the fiber. Applied negative strain was defined as the percentage contraction of the rubber blankets observed for a particular level of treatment. This was the controlled variable in all cases, and all treatment levels used in this study were at increments of 5% applied negative strain (i.e., 0, 5, 10, 15, and 20%). Actual negative strain was defined as the percentage decrease in length for all the fibers treated at any particular level of applied negative strain. Thus, the applied negative strain was determined from the fiducial marks on the rubber blankets, and the actual negative strain was determined from the changes observed in the fiber lengths.

LOAD-ELONGATION MEASUREMENT

Individual fiber tensile mechanical properties were determined on the IPC Fiber Load-Elongation Recorder (FLER) (88) at 73°F. and 50% R.H. The fibers were tacked to steel pins by applying ethylhydroxyethyl cellulose to the fiber ends except in the area where the epoxy resin was to go. Epon 907, a two-part Epoxy resin manufactured by Shell Chemical, was used to firmly fix the fibers to the pins. The glue mixture consisted of ten parts of Component A and six parts of Component B by weight. After careful mixing for approximately five

minutes, the glue was used immediately. As many fibers were glued at one time as could be mounted in 20 minutes.

The nominal span used throughout this investigation was 1.00 mm. The distance between the steel mounting pins was set at this span before the fiber was mounted. The actual span was determined as the distance between the glue lines measured with a calibrated eyepiece in a binocular microscope. The span length of fiber tested was long enough to be convenient but short enough to avoid the necessity of using any fiber ends which might have been damaged during handling. A 10 r.p.m. motor was used for all testing except for the case of load-unload cycling where a 2 r.p.m. motor was used. Most of the fibers were loaded at a rate of 1.40 g./sec. Exceptions were the load-unload study where fibers were loaded at 0.28 g./sec. and the kraft fibers which were loaded 2.0 g./sec.

CROSS-SECTIONAL AREA MEASUREMENT

The cross-sectional area of each fiber was determined by means of the IPC Compacted Fiber Dimension Apparatus (CFDA) (89). This device laterally compressed the fiber segment between two sapphire plates until optical contact was gained, indicating that the lumen and larger pores had been collapsed. The thickness was measured by a variable permanence transducer which measured the separation between the plates. The width was measured with a Vickers (Dyson)* image-splitting eyepiece on the viewing microscope. All measurements were made at 73°F. and 50% R.H. Cross sections were determined after tensile testing, when presumably the cross section would be more uniform.

*Vickers Instrument Ltd., York and Croydon, England.

Cross-sectional area was calculated by an equation which took into account the rounded edges of the compressed fiber:

$$A = 0.001668TW - 0.0000971T^2$$

where T = the fiber thickness in transducer units, W = the difference in the micrometer readings from the image-splitting eyepiece (i.e., the fiber width), and A = the compacted cross-sectional area in $\mu m.^2$.

DENSITY MEASUREMENTS

Density was determined for some fibers. The fiber length was obtained from the photographic measurement of the fiber's dry length. The cross section was determined with the CFDA as outlined in the last section. The fiber weight was obtained with a Rodder* microbalance which permitted individual fibers to be weighed. No correction factor was applied to account for the tapered ends of the fibers. All measurements were made at 73°F. and 50% R.H.

CRYSTALLINITY AND FIBRIL ORIENTATION

X-RAY CAMERA

X-ray diffraction patterns were taken photographically with a Laue camera mounted on a Norelco x-ray unit, using CuKα radiation from a tube operated at 50 kilovolts and 20 milliamperes. The camera shown in Fig. 20 was designed and built by Jentzen (82) for use with single fibers and was modified only slightly for use with groups of fibers. Twenty fibers were mounted at a time on a small plastic rectangle with a 1.5-mm. hole positioned

*Rodder Instrument Co., Los Altos, California.

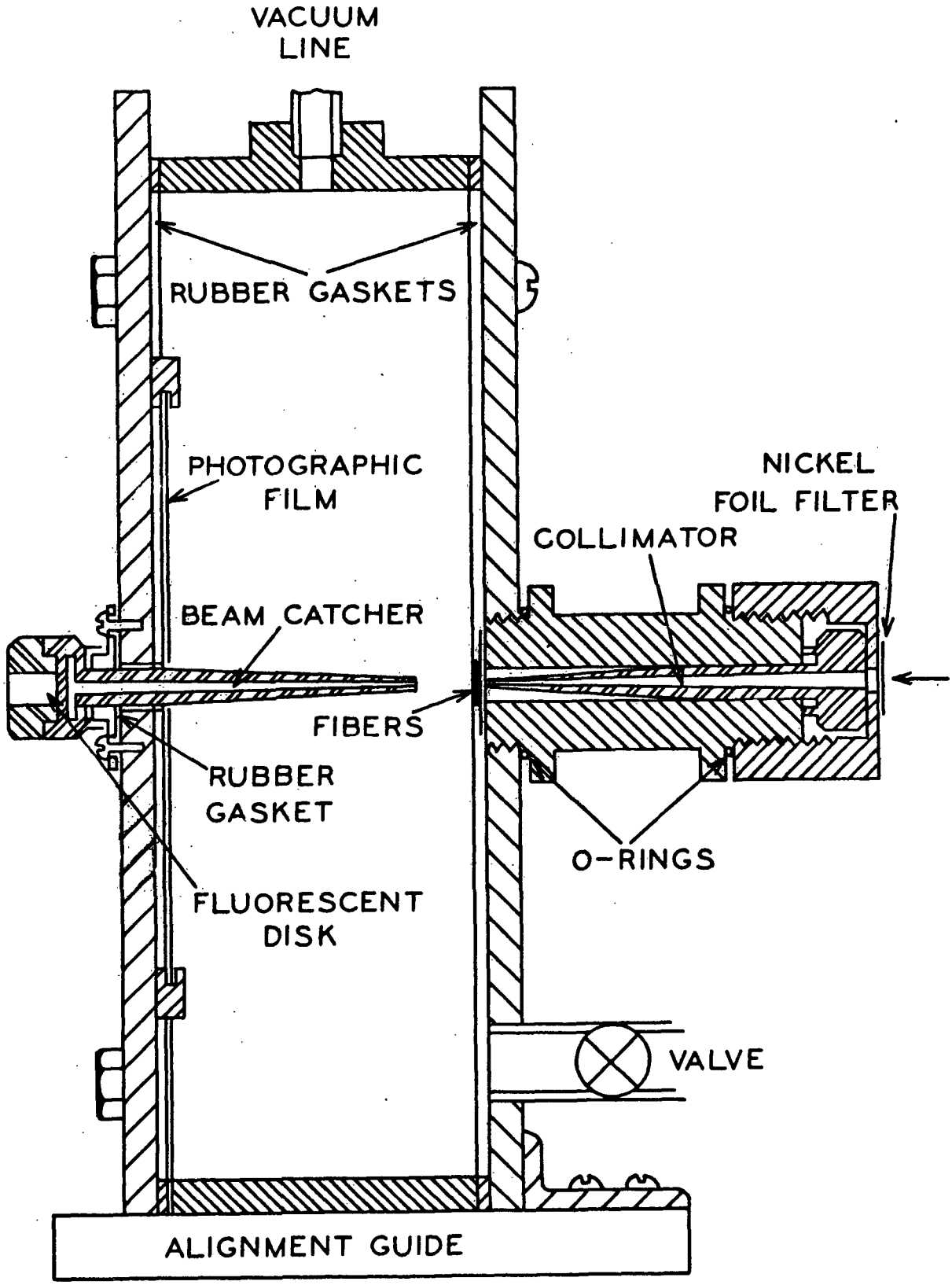

Figure 20. Schematic of Laue X-ray Camera. From Jentzen (82)

for the x-rays to pass through. The fibers were mounted across this hole in four rows of five fibers each using double-backed tape. Total sample depth was 0.25 mm. The fibers could be very well aligned with one another because they were quite straight. Mounting was carried out under a binocular microscope at 15X. The plastic plate was then placed over a pair of mounting screws inside the camera and aligned for shooting.

Once the fibers and film were mounted, the camera, constructed to be both air and light tight, was sealed and could be removed from the darkroom. After the camera was mounted on the x-ray unit, a vacuum was applied as shown in Fig. 20, which minimized scattering of the x-rays by air. X-rays passed into the camera through the nickel foil filter which served as a monochromator, and from there entered the collimator. The collimated beam of x-rays (less than 1 mm. in diameter) passed through the fibers where some of the beam was diffracted onto the photographic film. The undiffracted rays were caught by the beam catcher which had to be carefully aligned each time the camera was remounted. This was done by observing the undiffracted x-ray beam on the fluorescent disk and adjusting the beam catcher to center the x-ray beam. Lead glass covered the fluorescent disk to protect the observer.

FILM DEVELOPING AND CALIBRATION

Because Jentzen's work with single fibers required prohibitively long exposure times, groups of twenty fibers were used in this study. The relative speeds of Kodak Medical No-Screen X-ray Film and Kodak Type KK X-ray Film, the latter used by Jentzen (82) in his single fiber work, only differ by about 25%. No-Screen film was used exclusively because a ready supply of this type was available.

Calibration was carried out by exposing small areas of a single sheet of film for varying periods of time. The film-to-x-ray tube distance was 1.00 meter. CuKα radiation was used with the tube operated at 11 kilovolts and 8 milliamperes. The calibration curve for the No-Screen film based on measurements described below is shown in Fig. 21. The various considerations involved in determining the photographic effects of x-rays are discussed by Klug and Alexander (90). The important point to be made from Fig. 21 is that the plot is linear over the range of transmittances used in this study. Such linearity is characteristic of x-ray films of this type, and is essential for quantitative interpretation of diffraction patterns.

After exposure in the x-ray camera for 12-17 hours, all films were developed by the following procedure, designed for reproducibility and optimum pattern density: The film was immersed for five minutes in Kodak X-ray Developer followed by two minutes in Kodak Ektaflo Indicator Stop Bath and then ten minutes in Kodak X-ray Fixer. The films were then washed for thirty minutes in running water. All solutions and the wash water were controlled at 20°C. Throughout the procedure, the film was agitated at constant intervals according to a predetermined schedule.

MICRODENSITOMETER

For quantitative determination of the optical density of the developed x-ray film, a device was needed with which to scan the film. Two types of scan are required to obtain measurements of both crystallinity and crystallite orientation. A radial scan is required for crystallinity measurements and involves a linear progression across the film. For orientation, a circumferential scan is required. To obtain these, a microdensitometer designed and constructed by Jentzen (82) was reassembled.

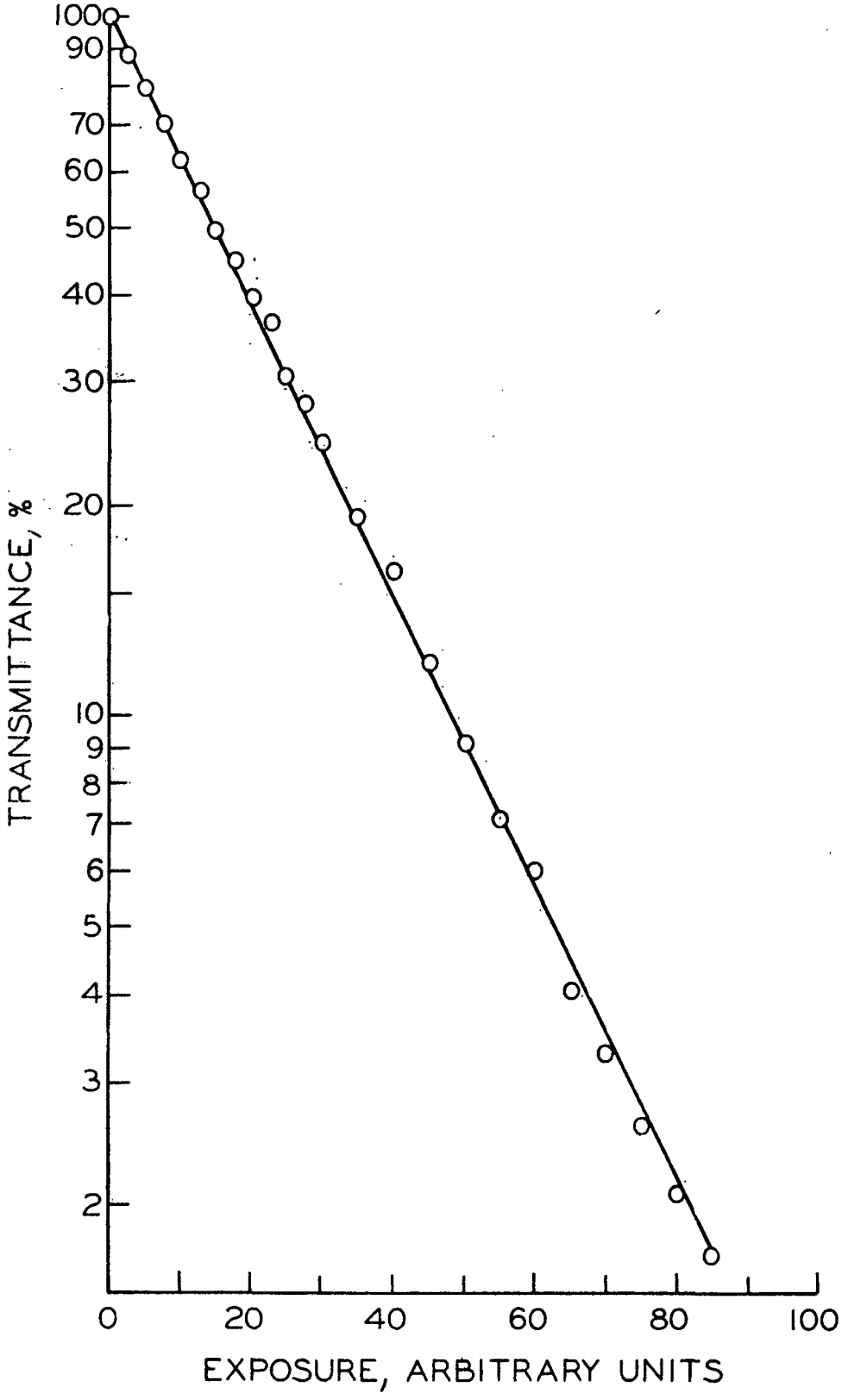

Figure 21. X-ray Film Calibration Curve

The illuminating system of the densitometer consisted of a light source and an inverted microscope to focus the light on the film. On the other side of the film was another microscope which focused the transmitted light on a photocell. A pinhole placed between the eyepiece of the second microscope and the photocell permitted a 0.5-mm. circle of film to be viewed at any one time.

The optical system described above was mounted in a fixed position and the film was mounted on a moveable carriage for scanning. The carriage was fitted with a constant-speed drive arrangement. A Sargent Model MR recorder was used with the Jentzen apparatus. Percentage transmittance was recorded versus film position for each scan and was interpreted as discussed in the following section.

CRYSTALLINITY

For descriptive purposes a typical Laue x-ray diffraction pattern of a group of twenty fibers is shown in Fig. 22. The fibers were oriented in the vertical position in front of the film. The darkest spots, which are also located the farthest from the center of the diagram, are due to diffraction by the 002 planes of the Cellulose I crystalline lattice. Closer to the center and lying on the same line (called the equator) as the 002 spots, are two more pairs of diffraction maxima. These are due to the 101 and $10\bar{1}$ crystallographic planes, but are not resolved in Fig. 22. This lack of resolution is due to small crystallite size and imperfections in the crystallites. The border of unexposed film was used as an optical density reference in each case. The amorphous background scatter is readily distinguished from the completely unexposed strips.

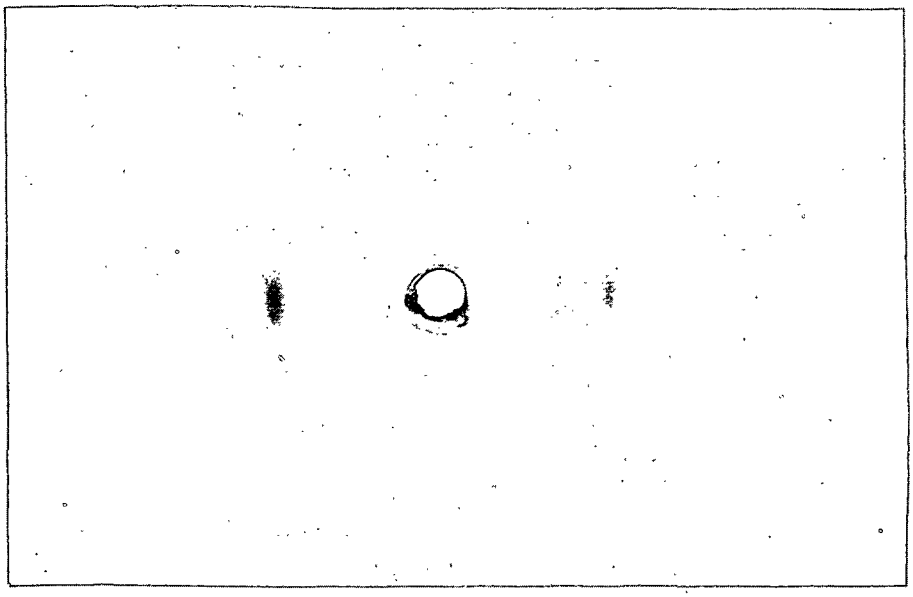

Figure 22. Laue X-ray Diffraction Pattern from 20 Summerwood Fibers Dried on a Teflon Sheet

Many methods of interpreting the x-ray diffraction patterns to give measures of crystallinity have been proposed and some will be discussed later in this section. Most of these require a radial scan of the diffraction maxima along the equator. This was obtained by means of the densitometer previously described. The unexposed portion of the film was used as the 100% transmittance reference, and a metal plate was used to cut off the light for a check of the 0% transmittance. The maximum of the 002 peak was set at a 2θ angle of 22.8° and all other angles were calculated with respect to this. The result was a plot of percentage transmittance against 2θ angle.

Percentage transmittance was then converted to x-ray intensity by means of the film calibration curve. Two correction factors were also required. The first of these, the film factor, converted the intensities to those which would have been observed by a goniometer at the same 2θ angle. This accounted

for the geometry of the film. The film factor equals $\cos^3 2\theta$ by which the corresponding intensity values were divided. The second correction was for polarization which was discussed by Klug and Alexander (90). The x-ray intensities were also divided by this factor, which was equal to $(1 + \cos^2 2\theta)/2$. All of these operations were carried out on transmittance data which had been reduced to digital form. This permitted the conversion to intensity, and application of correction factors by means of a digital computer. The converted data were then replotted by means of a Calcomp Model 110 and 565 combination plotter. Figure 23 shows a typical plot obtained after conversion and application of the correction factors.

Some of the earliest attempts to determine the relative amounts of crystalline and amorphous substance in cellulosic fibers were those of Hermans and Weidinger (91,92,93). These workers estimated the crystalline interference above some approximation of the background radiation due to the amorphous material. Although they calculated an absolute percentage crystallinity, such a quantity has no clearly defined physical significance. Instead, it is better to use such values to compare the relative order of different materials without making reference to absolute crystallinity. A planimetric method used to determine the relative order of the specimens of this study was based on the Hermans and Weidinger method, and employed the following equation:

$$RO_{HW} = 100A_{cr}/(A_{cr} + A_{am})$$

where RO_{HW} is the relative order, A_{cr} is the area between the diffraction curve and the lower dashed line of Fig. 23, and A_{am} is the area between that dashed line and the zero intensity line for $2\theta = 10$ to $32°$.

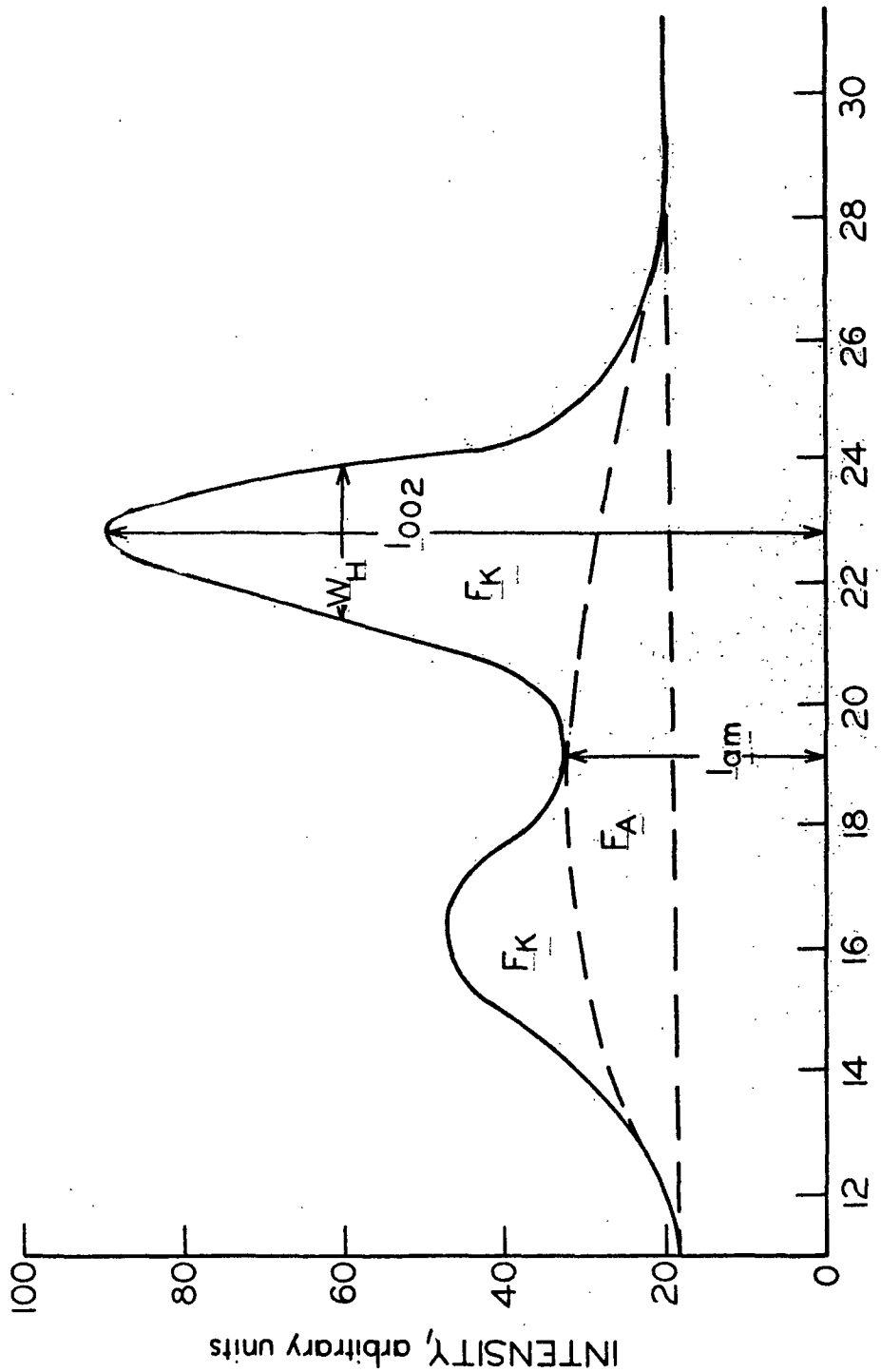

Figure 23. Typical Radial Intensity Distribution of a Laue X-ray Diffraction Pattern

Jayme and Knolle (94) used a very similar planimetric method and obtained excellent correlations for cellulosic substances whose crystallinities relative to one another were known from other studies. The Jayme and Knolle index was determined by the following equation:

$$KI = 100\ F_K/(F_K + F_A)$$

where KI is the Jayme-Knolle index of crystallinity, F_K is the sum of the two areas labeled F_K in Fig. 23, and F_A is the area enclosed by the dashed lines shown in Fig. 23.

A somewhat simpler method for determining relative crystallinity, and one which shows good correlation for most situations, is that of Segal, et al. (95). This commonly used method defines a crystallinity index by means of the equation

$$CrI = 100\ (I_{002} - I_{am})/I_{002}$$

where CrI is the crystallinity index, I_{002} is the maximum intensity of the 002 lattice diffraction as shown in Fig. 23, and I_{am} is the minimum intensity between the 002 and 101 maxima as in Fig. 23. A very similar index was more recently proposed by Ant-Wuorinen and Vispää (96), but offers no apparent advantage over the method of Segal, et al.

All of the above methods purportedly give quantitative comparisons of the relative order of different samples in terms of the amount of crystalline material present. A somewhat different line of approach was taken by Gjonnes, et al. (97), and Gjonnes and Norman (98). These workers reasoned that the width of the 002 lattice diffraction should be related to the diameter and state of disorder (lattice distortion) of the microfibrils. They found that

the width of the 002 lattice diffraction at one half the distance between the maximum and an arbitrary base line (W_H in Fig. 23) increased monotonically with the degree of amorphousness calculated by the method of Ellefsen, et al. (99). The Ellefsen method is similar to that of Hermans and Weidinger except that the base line comes in contact with the diffraction curve at the minimum between the 002 and 101 lattice diffractions. The half-width was determined for each of the samples of this study for purposes of comparison and because the physical significance of this measurement is somewhat different from that of the other quantities measured.

CRYSTALLITE ORIENTATION

Crystallite orientation is related to the width of the 002 lattice diffraction along an arc normal to the equator passing through the intensity maximum. All of the methods for determining orientation require circumferential scans along this arc. These were obtained for each diffraction pattern by using the microdensitometer. As before, the transmittance values were converted to intensities, but no correction factors were required in this case. The finished plot of the x-ray intensity versus azimuthal angle consisted of two sets of intensity distributions centered around 0 and 180° (the equator), with base lines somewhat above the zero intensity line. Figure 24 shows a typical example of a circumferential scan.

Jentzen (82) used a method which fitted the experimental data to a normal distribution and then described the orientation by means of the standard deviation of the fitted curve. However, many of the data for longitudinally compressed fibers do not fit the shape of a normal distribution. As a result, Jentzen's method was not used.

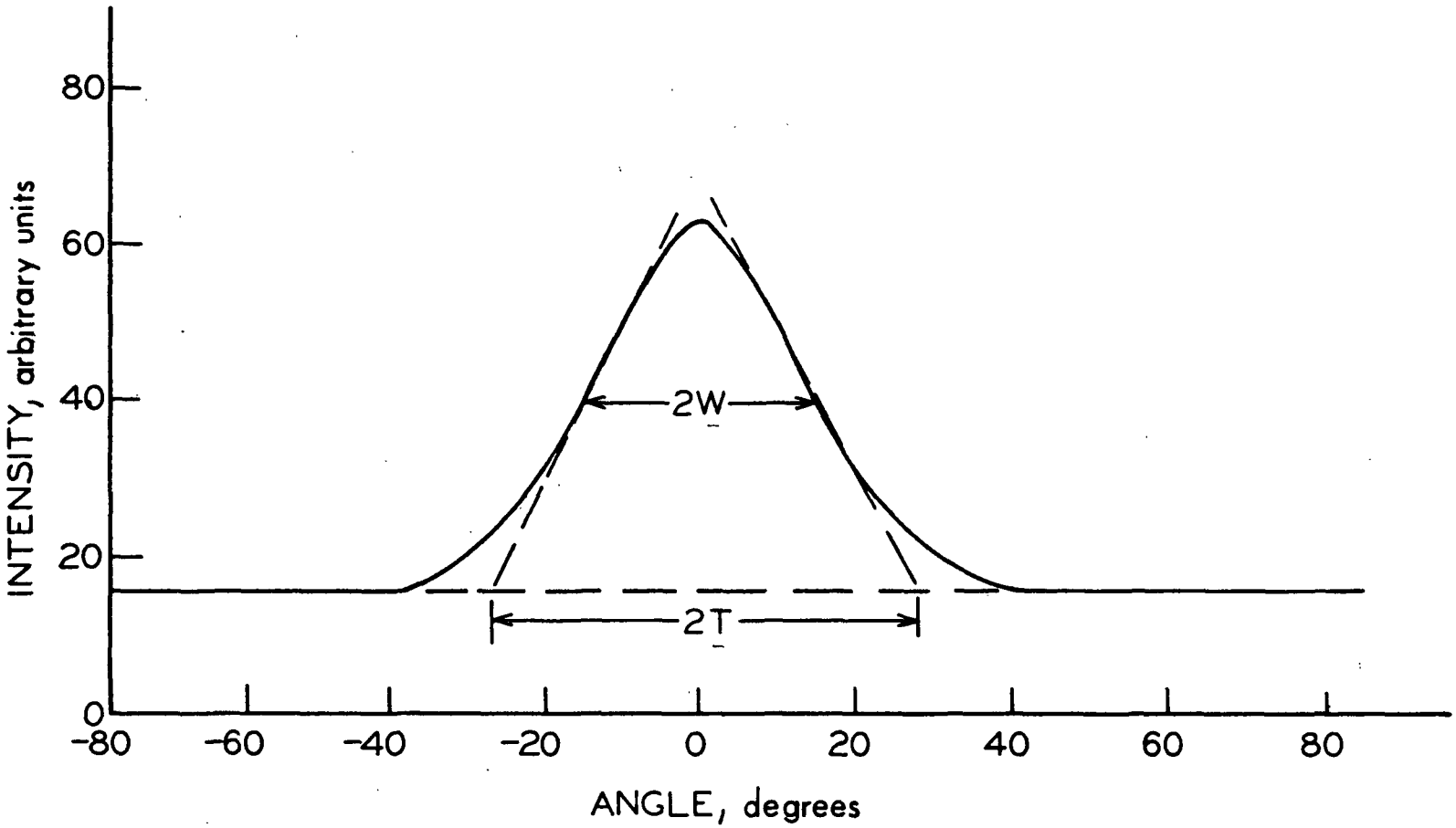

Figure 24. Typical Circumferential Trace of the 002 Lattice Diffraction from Uncompressed Fibers

The most common method for determining orientation was originally proposed by Sisson (100) and uses the width of the distribution curve at one half the distance from the base line to the maximum intensity (2W in Fig. 24). The average fibril orientation is then reported as one half of this value, or W. This quantity was determined for each sample of this study. However, because it depends on only two points and is thus sensitive to small variations in only these two points, an additional method was needed which would take into account the shape of the curve, and would not be dependent on so few points.

A method outlined by Hermans (101,102) requires circumferential traces of both the 002 and the 101-10$\bar{1}$ lattice diffractions. Hermans also derived an orientation factor which could be obtained from a single scan of the diatropic lattice diffractions of the 021 crystallographic planes. The 021 diffraction maxima would appear at an angle of 45° from the equator, but due to the weakness of the diffraction by these planes, the spots are not visible in Fig. 22. Jentzen used the equation developed for the diatropic planes to calculate an orientation factor from data derived from the paratropic 002 planes. Due to the necessity for extra circumferential scans, the slow speed of the microcomparator, and the fact that absolute values were not required for the comparisons to be made, the Hermans method was not used in this study.

A more direct approach to the determination of fibril orientation was taken by Meylan (103). Meylan's method was to draw tangents to the circumferential trace of the 002 arcs as shown in Fig. 24. From the intercepts with the dashed base line, he then obtained the quantity 2T as shown. He found that T was linearly related to the mean microfibril angle as determined by several methods of direct observation. Meylan's method was chosen for use

in this study for its sensitivity to curve shape, its dependence on a larger number of data points, and its excellent reproducibility and correlation with other accepted methods. Although $\underline{T}$ does not represent the exact value of the mean microfibril angle, it can be used directly for the purpose of comparing one sample with another.

One other consideration regarding the circumferential trace was important to this work. As has been mentioned, the circumferential scan is interpreted to represent the distribution of cellulosic fibrils around the fiber axis (i.e., 0 or 180°). Thus, a sample in which most of the fibrils were oriented very close to the fiber axis would give very intense spots for diffraction maxima. At the other extreme, a sample in which the fibrils were randomly oriented would have a pattern of concentric rings. Thus, the area of the curve above the dashed line of Fig. 24 can be interpreted to represent a quantity of fibrils preferentially oriented around the fiber axis. The area between the base line and the zero intensity line can be interpreted to represent a quantity of nonpreferentially oriented fibrils. The ratio of these two areas between the limits of $\pm$ 90° gives an indication of the relative proportion of preferentially oriented fibrils for a particular sample. The ratio between the maximum and minimum intensities observed during a 360° circumferential trace of the 002 arcs gives an indication of the degree of preferential orientation. Two samples can thus be compared by means of these ratios, if their relative crystallinities do not differ significantly. This will be further discussed in light of experimental results obtained.

MICROPHOTOGRAPHIC METHODS

Polarized light microscopy can be used to accentuate differences in the orientation of the crystallites within a fiber. Light is polarized and passed through the fiber where the angle of polarization is changed depending on the orientation of the crystallites. When the fiber is viewed through an analyzer oriented at 90° with respect to the original polarized light, only the crystalline material can be seen because all background light, which is still polarized at the original angle, is cut off. This causes the fiber to stand out as a bright body against a black background so that disturbances in the fiber structure can be readily determined. Many photographs were obtained using this method of observation, and were used in determining changes in fiber structure. The fibers were mounted in oil to minimize surface scatter.

Transmission electron microscopy was also used to determine submicroscopic changes in the longitudinal order of the fibers. Groups of fibers which had been examined by the x-ray technique were used for this work. The fibers, which were mounted in rows held in place by layers of double-backed tape across their ends, were tied in bundles with two nylon threads around the bundle as near the tape as possible. The fibers were then cut away from the tape. Bundling the fibers in this way caused many of them to assume a curved shape. This factor is important to later interpretations of the electron photomicrographs. The bundles of fibers were then imbedded in maraglas epoxy resin*.

*Erlandson, R. A., J. Cell Biol. 22:704-7(1964).

After they were imbedded, the fibers were sectioned longitudinally for examination under the electron microscope. This sectioning involved considerable trial and error manipulation to get the fibers properly oriented with respect to the microtome knife, but sections were ultimately obtained. Several cross sections were also made in order to determine the shape of the fiber ribbons after drying. All sections were stained with a 5% uranyl acetate solution to help in distinguishing the cellulosic material.

RESULTS AND DISCUSSION

CHEMICAL ANALYSIS OF PULPS

The fibers used in this study were characterized by means of chemical analyses of the pulps from which they came. The first two quantities listed in Table II (Extractives + Moisture, and Yield) were determined on the basis of the original wood, as has been described. The remaining data were determined from pulp samples which had been dried and completely pulverized, and the data are based on the dried sample.

TABLE II

CHEMICAL PROPERTIES OF EXPERIMENTAL PULPS

	Holocellulose		
	Springwood, %	Summerwood, %	Kraft, %
Extractives + moisture[a]	65	35	--
Yield	66[b]	66[b]	55.5
Extractives[c]	11.7	12.4	1.7
Klason lignin[d]	0.1	<0.1	0.4
Total sugars[e]	87.6	91.3	98.6
Glucan	63.6	69.4	81.4
Xylan	7.3	5.8	7.7
Mannan	13.4	13.7	8.2
Arabanan	1.2	0.9	0.7
Galactan	2.0	1.5	0.6

[a] Based on original wet wood.

[b] Based on extractive- and moisture-free wood.

[c] Pulverized pulp was extracted with hot alcohol and hot water.

[d] TAPPI Method T 13 m-54.

[e] Method of Borchardt, L. G., and Piper, C. V., Tappi 53, no. 2:257-60(1970).

Results of the analyses of the holocellulose pulps were similar to those reported by Jentzen (82) and Spiegelberg (20). The springwood and summerwood differ only slightly in their chemical composition. Note that the sum of the hot-water extractives and the total sugars for these pulps is greater than 100%. The sugar analysis was performed on pulverized pulp which had not been extracted with hot water. As a result, the sugar analysis also includes those sugars which are removable by hot-water extraction.

The kraft pulp differs considerably from the holocellulose pulps. Hot-water extraction removes far more material from the holocellulose pulp. This is probably due to the larger quantities of lignin residue, pectins and degraded sugars in the chlorite holocellulose pulps (104,105). Glucomannans and arabinogalactans were also removed to a greater extent during kraft pulping.

DETERMINATION OF FIBER COMPACTION

Using Van den Akker's theory (61), Jentzen (82) was able to determine the tension which might be expected in the individual fibers of a sheet of typical machine-made paper. In his derivation, the resulting maximum tensile loads for fibers oriented in the machine direction were about three times as great as the maximum longitudinal compressive loads on fibers oriented in the cross-machine direction. Jentzen then used the work of Schulz (105), who found maximum sheet drying tensions of 1.5 kg./sq.mm., to derive drying loads of 1.6 g. and 1.2 g. for summerwood and springwood fibers, respectively. Jentzen finally settled on 5.0 g. as a suitable maximum drying load to use in his work.

The drying load to be used was also important to this study. The longitudinal compressive drying load on the fibers could not be measured, but the load required to simulate the compressive forces during sheet drying could be

approximated. By analogy with the considerations noted above, it was reasoned that the maximum compressive drying load should be about one third of the maximum tensile drying load. As Jentzen used a 5-g. maximum tensile drying load in his work, a 2-g. compressive drying load was considered sufficient for this study. To obtain this using the experimental apparatus required the application of a lateral compressive force to hold the rubber blankets in intimate contact with the fiber. The lateral compression required was calculated, by the method shown in Appendix II, to be somewhat less than 60 p.s.i. By trial and error, it was determined that a lateral pressure of 85 p.s.i. was sufficient during longitudinal compression of the summerwood and about 50 p.s.i. was sufficient for the springwood.

Although known levels of longitudinal compressive strain were applied to the fibers, the actual negative strain, which was determined photographically, was usually found to be somewhat less than the applied negative strain. A comparison is presented in Table III for holocellulose fibers. The observed difference shown in Table III can be accounted for in two ways. There was undoubtedly a certain amount of hindrance to the rubber blanket contraction caused by pressing against the smooth lower plate. Slippage was also possible between the rubber mats and the fiber. This slippage was probably more significant for the summerwood which had somewhat more resistance to longitudinal compression. Even at the 0% level, a small decrease in fiber length was observed indicating that the fibers could slip to some extent to allow shrinkage during drying. In the two cases where the actual negative strain was slightly more than the applied strain, the inaccuracy in relaxing the rubber blankets to exactly the proper level and in the photographic method would easily account for the small differences observed.

TABLE III

ACTUAL NEGATIVE STRAIN OF HOLOCELLULOSE FIBERS

Applied Negative Strain, %	Actual Negative Strain, %			
	Springwood		Summerwood	
0.0	Av.	0.23	Av.	0.85
	S.E.	0.28	S.E.	0.30
5.0	Av.	3.42	Av.	3.69
	S.E.	0.36	S.E.	0.21
10.0	Av.	9.00	Av.	7.81
	S.E.	0.33	S.E.	0.43
15.0	Av.	15.08	Av.	12.41
	S.E.	0.25	S.E.	0.30
20.0	Av.	19.65	Av.	20.71
	S.E.	0.34	S.E.	0.38

Each average represents negative strain values of 40 fibers.

MECHANICAL PROPERTIES OF FIBERS

Parallel determinations of the mechanical properties of springwood and summerwood fibers were made throughout most of this study. The properties of the two fiber types differed markedly enough to give sufficient reason for testing both. The mechanical properties of the springwood fibers are listed in Table IV; those of the summerwood fibers in Table V. The column labeled 0% contains the results for fibers which were dried in the experimental apparatus under the same lateral air pressure as the other fibers, but the rubber blankets were only partially prestrained and were not allowed to contract. All references made to statistical significance in this section will be based on the 95% confidence limits. Because each average represents 40-50 determinations, the 95% confidence limits for each average are approximately $\pm$ 2.0 times the standard error of that average ($10\bar{1}$).

TABLE IV

MECHANICAL PROPERTIES OF HOLOCELLULOSE SPRINGWOOD FIBERS DRIED UNDER VARIOUS NEGATIVE STRAINS

		Negative Strain Applied During Drying				
		0%	5%	10%	15%	20%
Cross-sectional area, $\mu m.^2$	Av.	308	271	329	335	284
	S.E.	7.0	7.3	9.3	8.7	5.9
Breaking load, g.	Av.	17.6	16.3	12.8	11.8	11.1
	S.E.	0.9	0.5	0.4	0.7	0.5
	Change, %	0.0	-7.5	-27.1	-33.0	-37.2
Tensile strength, $kg./mm.^2$	Av.	58.2	61.0	39.3	35.1	38.9
	S.E.	3.3	1.9	1.2	1.8	1.4
	Change, %	0.0	+4.8	-32.5	-39.7	-33.2
Ultimate elongation, %	Av.	2.51	5.63	9.54	14.96	21.50
	S.E.	0.11	0.09	0.20	0.42	0.26
Initial modulus $kg./mm.^2$	Av.	3250	1900	1500	770	470
	S.E.	165	96	117	39	19
	Change, %	0.0	-41.3	-53.8	-73.4	-85.6
Work-to-rupture, $kg.\ mm./mm.^3$	Av.	0.87	1.30	1.36	1.85	2.28
	S.E.	0.07	0.05	0.05	0.08	0.08
	Change, %	0.0	+49.3	+56.3	+112.7	+162.0
Length, mm.	Av.	5.06	5.25	5.14	5.13	5.15
	S.E.	0.08	0.07	0.07	0.12	0.07
No. of fibers tested		47	48	43	41	49

Span = 1 mm.
Loading rate = 1.4 g./sec.
CSA determined after tensile test.
All fibers were dried under a lateral compression of 50 p.s.i.g.

TABLE V

MECHANICAL PROPERTIES OF HOLOCELLULOSE SUMMERWOOD FIBERS DRIED UNDER VARIOUS NEGATIVE STRAINS

		Negative Strain Applied During Drying				
		0%	5%	10%	15%	20%
Cross-sectional area, $\mu m.^2$	Av.	352	356	316	325	354
	S.E.	7.2	9.1	10.2	9.1	7.6
Breaking load, g.	Av.	31.1	19.8	17.4	17.3	15.9
	S.E.	1.2	0.7	0.5	0.6	0.5
	Change, %	0.0	-36.3	-43.9	-44.3	-49.0
Tensile strength, $kg./mm.^2$	Av.	88.7	55.9	56.1	53.5	44.9
	S.E.	3.1	1.5	1.4	1.4	1.2
	Change, %	0.0	-37.0	-36.7	-39.7	-49.4
Ultimate elongation, %	Av.	3.71	5.64	10.22	16.73	23.38
	S.E.	0.12	0.19	0.21	0.23	0.29
Initial modulus, $kg./mm.^2$	Av.	3970	2160	1150	840	420
	S.E.	126	68	47	55	19
	Change, %	0.0	-45.6	-70.9	-78.8	-89.5
Work-to-rupture, $kg. mm./mm.^3$	Av.	1.85	1.55	2.29	2.83	3.15
	S.E.	0.08	0.07	0.08	0.08	0.10
	Change, %	0.0	-16.2	+23.8	+53.0	+70.3
Length, mm.	Av.	5.59	5.58	5.37	5.32	5.51
	S.E.	0.06	0.07	0.07	0.08	0.08
No. of fibers tested		49	49	48	49	48

Span = 1 mm.
Loading rate = 1.4 g./sec.
CSA determined after tensile test.
All fibers were dried under a lateral compression of 85 p.s.i.g.

The shape of the load-elongation curves of these different fibers is of interest. In Fig. 25, such curves are shown for three different negative strain levels. Unlike the commercial fibers tested by Hardacker (88) which had about eight different curve types, the fibers of any particular treatment level in this study had remarkably similarly shaped load-elongation curves. The 5 and 15% negative strain curves are not included in Fig. 25, but they also had the sigmoidal shape and exhibited behavior intermediate between the levels shown in Fig. 25, as would be expected. Although the stress values of Fig. 25 are more typical of a summerwood fiber, the curve shapes were the same for both fiber types.

It is apparent from Fig. 25 that drying fibers under longitudinal compression caused some drastic changes in the ability of the fibers to respond to a load. The uncompressed fibers exhibit the behavior typical of viscoelastic solids. Contrastingly, the longitudinally compressed fibers are much more deformable. These fibers all show small response to load up to a low level where they then begin to elongate readily with only small increases in applied load. Finally, as they near the break point, their rate of deformation begins to decrease. Such curves indicate that the longitudinally compressed fibers are behaving more plastically. This observation will be investigated in detail later in this section.

For purposes of comparison, the various mechanical properties are plotted in Fig. 25-30 against the actual negative strains which were obtained photographically.

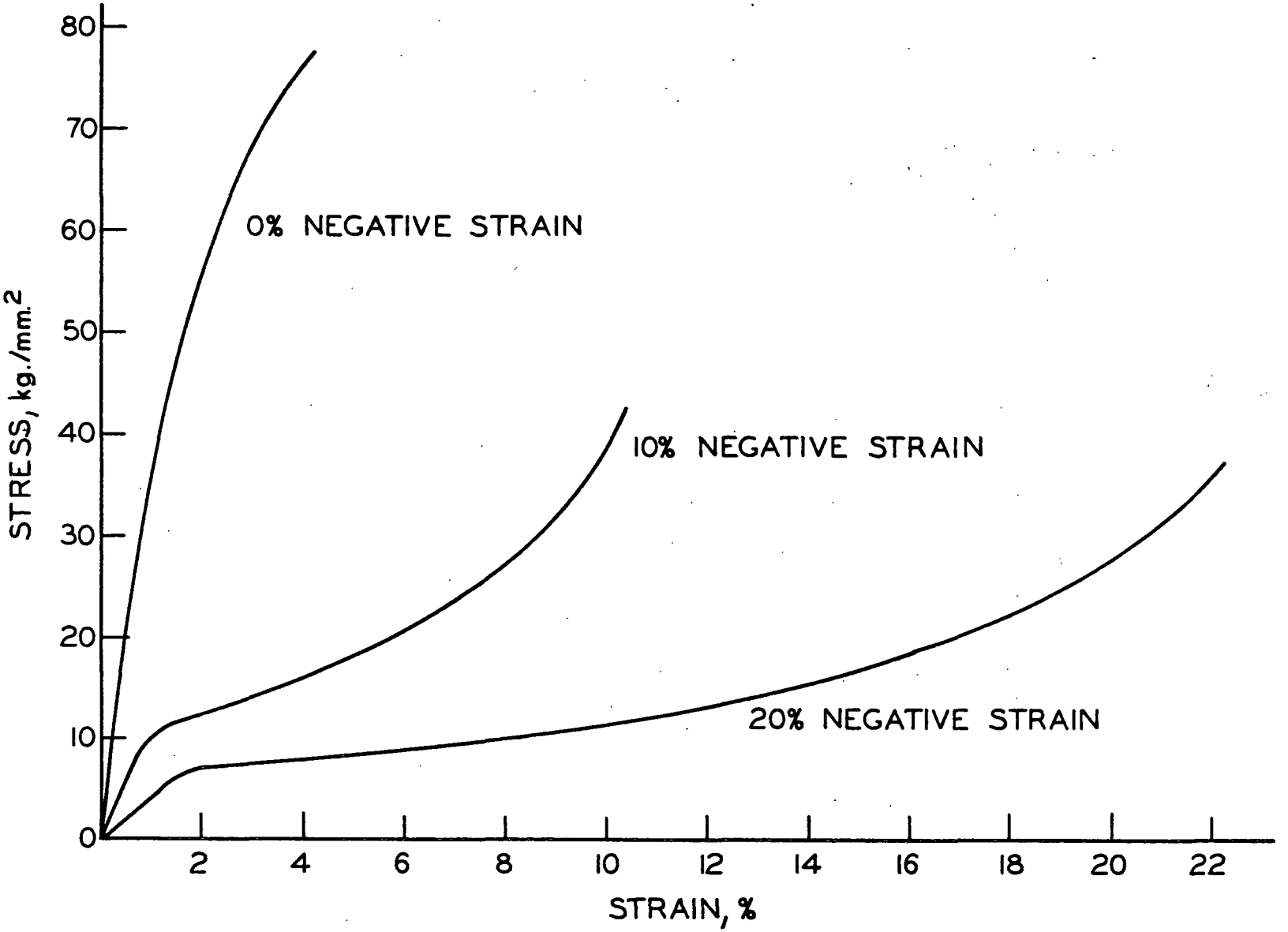

Figure 25. Typical Load-Elongation Behavior of Holocellulose Fibers Dried at Various Negative Strain Levels

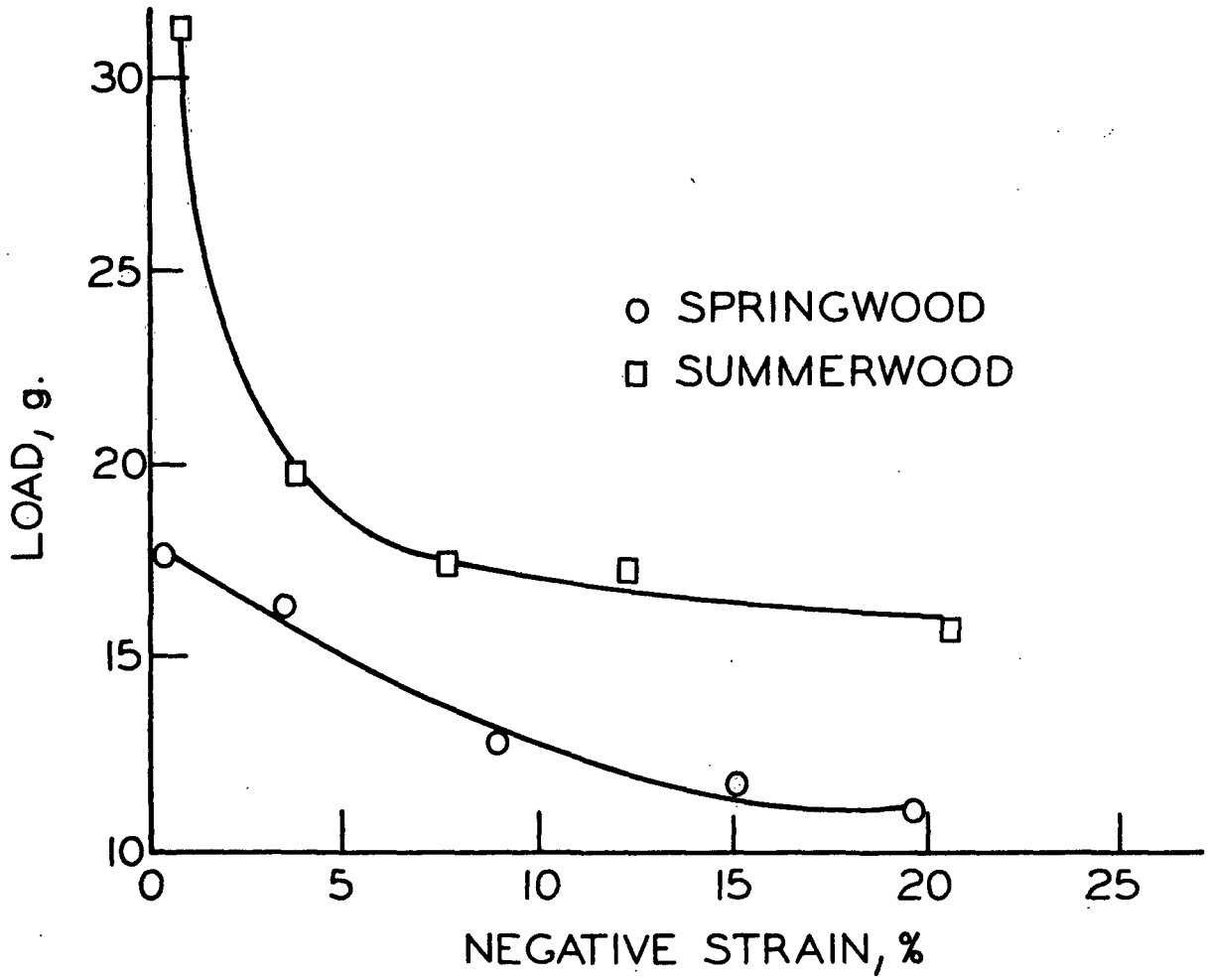

Figure 26. Effects of Longitudinal Compression During Drying on the Breaking Load of Holocellulose Fibers

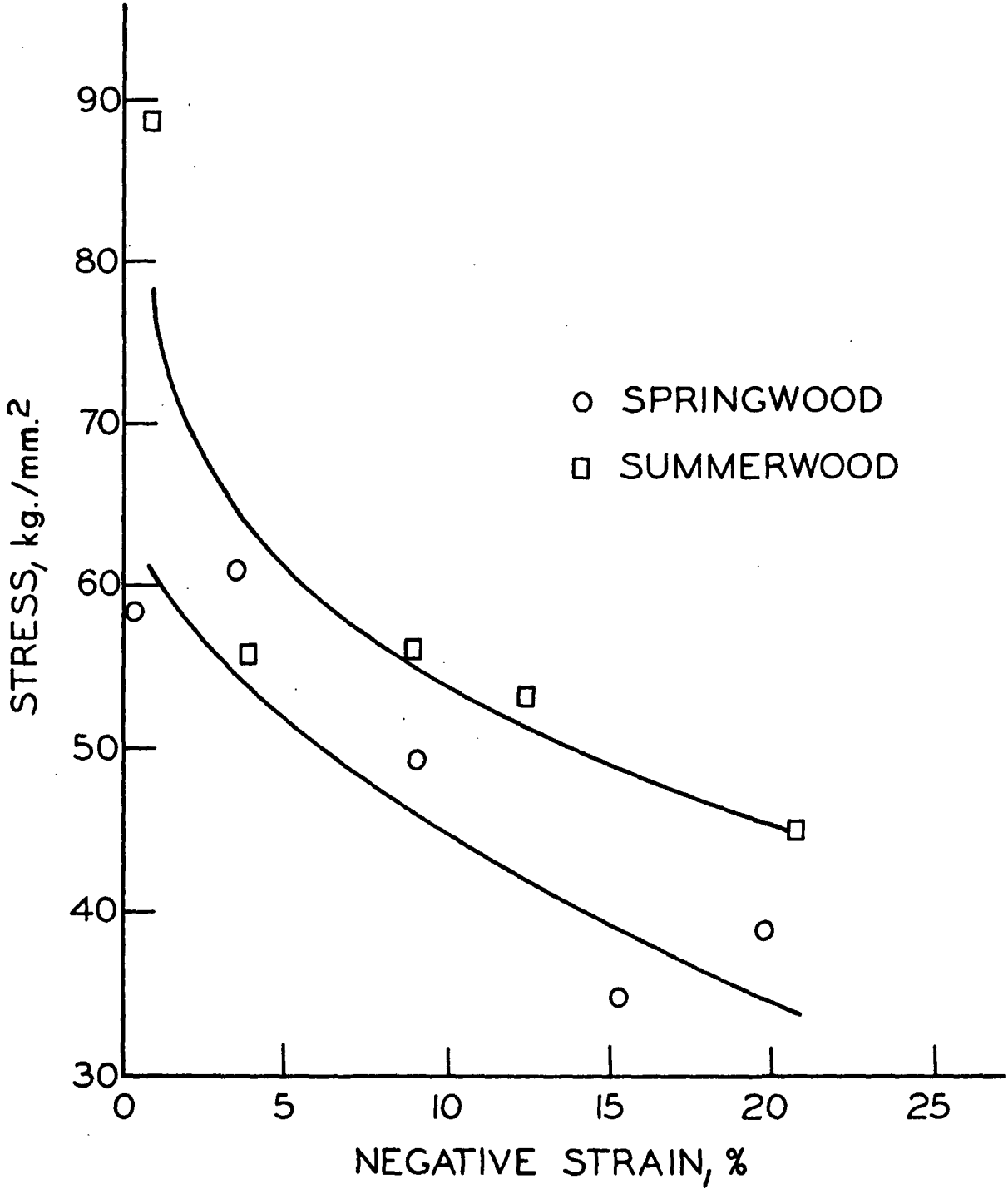

Figure 27. Effect of Longitudinal Compression During Drying on the Tensile Strength of Holocellulose Fibers

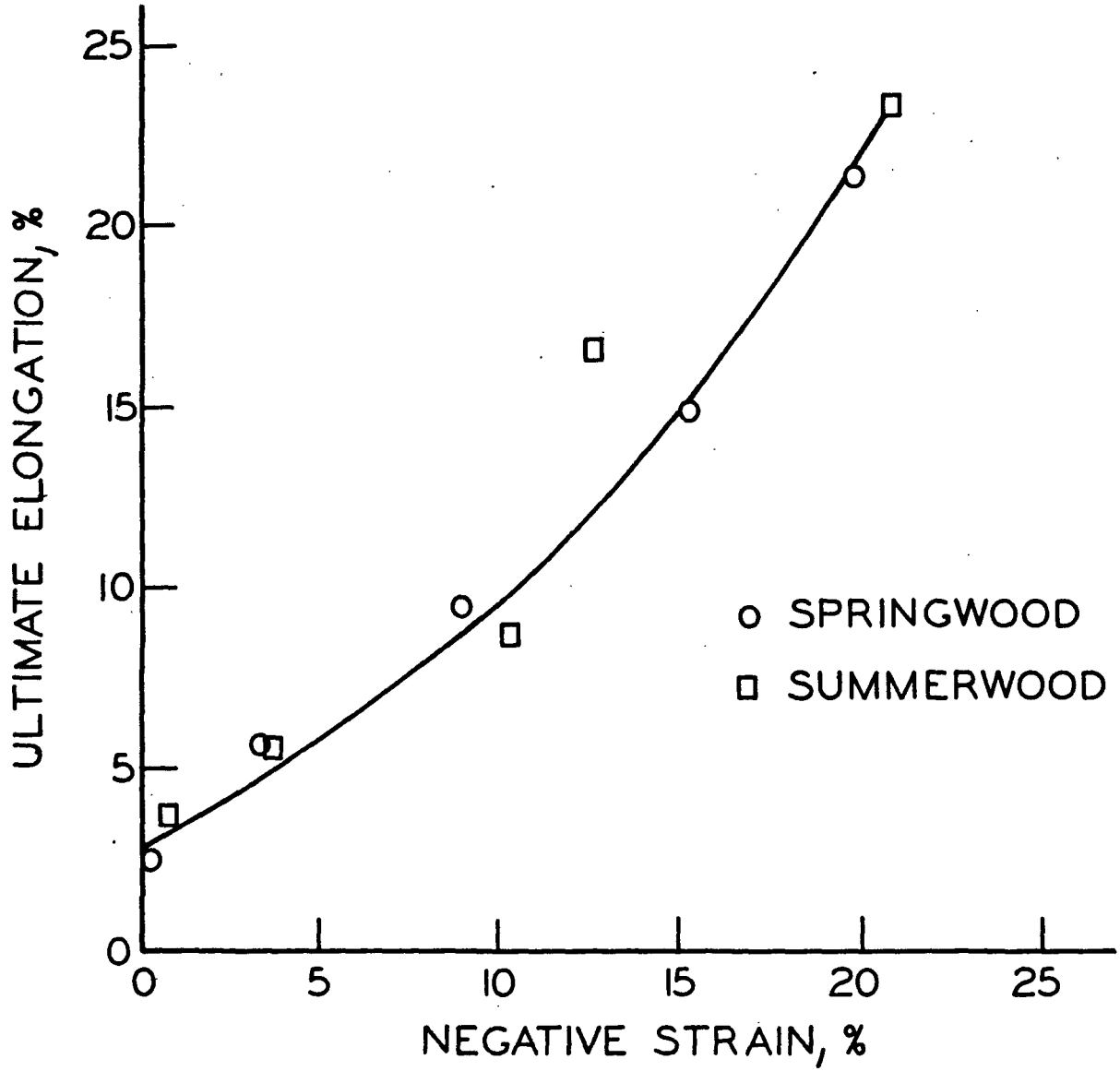

Figure 28. Effect of Longitudinal Compression During Drying on the Ultimate Elongation of Holocellulose Fibers

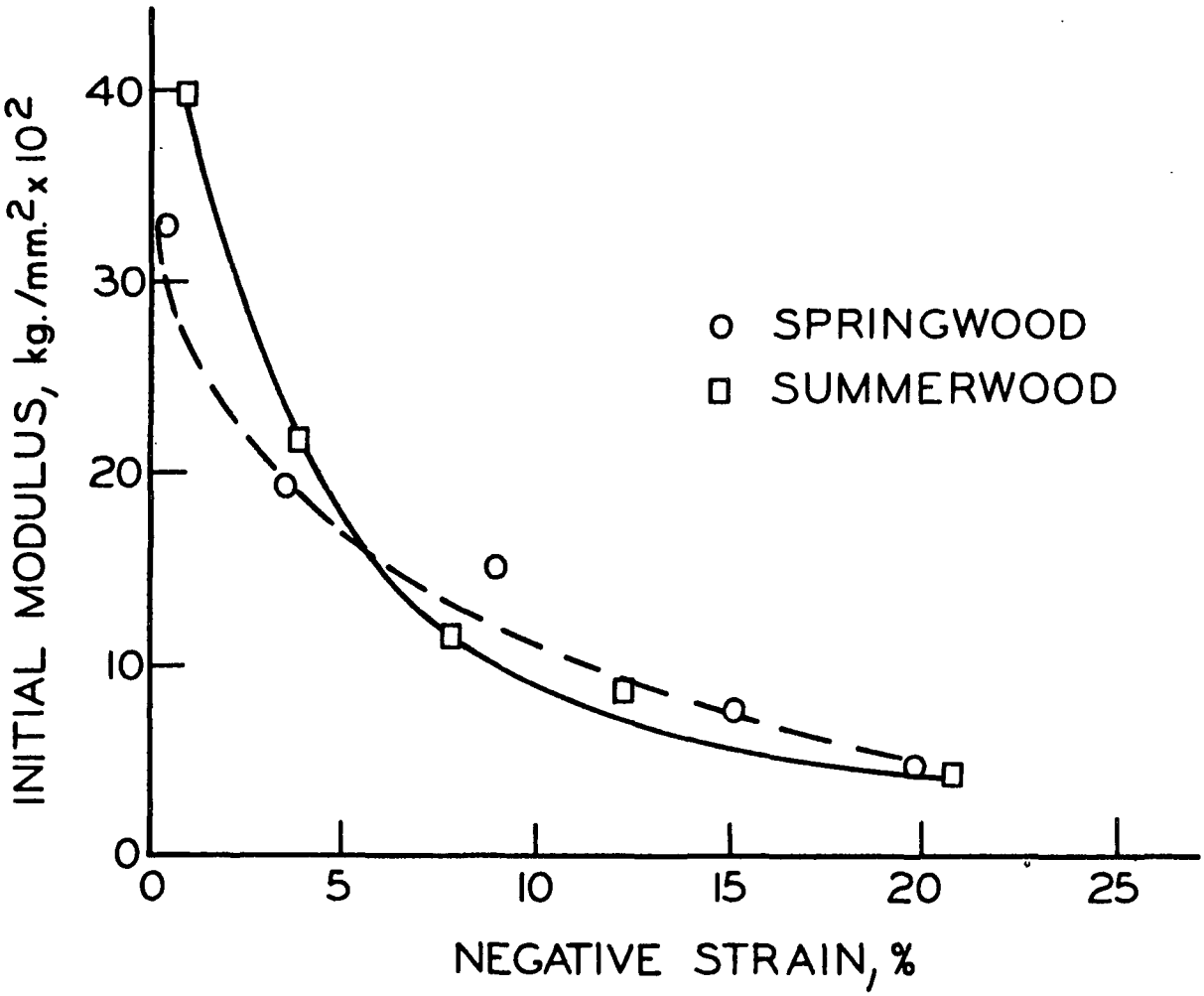

Figure 29. Effect of Longitudinal Compression During Drying on the Initial Modulus of Holocellulose Fibers

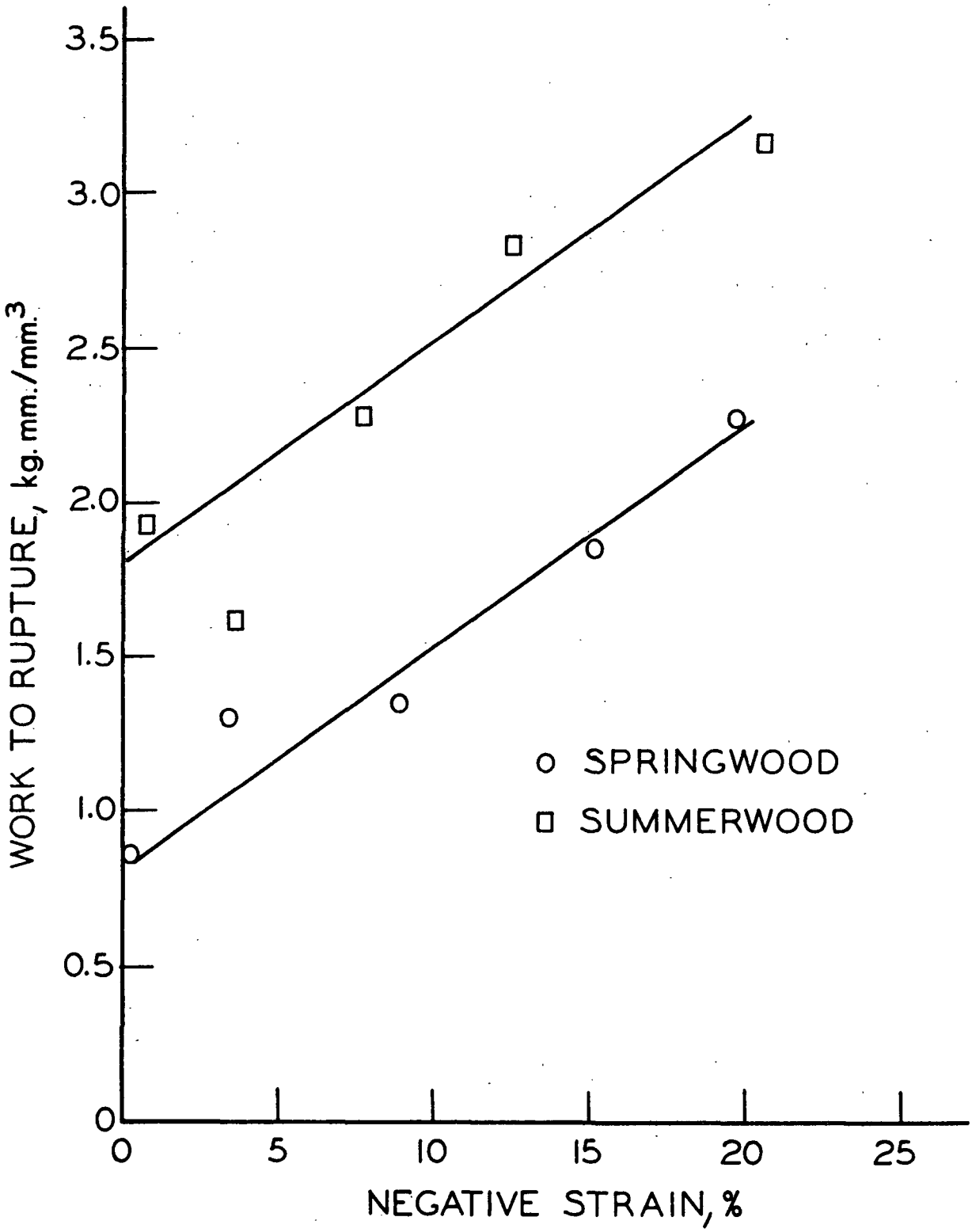

Figure 30. Effect of Longitudinal Compression During Drying on the Work-to-Rupture Holocellulose Fibers

Both load-to-break and tensile strength were plotted (Fig. 26 and 27) to demonstrate the additional variation which the use of cross-sectional area introduces. Breaking load is seen to decrease as the level of applied negative strain is increased for both summerwood and springwood. There were significant differences between the 0, 10, and 20% levels in all cases. Breaking stress also shows significant decreases for the 0, 10, and 20% negative strain levels, but the introduction of cross-sectional area, which is used in calculating stress, causes additional scatter in the data, as seen in Fig. 27. It was considered possible that the Compacted Fiber Dimension Apparatus (CFDA) might be sensitive to irregularities caused in the fiber structure by longitudinal compression. As a result, the compacted density might have been different in each case. No trend is observed in the cross-sectional area data of Tables IV and V to suggest this, but some densities were determined to indicate possible errors in determining compacted cross section. The results are presented in Table VI. Due to the larger standard error observed for the 20% sample, the difference between these fibers and those from the 0% level is not significant at the 95% level. Yet the trend does seem to be toward lower densities for the longitudinally compressed fibers. The fibers dried on teflon had even lower densities as tested on the CFDA and were significantly different from the fibers dried in the experimental apparatus under 0% longitudinal compression. The teflon-dried fibers might also be expected to be irregular because no uniform force was applied to hold them in place during drying. It therefore seems likely that the variations in fiber density which occur on the CFDA can cause errors in the determination of the quantity of material present in the fiber cross section. Because the CFDA measures only the cross-sectional dimensions, two fibers may have the same cross-sectional area but have different mass per unit length values if they are measured at the different densities observed.

TABLE VI

COMPARISON OF COMPACTED DENSITIES OF SPRINGWOOD FIBERS AS TESTED ON THE CFDA

	0% Neg. Strain	20% Neg. Strain	Teflon Dried[a]
Av. x-sec. area, μm.^{2}	331	373	315
standard error	12	8	13
Av. weight, μg.	2.72	2.38	2.23
standard error	0.14	0.13	0.11
Av. density, g./cm.^{3}	1.54	1.46	1.40
standard error	0.02	0.06	0.02
No. of fibers tested	11	12	13

[a]Dried without lateral compression in contact with a teflon surface.

Ultimate elongation increased regularly with increases in negative strain level (Fig. 28). Even when no longitudinal compression was applied, a certain strain was required to rupture the fibers. The values obtained for the 0% level fibers were similar to those obtained by Jentzen (82) for fibers dried under no load. Intuitively, one would then expect the strain required to rupture the fiber to increase linearly with increases in the compressive strain dried in. The plot of Fig. 28 is not quite linear, however, indicating that not quite all of the negative strain applied to the fiber is recovered during the tensile test.

Changes in initial modulus were significant at all levels (Fig. 29). Large decreases in initial modulus were observed for even small negative strains, but the modulus continued to decrease with each increase in negative strain level. Thus, the fiber stiffness can be altered decisively by the application of a longitudinal compressive strain to the wet fiber. Samuelsson (59) found

similar changes in the flexural rigidity of fibers in which structural damage had been observed.

The changes in all the properties described above were those expected on the basis of an analogy which assumed that the effects of compression drying would be the opposite of those of drying under tensile loads. However, in the case of work-to-rupture changes, this was not the case. Jentzen (82) found that drying fibers under tensile loads caused an increase in work-to-rupture values. Longitudinal compression during drying was also found to significantly increase the work-to-rupture values (Fig. 30). Apparently, either type of work input increases the ability of the fibers to absorb energy during tensile testing. However, the changes by which this increase in energy absorption ability occur are different in the two cases. Fibers dried under tensile load show increased work-to-rupture values because the fibers have higher tensile strengths which increase the area under the load-elongation curve. Fibers dried under compression have higher rupture energies because of a large increase in ultimate elongation, even though the tensile strength decreased.

Because the data in Tables IV and V are based on fibers from a single growth ring of springwood and another of summerwood, it was desirable to test other samples to make certain that the effects observed were not caused by a possibly anomalous behavior of a single growth ring. Several chips from the summerwood cook were combined to make up a fiber sample for additional testing. The results of this testing are presented in Table VII. Examination of these results shows that the effect of longitudinal compression was about the same as in the first group. A 56% decrease in tensile strength was observed; even larger than for the first fiber sample. The other mechanical properties change as well, though the work-to-rupture value did not increase as much as previously.

TABLE VII

MECHANICAL PROPERTIES OF HOLOCELLULOSE SUMMERWOOD FIBERS OBTAINED FROM SEVERAL GROWTH RINGS AND DRIED UNDER VARIOUS NEGATIVE STRAINS

		Applied Negative Strain		
		0%	10%	20%
Actual negative strain, %	Av.	1.46	9.17	18.80
	S.E.	0.27	0.15	0.32
Breaking load, g.	Av.	47.1	24.2	20.4
	S.E.	2.7	1.2	1.0
Cross-sectional area, $\mu m.^2$	Av.	416	416	422
	S.E.	13	12	12
Tensile strength, $kg./mm.^2$	Av.	109	56	48
	S.E.	4.2	1.7	1.7
Initial modulus, $kg./mm.^2$	Av.	4130	1320	380
	S.E.	152	54	17
Ultimate elongation, %	Av.	4.0	8.1	20.1
	S.E.	0.15	0.24	0.37
Work-to-rupture, $kg.\ mm./mm.^3$	Av.	2.16	1.93	3.04
	S.E.	0.08	0.07	0.09
No. of fibers tested		77	75	77

Span = 1 mm.
Loading rate = 1.4 g./sec.
CSA determined after tensile test.

Similar testing was carried out on the kraft fibers. The kraft pulp consisted of a mixture of spring- and summerwood, but only summerwood fibers were selected for testing. There was no difficulty in making this selection because there are very obvious difference in the appearances of the two fiber types. In order to insure random samples, all the fibers to be tested were selected at one time and then arbitrarily divided into three identical groups. The results of the testing are presented in Table VIII. Again, the changes were all significant, and of the same order as those observed for the holocellulose

fibers. Note, however, that the initial modulus, though quite high for the uncompressed fibers, plunges dramatically for all the kraft fibers dried under longitudinal compression. The explanation is that the load-elongation curves were somewhat different in this case. Instead of showing an initial straight-line portion of relatively high modulus, as in Fig. 25, the curves for these fibers began the rapid elongation behavior almost immediately when the tensile test was begun. As a result, the initial moduli observed for such fibers were much lower. With the addition of these results for kraft fibers, conclusions regarding the effects of longitudinal compression on pulp fibers in general are much better founded.

TABLE VIII

MECHANICAL PROPERTIES OF KRAFT SUMMERWOOD FIBERS
DRIED UNDER VARIOUS NEGATIVE STRAINS

		Applied Negative Strain		
		0%	10%	20%
Actual Negative strain, %	Av.	0.38	8.51	17.71
	S.E.	0.34	0.40	0.43
Breaking load, g.	Av.	57.5	37.9	31.5
	S.E.	2.4	1.4	0.9
Cross-sectional area, $\mu m.^2$	Av.	370	390	380
	S.E.	9	11	8
Tensile strength, $kg./mm.^2$	Av.	155	98	83
	S.E.	5.6	3.0	11.9
Initial modulus, $kg./mm.^2$	Av.	4500	177	64
	S.E.	136	13	1.9
Ultimate elongation, %	Av.	4.2	12.9	25.9
	S.E.	0.1	0.3	0.5
Work-to-rupture, $kg.\ mm./mm.^3$	Av.	3.46	3.60	5.12
	S.E.	0.19	0.17	0.21
No. of fibers tested		55	50	49

Span = 1 mm.; Loading rate = 2.0 g./sec.; CSA determined after tensile test.

The apparent plastic behavior of the fibers, based on their load-elongation curves led to an additional investigation. In order to determine the recoverability of the large tensile strains observed, load-unload cycles were run. Because of the great differences in the ability of the fibers treated at different levels of applied negative strain to elongate, they could not be directly compared by straining each type to the same level and then unloading. Instead, different tensile strain cycling levels were used for fibers from each negative strain level in order to examine the recoverability of each type of fiber over its whole range of elongations. Load-unload cycles are illustrated for the 0 and 10% negative strain levels in Fig. 31. The results of the load-unload cycling for three levels of applied negative strain are tabulated in Table IX.

Fibers dried under negative strain are seen to be very inelastic from the results shown in Fig. 31 and Table IX.

Jentzen (82) considered the shape of the load-elongation curves to be governed by two competing mechanisms: (1) secondary creep effects tending to make the curve concave toward the strain axis, and (2) redistribution of stress within the fiber (i.e., stiffening) tending to make the curve concave toward the stress axis. This type of interpretation is admirably suited to explaining the load-elongation curves observed in Fig. 25 in terms of the results obtained by load-unload cycling.

Two results from the load-unload experiments are pertinent. First, large increases in initial modulus are observed for each successive cycle of the fibers dried under longitudinal compression. Thus, the fibers become stiffer with increasing loads, indicating a redistribution of stress (i.e., a strain

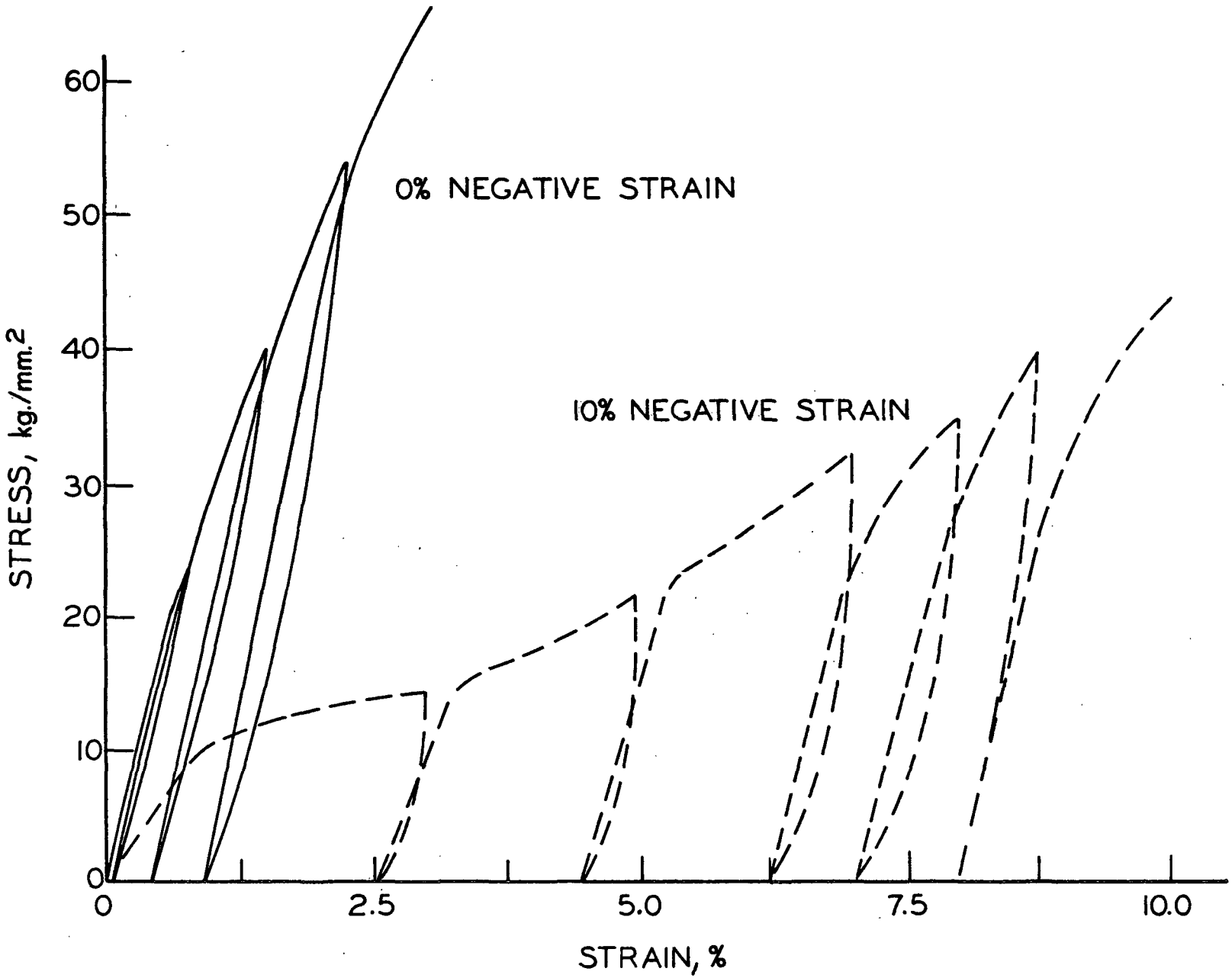

Figure 31. Load-Unload Cycles for Summerwood Fibers Dried with and Without Longitudinal Compression

TABLE IX

RESULTS OF LOAD-UNLOAD CYCLING OF HOLOCELLULOSE SUMMERWOOD FIBERS DRIED UNDER VARIOUS NEGATIVE STRAINS

Applied Negative Strain, %			Cycle Number 1	2	3	4	5	6
0	Strain reached during cycle, %		0.75	1.50	2.25	3.00	--	--
	Nonrecoverable deformation after cycle, %	Av.	0.07	0.41	0.84	1.34	--	--
		S.E.	0.00	0.01	0.02	0.03	--	--
	Initial modulus at start of cycle, kg./mm.^{2}	Av.	3380	3560	3720	3940	4040	--
		S.E.	90	100	110	100	110	--
10	Strain reached during cycle, %		3.00	5.00	7.00	8.00	9.00	--
	Nonrecoverable deformation after cycle, %	Av.	2.61	4.48	6.23	7.05	8.01	--
		S.E.	0.02	0.03	0.03	0.19	0.06	--
	Initial modulus at start of cycle, kg./mm.^{2}	Av.	1140	1970	2590	3090	3160	3285
		S.E.	40	60	90	110	140	150
20	Strain reached during cycle, %		10.00	15.00	20.00	22.50	25.00	--
	Nonrecoverable deformation after cycle, %	Av.	9.03	14.06	18.94	21.22	23.60	--
		S.E.	0.17	0.11	0.13	0.15	0.14	--
	Initial modulus at start of cycle, kg./mm.^{2}	Av.	400	840	1400	2020	2160	2300
		S.E.	10	50	70	90	90	90

No. of fibers tested for each negative strain = 46.
Span = 1 mm.
Loading rate = 0.28 g./sec.

hardening effect). Second, the fibers are very inelastic, indicating the importance of secondary creep effects. With these considerations in mind, the shape of the load-elongation curves for fibers dried under longitudinal compression can be readily interpreted. As stress is applied to these fibers, the initial short straight zone can be considered a region where neither the stiffening effect nor the secondary creep effect predominates, but instead they seem to balance one another. However, at a rather low stress level, the secondary creep takes over and causes the rapid extension region of the curve. When secondary creep predominates, the curve is bent toward the strain axis. As elongation proceeds, the stiffening mechanism overshadowed at first begins to assert an influence. The result is a gradual bending back toward the stress axis, which gives the final portion of the curve a concave upward appearance. The result of the variation in the influence exerted by these two mechanisms is the sigmoidal curve observed.

One of the characteristics of viscoelastic materials is that the recovery (the ratio of the elongation recovered to the total elongation on loading) for that cycle decreases as the maximum load applied during a load-unload cycle increases (76). An examination of Fig. 31 shows that this is not the case for fibers which have been dried under longitudinal compression. Indeed, due to the initial predominance of secondary creep, the elastic recovery increases as higher loads are reached. Presumably, a series of load-unload cycles at small increments of increasing load near the breaking point would show a reversal in this trend.

The increase in initial modulus for successive cycles is characteristic of natural fibers (76). It is important to note that the effect was observed for the fibers which had not been negatively strained as well as for

the ones which had. This is of some importance since Jentzen (82) observed that fibers dried under load did not show this behavior. Because fibers which were dried under negative strain were still held by the rubber mats during drying, there was some fear that the effect on them might be the same as drying under load. However, these fibers exhibited behavior typical of those dried under no load. Also, the tensile strengths observed by Jentzen (82) for fibers dried under no load were identical with those observed in this study for unstrained fibers, even though Jentzen used a different method for determining cross-sectional area.

The permanence of the mechanical effects observed is also of considerable importance to practical application of the findings of this study. If by rewetting a fiber which has been dried under longitudinal compression the mechanical property changes can all be recovered, then the only longitudinal compressive forces having significant effects on ultimate use properties of fibers would be those occurring during sheet drying. An experiment was carried out to ascertain the permanence of these effects.

Groups of holocellulose springwood and summerwood fibers were dried at three levels of longitudinal compressive strain in the usual way. The actual negative strain was also measured for these treatments. The fibers were then individually immersed in distilled water. Because the dried fibers tended to float on the surface of the water, they had to be dragged under by pulling on their ends with jeweler's forceps. After two days immersion, the fibers were dried again in the experimental apparatus, but without the application of longitudinal compressive strains. Their lengths were then checked again to determine the total negative strain. The results of these determinations of actual negative strain are listed in Table X.

TABLE X

ACTUAL NEGATIVE STRAINS OF HOLOCELLULOSE FIBERS AFTER LONGITUDINAL COMPRESSION AND AFTER REWETTING AND REDRYING

Applied Neg. Strain, %	No. of Fibers Tested		Actual Negative Strain, %[a] After Compression	Rewet & Redried
		Springwood		
0.0	49	Av.	-0.8[b]	-1.2[b]
		S.E.	0.22	0.24
10.0	46	Av.	8.0	4.3
		S.E.	0.23	0.17
20.0	49	Av.	14.9	7.5
		S.E.	0.39	0.42
		Summerwood		
0.0	49	Av.	0.5	0.3
		S.E.	0.14	0.14
10.0	49	Av.	6.3	5.2
		S.E.	0.54	0.36
20.0	49	Av.	16.4	10.7
		S.E.	1.15	1.35

[a]All percentages based on original wet fiber length.

[b]Negative value indicates average length increased during drying.

Load-elongation properties were determined for the rewet and redried fibers in the usual way. The curve shapes of the fibers dried under longitudinal compression still exhibited the characteristic sigmoidal shape. However, the average mechanical properties were altered by rewetting as shown in Tables XI and XII.

The effect of rewetting is considerably more severe in spring- than in summerwood fibers. When the changes observed in Table XI are compared with those in Table IV, it can be seen that the rewetting causes nearly a total loss of the ultimate elongation increases imparted by longitudinal compression.

TABLE XI

MECHANICAL PROPERTIES OF SPRINGWOOD FIBERS DRIED UNDER VARIOUS NEGATIVE STRAINS FOLLOWED BY REWETTING AND REDRYING UNDER 0% NEGATIVE STRAIN

		Applied Negative Strain		
		0%	10%	20%
Cross-sectional area, $\mu m.^2$	Av.	304	329	323
	S.E.	7.1	7.2	9.0
Breaking load, g.	Av.	22.8	13.0	13.0
	S.E.	0.7	0.5	0.4
	Change, %	0.0	-43.0	-43.0
Tensile strength, $kg./mm.^2$	Av.	75.8	39.7	40.8
	S.E.	2.0	1.4	1.1
	Change, %	0.0	-49.1	-46.2
Ultimate elongation, %	Av.	3.3	3.7	5.7
	S.E.	0.1	0.2	0.2
Initial modulus, $kg./mm.^2$	Av.	3370	2110	1360
	S.E.	73	56	47
	Change, %	0.0	-37.4	-59.6
Work-to-rupture, $kg.mm./mm.^3$	Av.	1.44	0.82	1.18
	S.E.	0.05	0.04	0.04
	Change, %	0.0	-43.0	-18.0
Length, mm.	Av.	5.50	5.53	5.46
	S.E.	0.07	0.07	0.07
No. of fibers tested		49	46	49

Span = 1 mm.
Loading rate = 1.4 g./sec.
CSA determined after load-elongation testing.

TABLE XII

MECHANICAL PROPERTIES OF SUMMERWOOD FIBERS DRIED UNDER VARIOUS NEGATIVE STRAINS FOLLOWED BY REWETTING AND REDRYING UNDER 0% NEGATIVE STRAIN

		Applied Negative Strain		
		0%	10%	20%
Cross-sectional area, $\mu m.^2$	Av.	363	346	356
	S.E.	7.5	8.8	10.2
Breaking load, g.	Av.	31.6	18.9	18.0
	S.E.	1.3	0.8	0.6
	Change, %	0.0	-40.2	-43.0
Tensile strength, $kg./mm.^2$	Av.	87.2	55.2	51.2
	S.E.	2.9	2.2	1.3
	Change, %	0.0	-36.7	-41.4
Ultimate elongation, %	Av.	4.3	5.3	14.4
	S.E.	0.1	0.2	0.2
Initial modulus, $kg./mm.^2$	Av.	3600	2190	1010
	S.E.	108	107	39
	Change, %	0.0	-39.1	+72.0
Work-to-rupture, $kg.\ mm./mm.^3$	Av.	2.15	1.47	3.25
	S.E.	0.09	0.07	0.09
	Change, %	0.0	-31.5	+51.1
Length, mm.	Av.	5.58	5.61	5.40
	S.E.	0.06	0.06	0.08
No. of fibers tested		49	49	49

Span = 1 mm.
Loading rate = 1.4 g./sec.
CSA determined after load-elongation testing.

Likewise, the work-to-rupture values were even lower for the rewet fibers than they were for the original uncompressed fibers. Initial modulus recovered about half of the loss caused by compression drying. However, the tensile strength did not recover at all. The effects were similar, though not as pronounced, in summerwood, as seen by comparing Table XII with Table V. Ultimate elongations decreased a few percent and initial modulus increased somewhat due to rewetting. Rewetting likewise caused a small decrease in the rupture energy. However, tensile strength remained nearly unchanged, just as in the springwood fibers. Thus, the result of rewetting seems to be a loss in the desirable properties imparted by longitudinal compression, with no parallel improvement in the fiber strengths which are so drastically reduced by compressive straining.

X-RAY DIFFRACTION STUDY

CRYSTALLINITY

Relative crystallinities were determined by the several methods previously described. Results are listed in Table XIII for 0 and 20% negative strain levels of both spring- and summerwood fibers.

In the case of the springwood fibers, all four methods of determining crystallinity were in agreement that no significant change occurred. The results for the summerwood fibers were not so clear cut. The crystallinity index (CrI of Segal, et al.) indicates a significant decrease in the relative crystallinity of the longitudinally compressed fibers. The width at half-height measurement indicates a probable decrease in crystallite order or size, but the differences are small enough to be barely significant at the 95% confidence level. The relative order planimetric method of Hermans and Weidinger also indicates a definite decrease in crystallinity. The planimetric

crystallinity index of Jayme and Knolle, on the other hand, shows an increase in crystallinity for the fibers dried under compression. It must be mentioned that this last method is sensitive to the selection of the base line on the intensity trace. Since this was sometimes rather ill-defined, the last method listed should probably be given less credibility than the others.

TABLE XIII

CRYSTALLINITY OF HOLOCELLULOSE FIBERS

Applied Negative Strain		Springwood 0%	Springwood 20%	Summerwood 0%	Summerwood 20%
Crystallinity index CrI[a]	Av.	46.6	47.0	60.3	55.7
	S.E.	1.2	0.7	1.6	1.0
Width at half height[b]	Av.	3.92°	3.90°	3.37°	3.49°
	S.E.	0.11	0.08	0.05	0.06
Relative order[c]	Av.	27.5	28.1	41.4	32.3
	S.E.	0.9	1.0	1.1	1.3
Crystallinity index KI[d]	Av.	67.1	65.9	69.0	74.5
	S.E.	1.5	1.3	1.3	0.9
No. of diffraction patterns[e]		10	10	10	10

[a]Method of Segal, et al. (95).
[b]Method of Gjonnes, et al. (97).
[c]Method of Hermans and Weidinger (91-93).
[d]Method of Jayme and Knolle (94).
[e]Each pattern represents 20 fibers.

A decrease in relative order due to longitudinal compression is not inconceivable, yet some doubt must be cast on the significance of the changes observed in the summerwood fibers. Hermans and Weidinger (91) demonstrated in a carefully designed experiment that, for nonrandomly oriented specimens, the crystallinity was directly related to the degree of orientation of the sample.

In the next section it will be shown that there was a large decrease in the orientation of the summerwood fiber crystallites due to longitudinal compression. This means that the crystalline lattice diffraction from the 002 planes is spread over a wider arc than before. Because the crystallinity measurements only used intensities along the equator, a decrease in the amount of crystalline diffraction at the equator can be detected and interpreted incorrectly as a change in crystallinity.

ORIENTATION

Two methods were used to determine the crystallite orientation. These are presented in Table XIV together with two quantities to indicate relative proportions of well-oriented and randomly oriented crystallites. The average crystallite orientations were changed significantly by drying fibers under longitudinal compression. Summerwood fibers showed significant decreases in orientation for each increase in the negative strain level. The springwood fibers behaved somewhat differently in that most of the change occurred when the negative strain was increased from 0 to 10%. Between 10 and 20%, the orientation decreased very little.

Some interesting observations during the diffraction study gave rise to the last two quantities listed in Table XIV. These are best explained by means of a comparison of the diffraction patterns obtained from fibers to which different longitudinal compressive strains had been applied. These patterns are shown in Fig. 32-35. The 002 and 101-10$\bar{1}$ diffraction maxima are readily distinguished. The additional dark narrow bands were caused by particles of talc which were originally on the surface of the rubber blankets and became stuck to the fibers during drying. These bands did not impede

the scanning of the patterns but, in fact, were helpful in centering for accurate circumferential traces. Note that these bands are somewhat oriented in the fibers which had not been longitudinally compressed. This is because the talc consists of flat platelets which become oriented so that their planar surfaces are parallel to the fiber surface.

TABLE XIV

CRYSTALLITE ORIENTATION OF HOLOCELLULOSE FIBERS

Applied Negative Strain		Springwood			Summerwood		
		0%	10%	20%	0%	10%	20%
W, degrees[a]	Av.	22.8	25.2	25.3	14.8	17.8	22.0
	S.E.	0.58	0.50	0.51	0.63	0.50	1.23
T, degrees[b]	Av.	36.0	39.6	41.0	26.9	31.8	38.5
	S.E.	0.54	0.49	0.54	0.95	0.66	1.27
I_{max}/I_{min}[c]	Av.	2.14	1.83	1.76	4.32	3.44	2.65
	S.E.	0.05	0.02	0.06	0.19	0.11	0.09
$A_{oriented}/A_{total}$[d]	Av.	0.230	0.197	0.181	0.359	0.349	0.291
	S.E.	0.009	0.004	0.010	0.012	0.007	0.010
No. of patterns[e]		10	10	10	10	10	10

[a] Half width at 50% of maximum 002 intensity relative to base line.

[b] Method of Meylan (103).

[c] Ratio of maximum to minimum intensity observed during circumferential scan of 002 diffraction maxima.

[d] $A_{oriented}$ = area between 002 intensity trace and the base line.
A_{total} = area between 002 intensity trace and the zero intensity line.

[e] Each pattern represents 20 fibers.

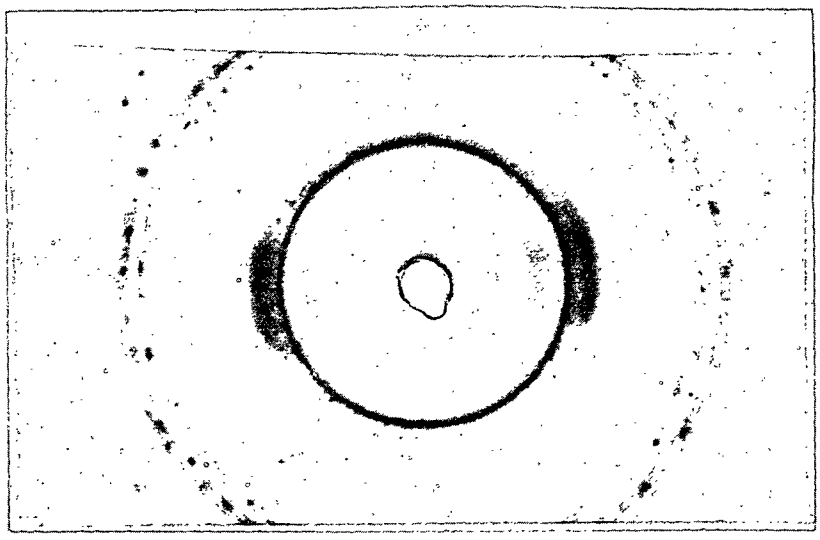

Figure 32. Laue X-ray Diffraction Pattern from 20 Holocellulose Springwood Fibers Dried Under 0% Negative Strain

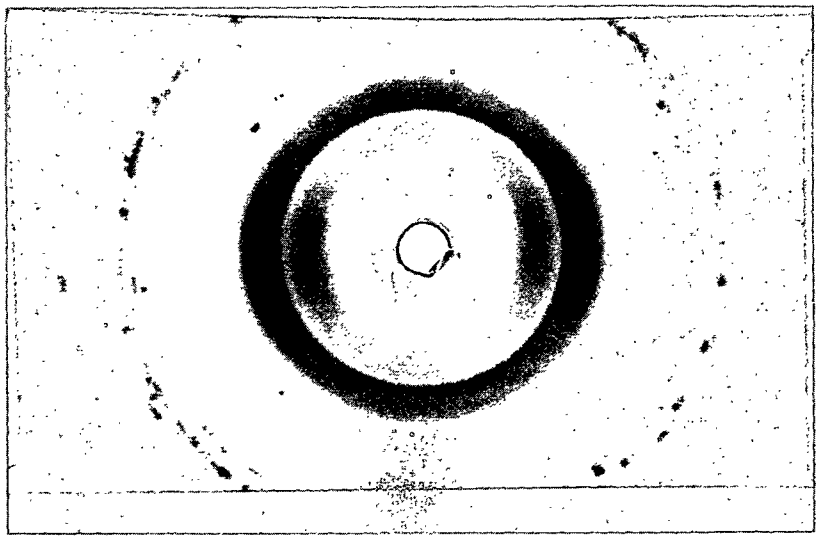

Figure 33. Laue X-ray Diffraction Pattern from 20 Holocellulose Springwood Fibers Dried Under 20% Negative Strain

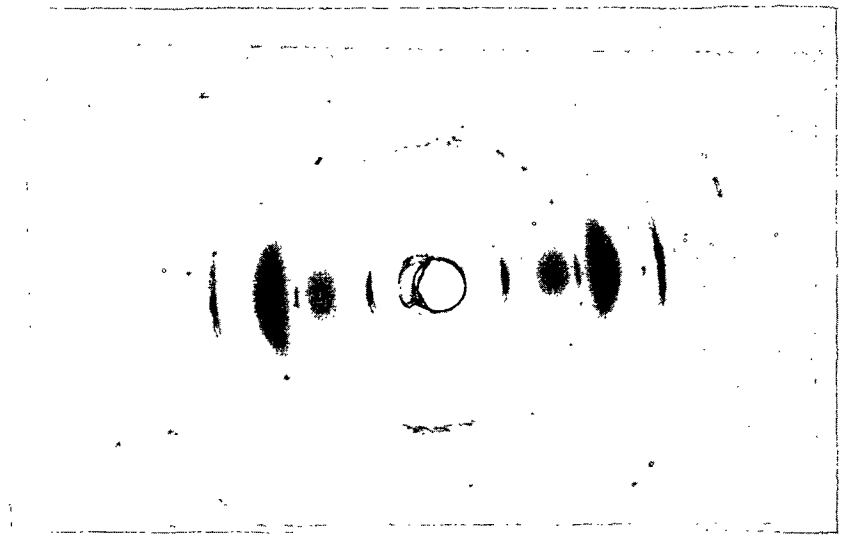

Figure 34. Laue X-ray Diffraction Pattern from 20 Holocellulose Summerwood Fibers Dried Under 0% Negative Strain

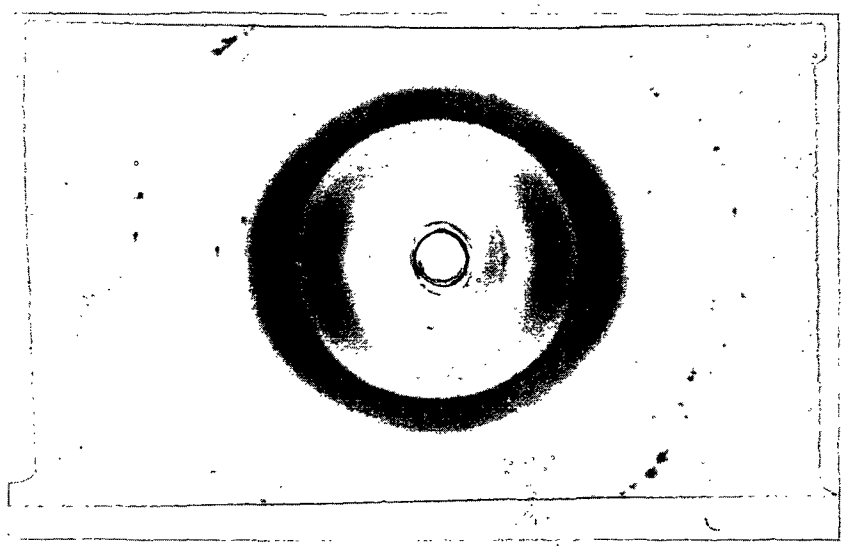

Figure 35. Laue X-ray Diffraction Pattern from 20 Holocellulose Summerwood Fibers Dried Under 20% Negative Strain

Differences are immediately apparent between the patterns corresponding to the 0% negative strain (Fig. 32 and 34) and those of 20% negative strain (Fig. 33 and 35). The summerwood can also be seen by comparison of Fig. 32 and 34 to be considerably better oriented in the unstrained state than are similar springwood fibers. Keeping in mind the fact that the darkening of the film around the 002 circle is proportional to the number of crystallites oriented at that particular angle, the observed differences can be interpreted in the following way. Longitudinal compression results in a redistribution of the crystallites of the fiber in two different ways. Many of the crystallites which originally showed preferential distribution relative to the fiber axes are randomly disoriented, causing a uniform increase in the diffraction intensity all around the ring. If this were the only change occurring, the resulting pattern would still have a rather sharp spot, as in Fig. 32 and 34, superimposed on a uniform diffraction ring. In addition, however, the crystallites which remained preferentially ordered around the fiber axes are oriented at angles considerably greater than before. The result is a wider intensity distribution from preferentially oriented crystallites superimposed on a uniform circumferential intensity distribution due to randomly oriented crystallites. The last two quantities listed in Table XIV are an attempt to quantify these observations. The differences in the circumferential traces of the 002 lattice diffractions are illustrated in Fig. 36. Although the increased intensity of the entire circumferential trace of the 002 ring could have been caused by an increase in amorphous material, this was considered unlikely for two reasons: (1) the increases were observed for springwood fibers even though there was no crystallinity change, and (2) the radial width of the ring at 90° from the equator was narrow, indicating that the diffraction was due to crystalline material.

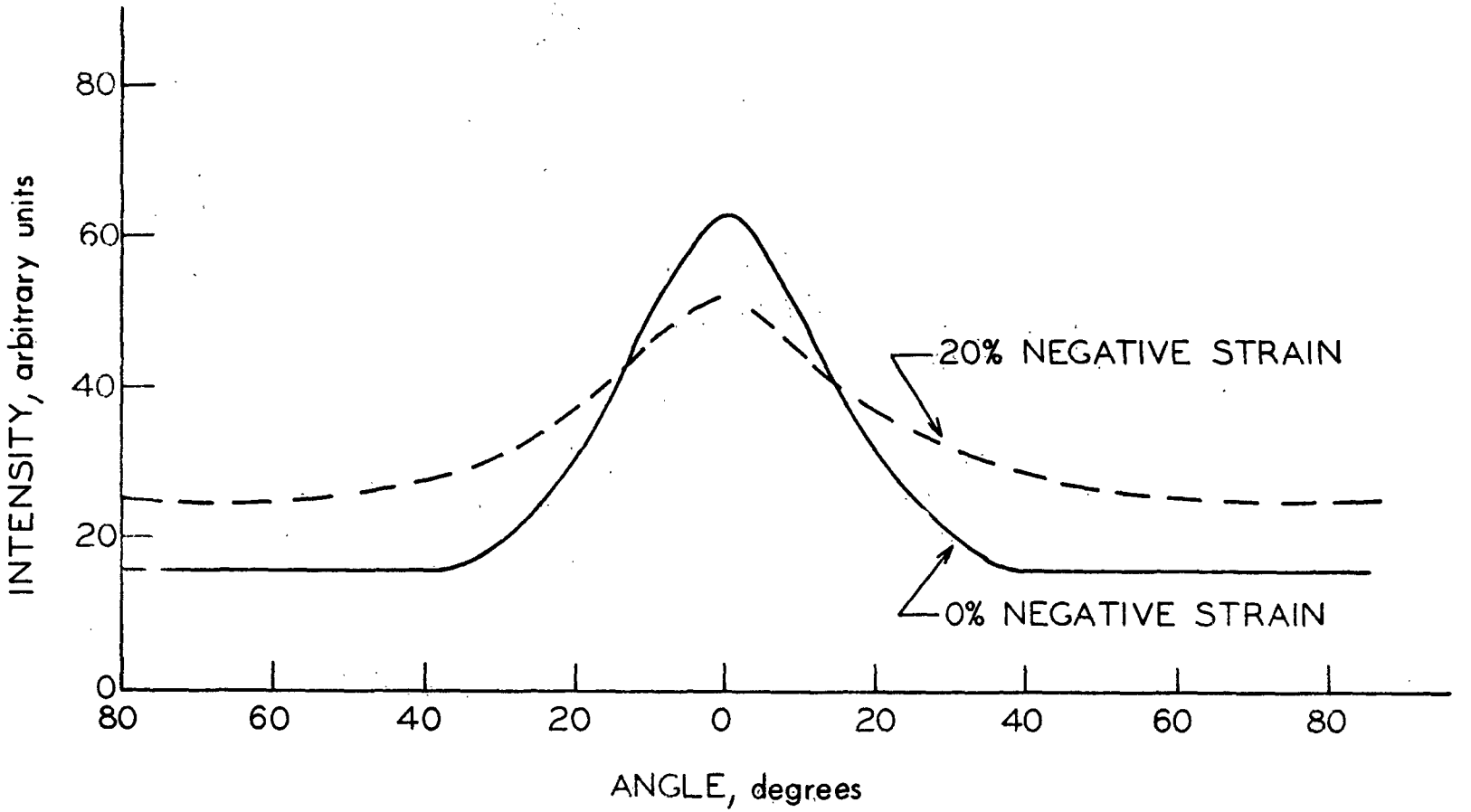

Figure 36. Circumferential Intensity Trace of 002 Diffraction Maximum from Holocellulose Summerwood Fibers

The first of these calculated values (i.e., I_{max}/I_{min}) is simply a comparison between the maximum intensity observed during a circumferential trace (i.e., at 0°) and the minimum intensity (at 90°). This gives an indication of the relative number of crystallites at the originally preferred orientation and the number oriented opposite to it. The second value listed is from a planimetric method which indicates the amount of crystallite diffraction from material preferentially ordered around the fiber axis. This was determined as the area of the intensity curve above the base line defined by the random intensity distribution. The value which is listed is this area divided by the area under the whole curve between the limits of 0-90°.

Examination of Table XIV shows that these attempts to quantify the decrease in preferred orientation do indicate changes. Statistical differences were observed for both spring- and summerwood. The last quantity listed shows some differences between the behavior of springwood and summerwood. In springwood, the largest changes in this value occurred between the 0 and 10% levels. In summerwood, most of the changes occurred between the 10 and 20% levels. The significant differences observed are offered as quantitative evidence in favor of the interpretation outlined above.

It has been shown by Jentzen (82) that the change in fiber length due to drying under load can be related to a uniform change in the helix angle of the fiber structure as measured by the change in orientation. The relationship between lengths and fibril orientations is

$$L/L_1 = \cos \theta / \cos \theta_1$$

where L is the length of the original fiber having a circular helix angle θ, and L_1 is the length of the fiber of helix angle θ_1 after drying under load.

The quantity W in Table XIV is close enough to the helix angle to be used for making this comparison. As the maximum change observed is from 14.8 to 22.0°, this type of analysis can account for only a little over 4% decrease in length. Apparently, the decrease in length of fibers during longitudinal compression is occurring by some mechanism other than a uniform change in helix angle. This conclusion is further strengthened by the microscopic examination of fibers to be discussed in the next section.

MICROSCOPIC EXAMINATION OF FIBERS

LIGHT AND POLARIZED LIGHT PHOTOMICROGRAPHY

Microscopic examination of longitudinally compressed fibers for determination of actual negative strain gave early indications that some type of regularly distributed misalignments was being produced. Photographs of fibers at different levels of applied negative strain are shown in Fig. 37-39. The cross-striations were readily visible for all negatively strained fibers. As the level of negative strain increased, the striations became more prominent. The photographs of Fig. 37-39 were obtained using white light reflected from the surface of the fibers. Very little detail can be obtained from such examination by increasing the magnification. A better microscopic technique for illuminating structural variations was available, however.

Because many workers have shown that polarized light microscopy is admirably suited to bringing out structural discontinuities in cellulosic fibers, the technique was adopted for this study. Many polarized light micrographs were examined and a few examples are presented in Fig. 40-48. In Fig. 40-43, a comparison between negatively strained and unstrained fibers at two levels of magnification is presented. The differences are obvious,

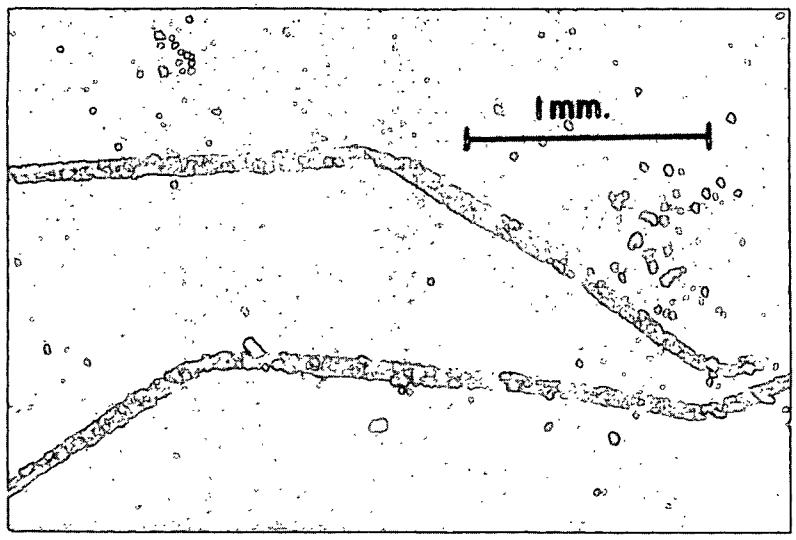

Figure 37. Springwood Fibers Dried Under 0% Negative Strain

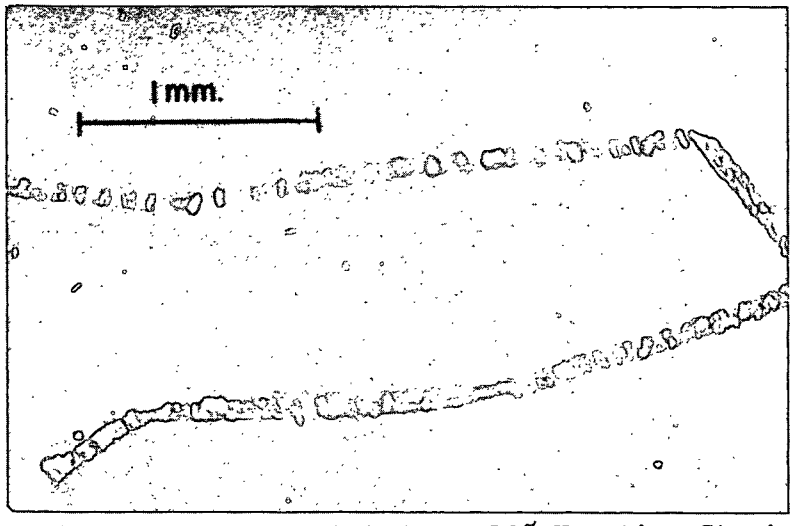

Figure 38. Springwood Fibers Dried Under 10% Negative Strain

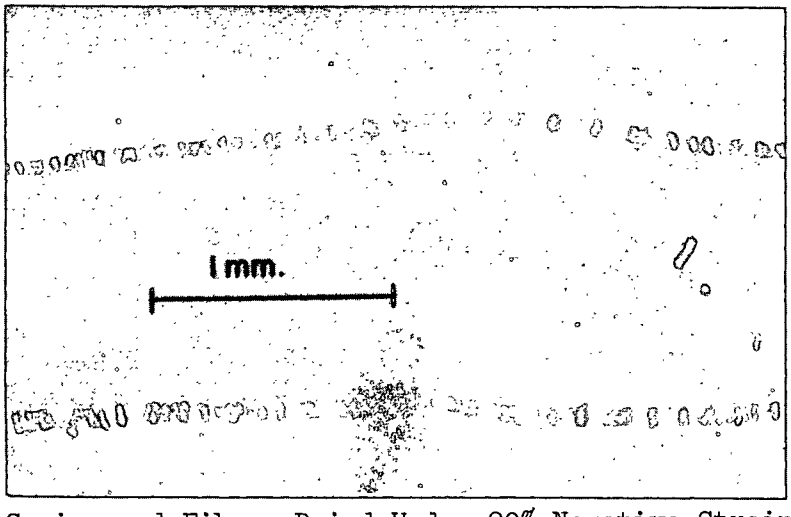

Figure 39. Springwood Fibers Dried Under 20% Negative Strain

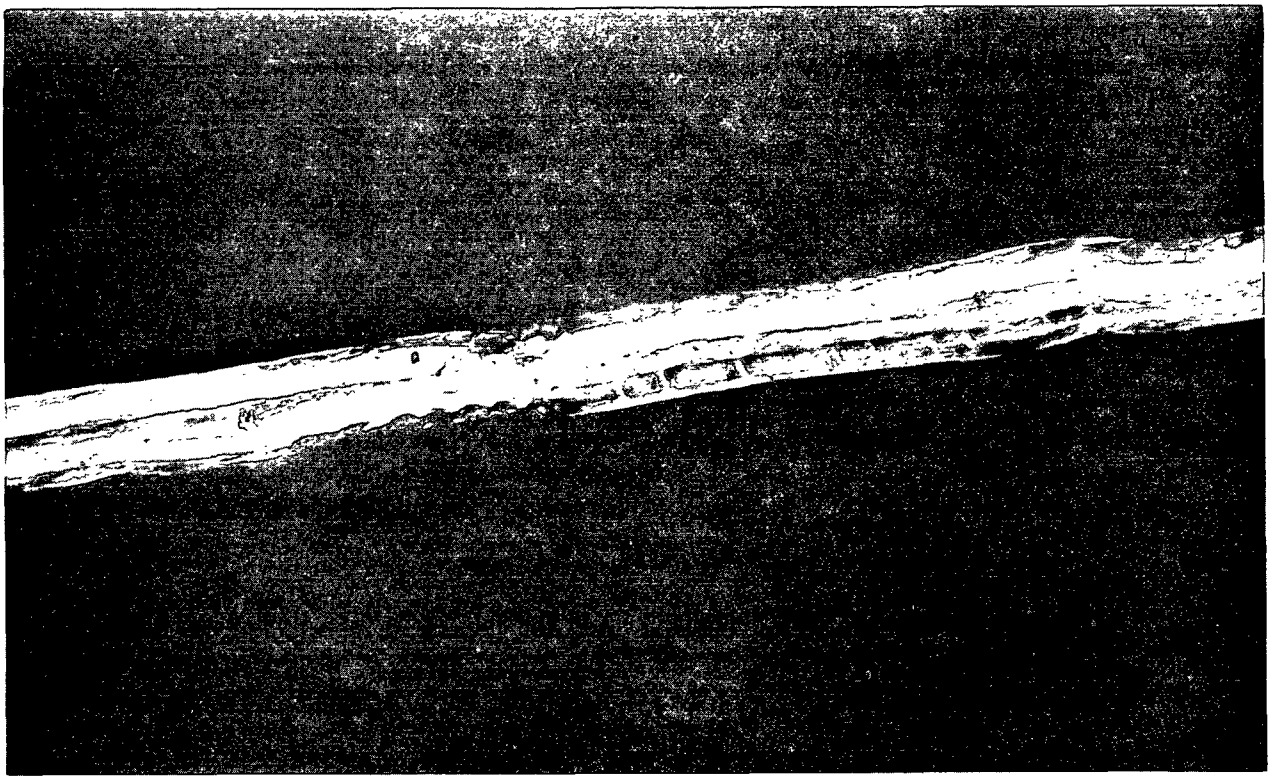

Figure 40. Springwood Fiber Dried Under 0% Negative Strain

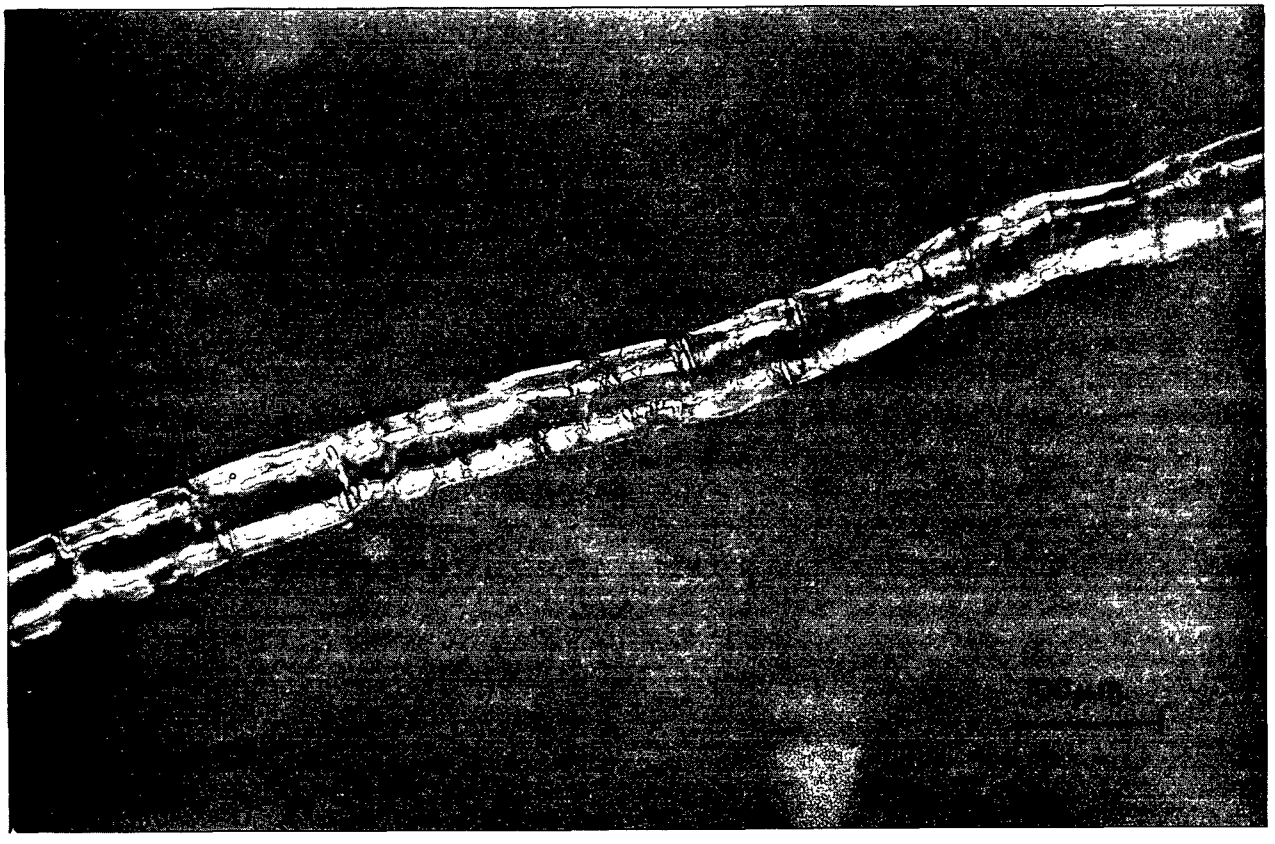

Figure 41. Springwood Fiber Dried Under 20% Negative Strain

Figure 42. Springwood Fiber Dried Under 0% Negative Strain

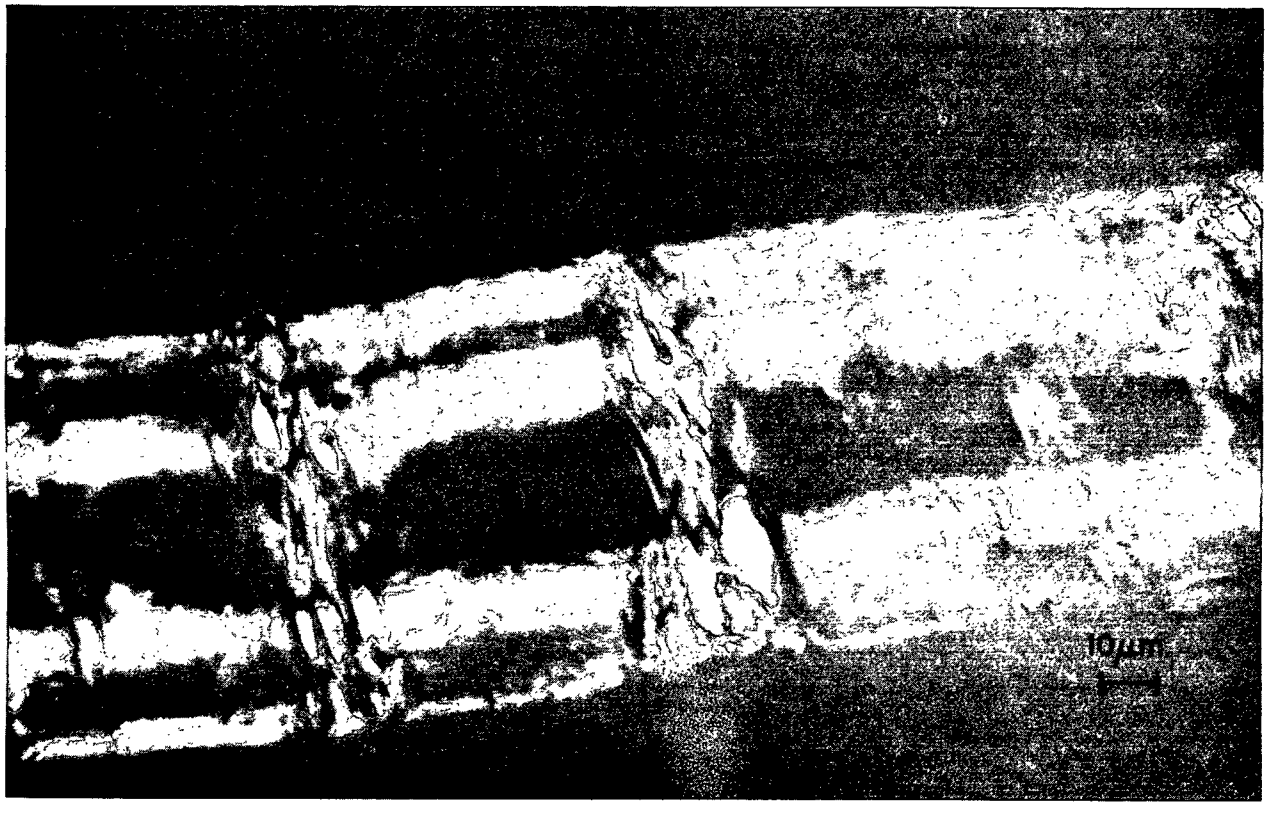

Figure 43. Springwood Fiber Dried Under 20% Negative Strain

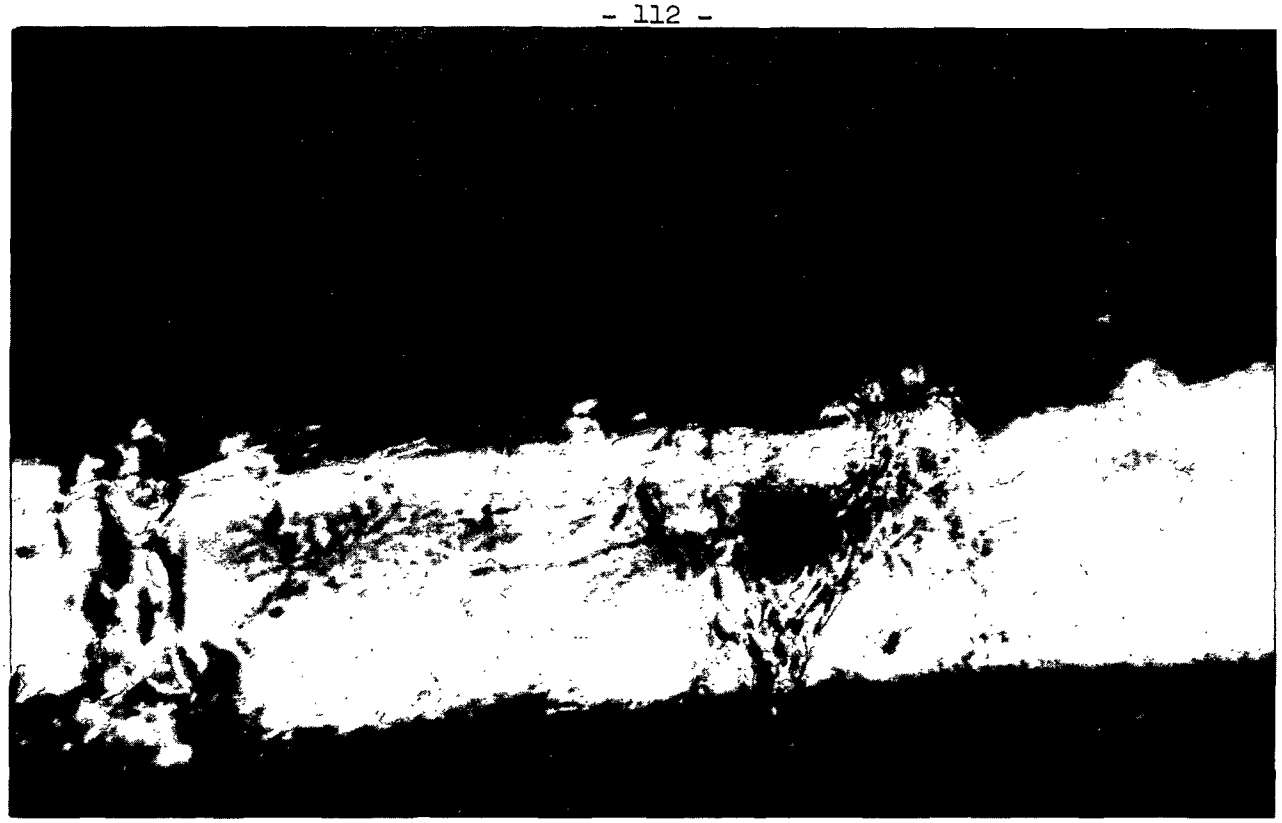

Figure 44. Springwood Fiber Dried Under 10% Negative Strain

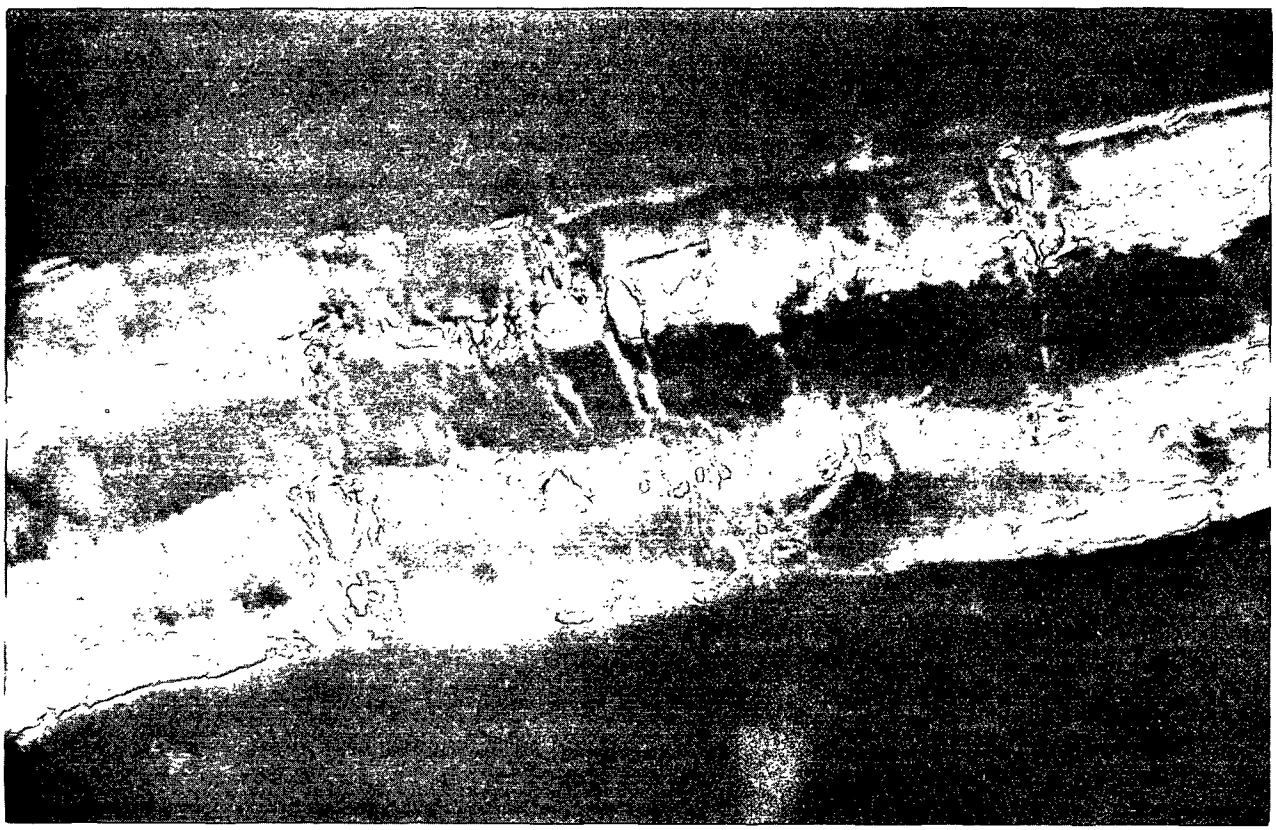

Figure 45. Springwood Fiber Dried Under 20% Negative Strain

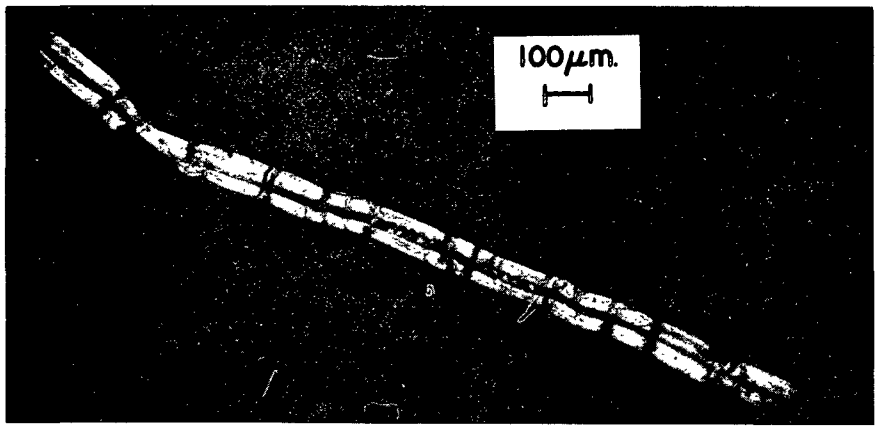

Figure 46. Holocellulose Summerwood Fiber Dyed with Congo Red and Dried Under 20% Negative Strain

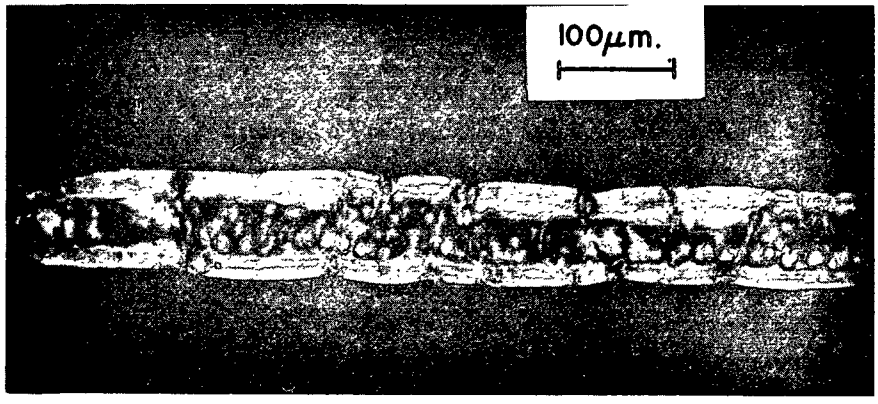

Figure 47. Holocellulose Summerwood Fiber Dyed with Congo Red and Dried Under 20% Negative Strain

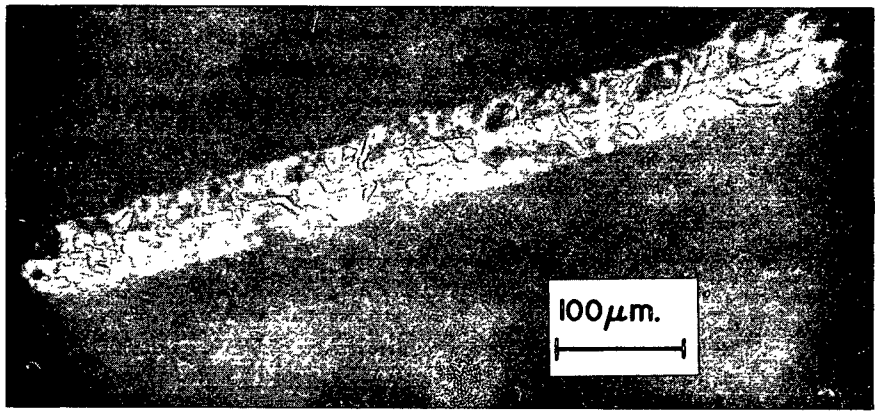

Figure 48. Same Fiber as in Fig. 47 with Crossed Polars Slightly Rotated

and the misaligned zones appearing in the negatively strained fibers can be examined in more detail. The misalignments are seen to be fairly evenly distributed along the fiber length.

At first it seemed that the number of misaligned zones might be related to the level of applied negative strain. However, the number of zones was difficult to count. The reason for this can be seen in Fig. 44 and 45 which show fibers from two negative strain levels. It is apparent from these photographs that misaligned zones are not well defined and isolated in these fibers. Particularly in Fig. 45, the cross-striations can be seen to spread over the fiber surface extensively. They are not really separable into individual zones. Qualitative examination of fibers from several negative strain levels indicated that there was not much difference in the general appearance of any of them.

Pleochroic dyes also help bring out structural discontinuities. A number of fibers were dyed in Congo Red stain and dried under 20% negative strain. Figures 46-48 are examples of the photographs obtained from these fibers using polarized light. The photographs of Fig. 46 and 47 show the same type of structural discontinuities as have been seen in the previous figures. Figure 48 was taken slightly out of focus and with fiber adjusted only slightly differently relative to the crossed polars. The result makes the fiber look finely crinkled and gives it a much different general appearance. This type of photograph has been shown frequently in the literature (50,53,60) and is offered to indicate how variations in microphotographic technique can change the appearance of a structure markedly.

Some important generalizations can be made from the polarized light microscopy. The structural misalignments are well distributed along the length of the longitudinally compressed fibers. The lengths of the apparently

undamaged regions between the misaligned zones vary from perhaps 20 μm. to over 100 μm. The widths of the misaligned zones vary considerably. The misaligned zones seem to be locations at which the fiber has collapsed, and they have an accordion-pleated appearance. Despite the fact that the fibers have decreased in length by as much as 20%, however, no bulging can be detected to account for the fiber material which was lost. This last point led to additional microscopic examination of the fiber structure.

The misaligned zones appear to be somewhat denser when they are examined by transmitted light, but it did not seem likely that the density of the cellulosic material could actually increase enough to account for all of the fiber length lost during compression. To compress 20% of the mass of the fiber into misaligned zones representing at most one third of the remaining fiber would have required densities higher than those of crystalline cellulose. To determine whether the extra fiber material was residing in the misaligned zones in some way, an interesting experiment was performed.

It will be recalled that the IPC Compacted Fiber Dimension Apparatus was used to laterally compact fiber segments between two sapphire crystals until optical contact would be gained first in the regions which were thickest relative to the rest of the fiber. This situation was ideally suited to demonstrating whether the longitudinally compressed fibers were uniform along their lengths, or whether there were thickened areas. Fiber segments were placed between the sapphire crystals and photographed. Compaction pressure was then applied very slowly and other photographs were taken at increments of compaction pressure. The appearance of the regions of optical contact was observed; some representative results are presented in Fig. 49-54.

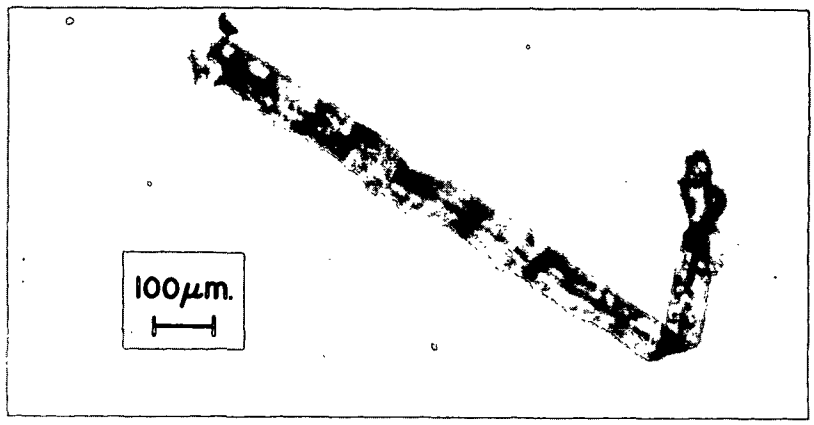

Figure 49. Negatively Strained Springwood Fiber Segment Between Two Sapphire Crystals Under No Lateral Compaction

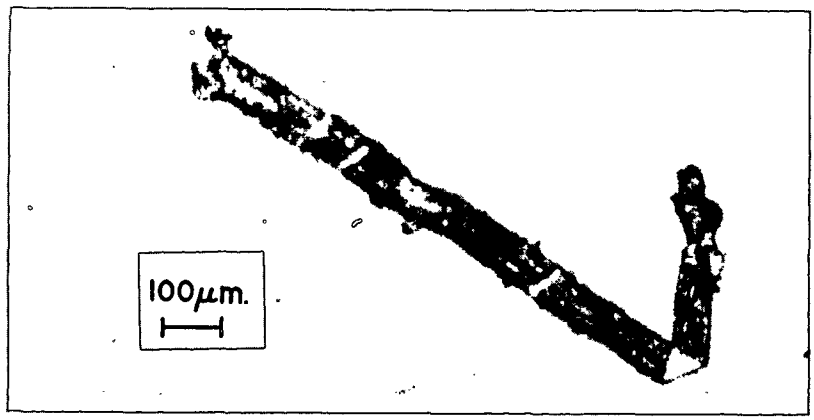

Figure 50. Same as Above Under Small Lateral Compaction Pressure

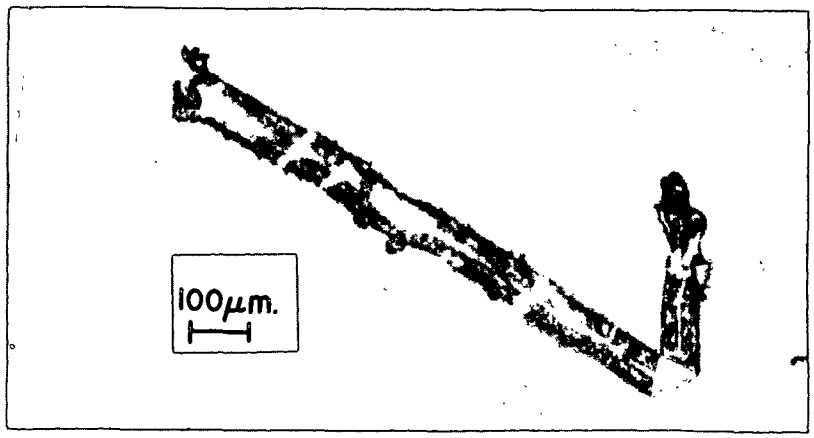

Figure 51. Same as Above Under Larger Lateral Compaction Pressure

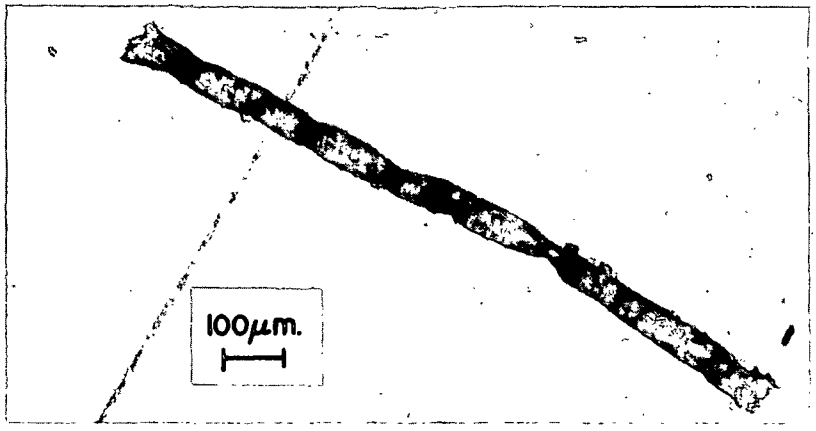

Figure 52. Negatively Strained Summerwood Fiber Segment Between Two Sapphire Crystals Under No Lateral Compaction

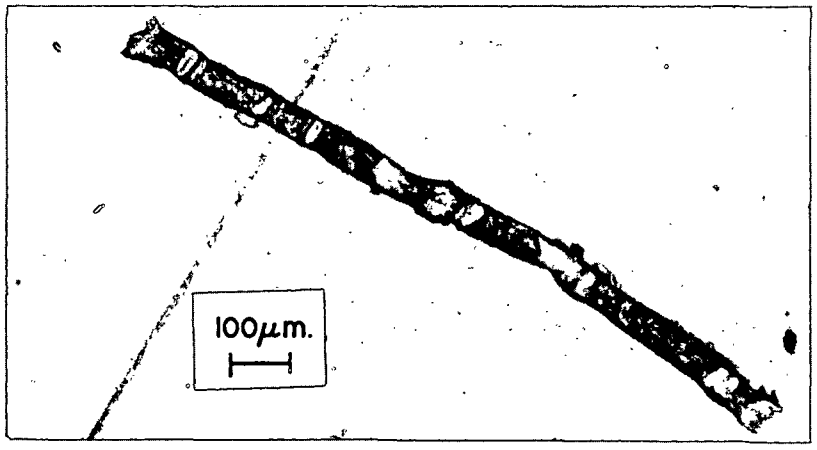

Figure 53. Same as Above Under Small Lateral Compaction Pressure

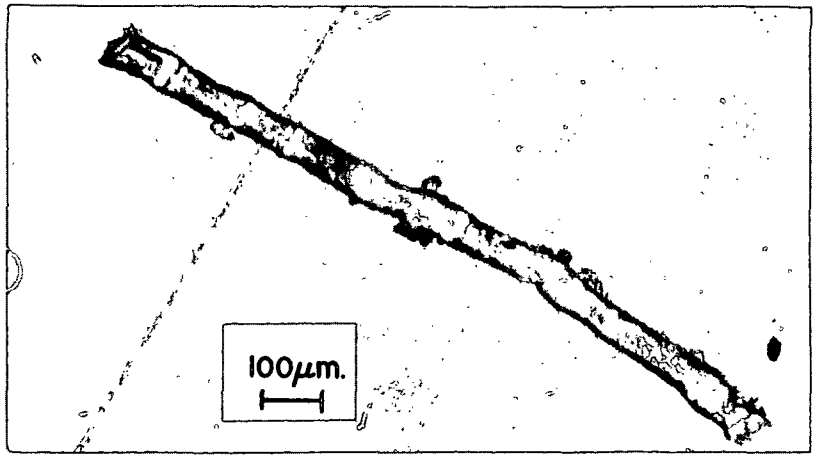

Figure 54. Same as Above Under Larger Lateral Compaction Pressure

These are sequential photographs of a springwood fiber segment and a summerwood fiber segment which have been 20% longitudinally compressed. The development of optical contact can be readily seen in these pictures. In Fig. 49 and 52 the fibers, with their misaligned zones of denser appearance are shown. Figures 50 and 53 show the fibers under lateral compaction between the crystals. Optical contact is observed as light areas, and these can be seen to correspond to the misaligned zones without exception. Note also that, in the case of the springwood, the segment is doubled over at the bend. Optical contact has been gained at this bend where the fiber is obviously twice as thick. Note also that optical contact has begun to develop for the misaligned zones too, indicating that they may be almost twice as thick as the regions between the misalignments. The summerwood demonstrates the effect very well in Fig. 53. In Fig. 51 and 54, the compacting pressure is higher, and optical contact is very well developed. Note that the areas of optical contact seem to spread out from the misaligned zones, indicating a region of transitional thickening up to the zone itself. This gives direct proof that the apparently lost mass of fiber material is located in the misaligned zones in some manner. Additional investigation demonstrated how this happened.

It will be demonstrated in the next section, and in Appendix III, that all of the dried fibers had the shape of flattened ribbons. It seemed logical that the narrow dimension (i.e., perpendicular to the plane of the fiber ribbon) might be the one in which failure and buckling came about. Because all of the micrographs shown so far have been taken looking straight down on the plane of the fiber, they gave no real indication of variations in the dimension out of the specimen plane. To simplify discussion, consider the $\underline{x}$-$\underline{y}$ plane to be the plane of the surface of the flat fiber ribbon. Thus, $\underline{z}$ is the direction normal to this ribbon surface.

Fibers were mounted on double-backed tape stuck to a glass slide. The fibers were oriented so that the thin edge of the fiber ribbon could be examined and, thereby, variations in the z direction readily determined. This examination proved that buckling was indeed occurring in the z direction. The fiber material was simply being forced into convolutions in the z direction to adjust to applied strains. Examples of the results of this examination are presented in Fig. 55-57.

That the fiber should collapse in its narrowest dimension is very logical, but the fact that this effect cannot be detected by examining the fiber from above is very interesting. Several fibers were examined from their edges, as in Fig. 55-57, and then flattened onto the tape and reexamined from the top as before. Indeed, it is quite amazing that the convolutions in the z direction, when examined from above the fiber surface, have only the appearance which has been demonstrated in all the preceding micrographs. The accordion pleats observed are undoubtedly real, but the variation which they reveal is actually in the z direction.

ELECTRON PHOTOMICROGRAPHY

One of the purposes of this part of the study was to examine the cross-sectional shape of longitudinally compressed and some uncompressed fibers. It was also hoped that cross sections might indicate some delamination of the internal lamellae of the fiber but, unfortunately, such detail becomes obscured during imbedding and sectioning. Some transmission electron micrographs of cross sections of holocellulose fibers are presented in Appendix III. Such cross sections, taken for several levels of negative strain, indicate that all dried fibers have the shape of flat ribbons.

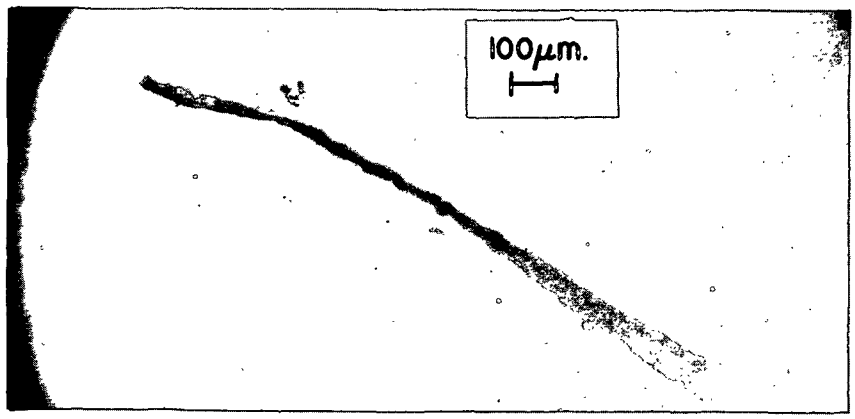

Figure 55. Edge View of a Negatively Strained Holocellulose Springwood Fiber in Transmitted Light

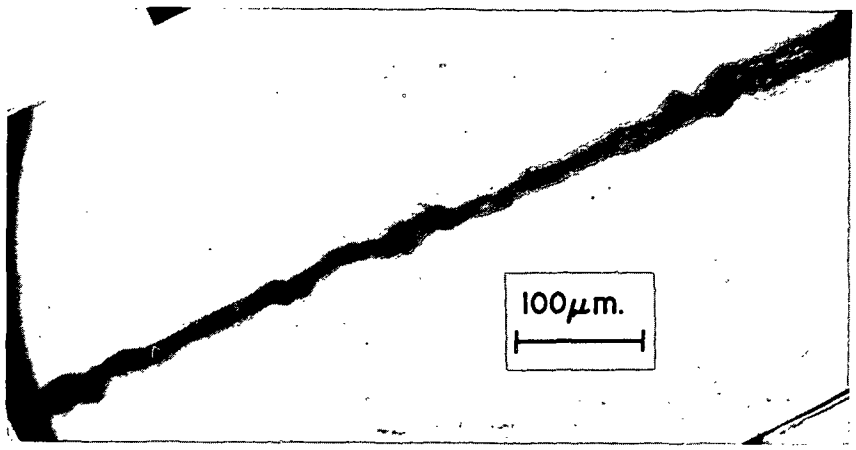

Figure 56. Edge View of a Negatively Strained Holocellulose Summerwood Fiber in Transmitted Light

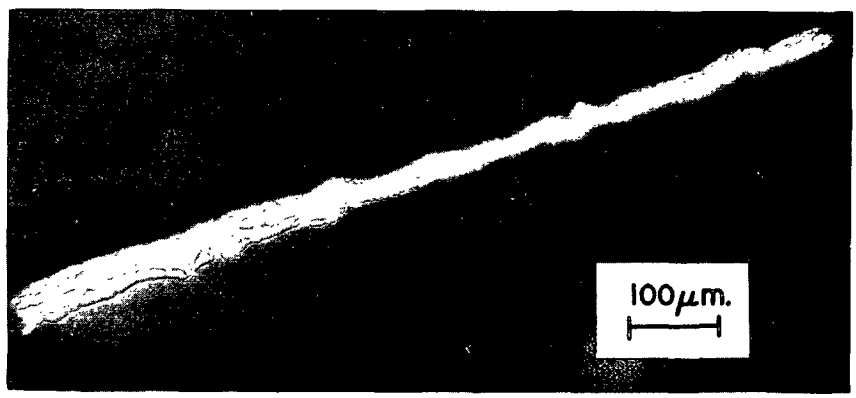

Figure 57. Edge View of a Negatively Strained Holocellulose Summerwood Fiber Observed with Crossed Polars

Longitudinal sections were also obtained from both spring- and summerwood fibers. The longitudinal sections were all cut to give edge views of the fiber ribbons. The resulting photographs show the structural disruption in the z direction at a much higher magnification than before. Figures 58-61 are a few samples of structural dislocations in the z direction. Additional examples are presented in Appendix IV. Sections were also obtained from fibers which had not been longitudinally compressed. These simply demonstrated that such fibers were indeed straight, and that the effects observed in Fig. 58-61 were not artifacts from the sectioning process. Examples of uncompressed fibers are not particularly instructive and will not be shown.

Many micrographs such as those presented were obtained. Series of overlapping photographs were taken along the lengths of some fiber segments. Such photographs could be pieced together to permit fiber segments of up to 0.5 mm. in length to be viewed at high magnification. Examination in this way showed long fiber segments (curved somewhat because of the bundling technique prior to imbedding) having many misaligned zones of the type displayed in Fig. 58-61. These zones appeared every 30-100 μm., intervals similar to those observed with polarized light microscopy. Because a photograph of a 0.5-mm. fiber segment is over two meters long at this magnification, space requirements prohibit the display of such composites.

The results of the electron microscope work indicate that the fiber structure is badly distended during longitudinal compression. The localization of the damage shows that there are some areas more susceptible to misalignment than others. The tortured contours into which fibers were dried are certain to result in localized stress concentrations when the fiber is subsequently loaded. Likewise, it is obvious from this work, and the x-ray study,

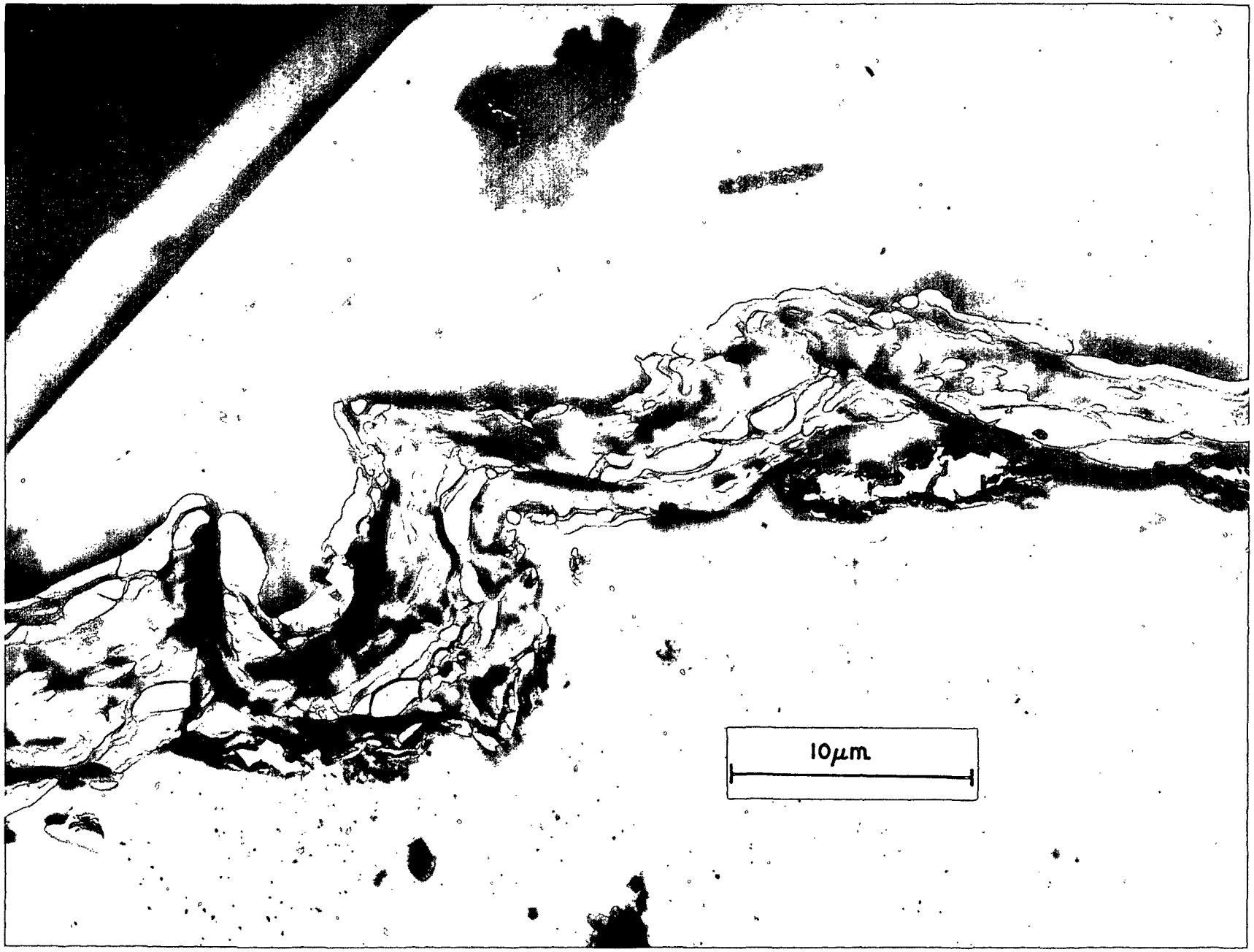

Figure 58. Longitudinal Section of a Holocellulose Springwood Fiber Dried Under 20% Negative Strain. Plate No. 8226 F

Figure 59. Longitudinal Section of a Holocellulose Springwood Fiber Dried Under 20% Negative Strain. Plate No. 8308 F

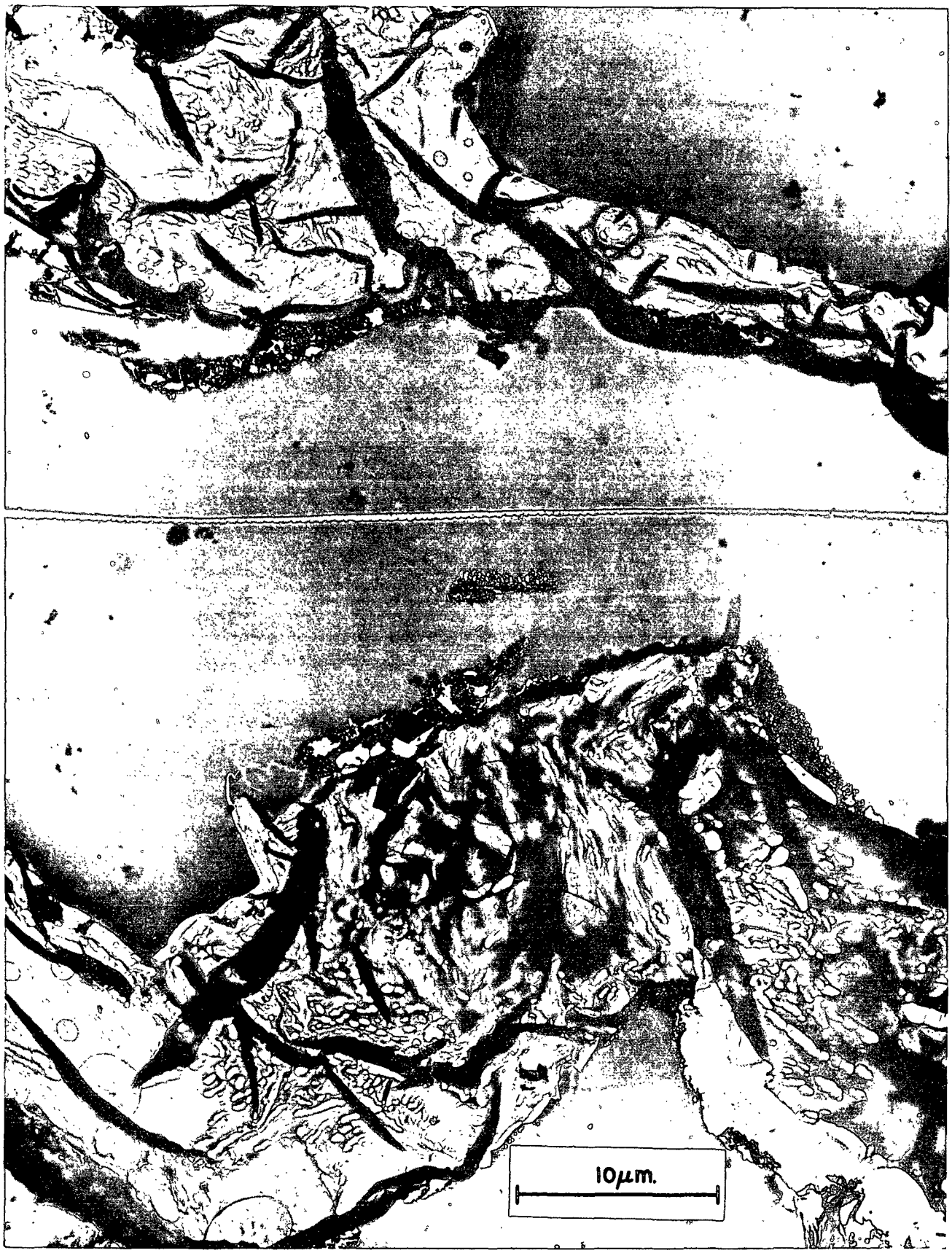

Figure 60. Longitudinal Section of Two Summerwood Fibers Dried Under 20% Negative Strain. Plate No. 8564 F

Figure 61. Longitudinal Section of a Summerwood Fiber Dried Under 20% Negative Strain. Plate No. 8557 F

that the misaligned zones observed with polarized light are not surface effects, but involve the entire fiber cross section. Delamination of the cell wall lamellae at the misaligned zones was not observed, yet it cannot be ruled out as a significant effect of longitudinal compression.

INTERPRETATION OF MECHANICAL PROPERTY CHANGES RELATIVE TO CHANGES IN FIBER STRUCTURE

Drying under longitudinal compression has been shown to have a great effect on the mechanical properties and on the structure of fibers. Changes in fiber structure can be interpreted as giving rise to the mechanical property changes. This discussion proposes to speculate upon the connection between various fiber mechanical properties and the structural changes at different levels of cellular organization. The structure of a longitudinally compressed fiber is hypothesized to consist of two distinct regions: (1) the buckled zones in which the fibrils are completely disoriented, and (2) the relatively intact segments in which the fibrils are still parallel to one another and maintain the helical arrangement, though the helix angle is somewhat altered. The mechanical properties are discussed in terms of this model.

Tensile strength of undamaged fibers has been demonstrated by other investigators to depend largely on the fibrillar orientation in the S_2 layer. Drying fibers under load causes an increase in tensile strength by increasing the fibrillar orientation and improving the uniformity of stress distribution (82). It is this writer's feeling that the lateral contraction of the fiber during such drying is also of importance. This lateral contraction can help to draw the various amorphous components of the fiber closer together, thus enhancing secondary bonding within these parts of the fiber, and thereby increasing the ability of the fiber to withstand tensile stresses.

If, on the other hand, a longitudinal compression is applied during drying, a decrease in fibrillar orientation would be expected, and is in fact observed. Wet fibers can very likely accommodate small compressive strains without buckling. The results from this study show that compressive strains of up to 4% might be absorbed by means of a uniform decrease in fibrillar orientation. However, buckling does become a significant factor at relatively low compressive strains. Once buckling has occurred, the uniform decrease in fibrillar orientation no longer predominates in determining tensile strength. In the buckled zones, the fibrils become very disorganized and are no longer oriented to maximize the ability of the fiber to withstand subsequent tensile stresses. Secondary bonds are undoubtedly broken and reform in these areas, but they are reformed in such a way as to accommodate the compression by means of a crumpling of the fiber wall. These new secondary bonds will not tend to be so aligned as to maximize resistance to tensile stresses, as was previously the case. It is hypothesized that the tensile strength of longitudinally compressed fibers is dependent only on the buckled zones, in which the fibrils are no longer well aligned, and bonded parallel with one another. Loads are no longer well distributed and stress concentrations cause failure in the buckled zones. Even after the fibrils within these zones have been straightened out, as outlined later in this discussion, the lateral secondary bonds, which aid in distributing the stress, will not be present. The result is, stress concentrations will build up within the buckled zones, causing failure.

Changes in initial modulus can also be attributed to the buckled zones. In an uncompressed fiber, the application of tensile stress causes an immediate tension in the well-oriented fibrils. There is no means by which a strain can be relieved in such fibers other than by internal slippage or a decrease in

orientation and lateral contraction of the fiber, causing lateral compression of the fibrils and amorphous matrix. This lateral contraction is resisted by the matrix, and as a result, the initial modulus of such fibers is relatively high.

In longitudinally compressed fibers, a strain relief mechanism is readily available in the buckled zones. The fibrils in these zones are not aligned to withstand a tensile stress. The only resistance to such a stress is from secondary bonds which happen to be oriented in the longitudinal fiber direction. These few secondary bonds are quite easily broken, giving a correspondingly lower initial modulus. The fiber then elongates very rapidly until the fibrils in the buckled zones are straightened out and reoriented along the fiber axis. This is the hypothesized mechanism by which the large ultimate elongation values can be accounted for. The hypothesis of permanent bond breakage is strongly supported by the observed inelastic nature of the longitudinally compressed fibers.

Rupture energy cannot be so readily attributed to the buckled zones. It has been shown in this study that the energy increase is due to the large increases in elongation of longitudinally compressed fibers. In the region of rapid elongation, the energy input is undoubtedly going to the buckled areas. But, near the end of the load-elongation curve, a good deal of stiffening occurs which causes the intact fiber segments to come into play. Whether the large increments of energy required near the end of a tensile test are being absorbed by the buckled zones, or by the intact segments or both is not clear. It seems possible that at least some of the increased rupture energy might be absorbed by the matrix as the fibrils of the intact segment try to return to their original orientation.

No mention has been made of the effects which changes in crystallinity might have. The discussion has revolved around the secondary bonds because it seems very likely that these bonds determine the mechanical properties almost exclusively. This idea has been offered by Hermans (102), according to whom the crystallinity has little bearing on the physicochemical behavior of cellulosic materials in comparison with the amorphous region. The only primary valence bonds which might be of some importance to changes observed in this work are those which are part of the cellulosic chains of the amorphous matrix and external to the crystallites. Some of these bonds do break during fiber rupture, but it is doubtful whether their breakage initiates fiber rupture.

Some differences were observed between spring- and summerwood fibers. The unstrained springwood fibers had tensile strengths about 35% lower than those of similar summerwood fibers. This can be only partially accounted for by the fact that summerwood fibers of this study were shown to have larger cellulose contents and that the S_2 layer constitutes about 10% more of the volume of the summerwood than of the springwood (27). It seems probable that the summerwood fiber is a more cohesive structure, having more internal bonding. This would help to explain the somewhat higher initial modulus of summerwood fibers. A comparison can also be made of the tensile strengths of spring- and summerwood fibers which have been 20% longitudinally compressed. When the tensile strengths are corrected for the 10% relative difference in S_2 material, they are found to be the same. Apparently, by adding imperfections in the form of buckled zones to both fiber types, the effect is stronger in the summer- than in the springwood and causes the former to become much like the latter in terms of tensile strength. After allowing for differences in the amount of S_2 layer in the two

fiber types, Jentzen (82) accounted for differences in tensile strength by saying that the springwood fibers had more imperfections or "weak links" which caused them to fail sooner.

INTERPRETATION OF MECHANICAL CHANGES IN TERMS OF THEIR PRACTICAL SIGNIFICANCE

That pulp fibers can come under longitudinal compressive strains in a number of commercial processes has been discussed in the literature review. This study has found that such compressive strains alter the fiber mechanical properties to a considerable extent. It is interesting to speculate on the effects which the changes in mechanical properties might have on the properties of the resulting paper sheet.

Sheets containing large proportions of longitudinally compressed fibers might be expected to demonstrate superior extensibility, more plastic deformation, and high-impact resistance due to the ability of the fibers to absorb energy. An example of this would be Clupak papers which do show the properties mentioned. Load-elongation behavior of the Clupak sheet is very similar to that of the fibers examined in this study. Although the Clupak treatment probably affects the fiber-to-fiber bond as well as the fiber structure, there is no reason to doubt that the important changes obtained in the process are the result of changes in the fiber structure. Sheet strength is also reduced by the Clupak process, but it is difficult to conclude whether this is caused by the reduced fiber strength or whether disrupted fiber-fiber bonds initiate the failure.

Fibers in the cross direction of machine-made papers also come under longitudinal compression during the drying process. The sheet is also found to be more extensible, more plastic, and weaker in this direction. All of

these properties are the same as those for longitudinally compressed fibers. It seems very likely that the changes in fiber properties are responsible for this behavior to at least some extent.

Page (60) has shown that longitudinal compression of fibers during high-consistency refining resulted in sheets having a higher stretch. In work by Brezinski and Hardacker (107) an unbeaten southern pine kraft pulp was found to contain a large number of very highly stretchable fibers. These fibers were examined by this writer and found to contain many misaligned zones similar to those described in this study. Examples of these are shown in Appendix V. Despite the high ultimate elongations of these fibers, many exceeding 20%, the paper made from this pulp did not exhibit abnormal stretchability. Perhaps it is necessary that most of the fibers be of the high stretch variety before the sheet will display properties similar to the fibers. It is possible that high-consistency refining results in more uniform longitudinal compression of all the fibers so that the effect can be seen in the sheet properties.

Conjecture is possible about the effect which the random addition of a significant quantity of longitudinally compressed fibers to a sheet might have. Such fibers will be more flexible and could affect sheet density. Even in a well-bonded sheet, many of the segments from the compressed fibers would not be capable of bearing a load and would deform very easily under stress. This would mean that the other undamaged segments would have to bear a greater share of the load. This might adversely affect sheet strength.

Such fibers might also contribute to the plastic deformation of paper as part of the intrafiber deformation mechanism postulated by Ebeling (7). He felt that the contribution of intrafiber irreversible structural changes

to the plastic deformation of paper might be more important than the contribution of interfiber irreversible structural changes. If this were true, then certainly the presence of fibers of the type observed in this study would have a strong influence.

Important implications can be derived from the rewetting experiments. A considerable loss in the extensibility of springwood fibers followed rewetting and redrying, but no recovery in tensile strength was observed. The mechanical manipulations performed during formation of the sheet might well eliminate most of the fiber extensibility which longitudinally compressed fibers possessed. The only effect retained would then be the decrease in fiber tensile strength. This effect could become significant for well-bonded sheets in which the strengths of the individual fibers are important.

SUMMARY OF RESULTS

The objectives of this thesis were to determine (1) the mechanical property changes in individual pulp fibers associated with drying under longitudinal compression, and (2) the structural changes in the fiber which accompanied the changes in mechanical properties. To accomplish this, an apparatus was constructed to compress individual fibers longitudinally while drying them. Holocellulose fibers were prepared from springwood and summerwood portions of mature growth rings of longleaf pine. In addition, kraft fibers were prepared from the same species for purposes of comparison. The load-elongation properties of the fibers were measured for several levels of longitudinal compressive straining. Structural changes were determined by the use of Laue x-ray diffraction, polarized light microscopy, and electron microscopy. This work produced the following results:

1. The holocellulose springwood fibers showed a maximum decrease of 40% in tensile strength, 86% in initial modulus, and an increase of 160% in work-to-rupture after application of a 20% longitudinal compressive strain.

2. The holocellulose summerwood fibers showed a maximum decrease of 40% in tensile strength, 90% in initial modulus, and an increase of 70% in work-to-rupture after application of a 20% longitudinal compressive strain.

3. The kraft summerwood fibers showed a maximum decrease of 46% in tensile strength, 95% in initial modulus and an increase of 50% in work-to-rupture after application of a 20% longitudinal compressive strain.

4. The principal structural manifestation of longitudinal compression drying is the formation of multiple buckled zones distributed along the fiber length.

5. The crystallite orientation of both springwood and summerwood holocellulose fibers decreased due to drying under longitudinal compression. In addition, both fiber types showed a decrease in the proportion of crystallite material oriented about the fiber axis relative to the crystallite material which was randomly oriented.

6. No significant changes in relative crystallinity were observed for springwood fibers dried under longitudinal compression. However, the relative crystallinity of summerwood fibers was observed to decrease significantly from this treatment.

7. The ultimate elongation of all fiber types increased by an amount approximately equal to the axial compressive deformation applied during drying.

8. Rewetting of longitudinally compressed fibers followed by redrying without compression did not result in a recovery of the strength properties, but did reduce the ultimate elongation.

9. Load-unload cycling of fibers which had been dried under longitudinal compression showed them to be much less elastic. Large increments of permanent set were added with each successive cycle.

10. Fibers which had been dried under longitudinal compression showed increased initial moduli with each successive load-unload cycle. Those which were most highly compressed showed the greatest changes.

11. The initial modulus observed in the final cycle of the fibers which had been longitudinally compressed by ten percent was the same as that of the first cycle for uncompressed fibers. However, the initial moduli of the

cycles of the twenty percent negatively compressed fibers never reached this level.

12. There were small chemical differences between the springwood and the summerwood fibers. The springwood fibers contained 59% cellulose, 29% hemicellulose, and 12% lignin residue, pectins and arabinogalactans. The summerwood contained 65% cellulose, 27% hemicellulose, and 8% lignin residue, pectins and arabinogalactans.

13. The average compacted cross-sectional area of the summerwood fibers was approximately 15% greater than that of the springwood fibers.

CONCLUSIONS

Tensile mechanical properties of dry pulp fibers are strongly affected by previous longitudinal compressive forces applied to the fibers while still wet. Breaking stress and initial modulus are both drastically reduced, although the fibers' ability to absorb energy is considerably enhanced as evidenced by the increase in work-to-rupture values. These effects have been found to be associated with the formation of structural discontinuities in the fiber wall due to buckling. The buckled zones are irregularly distributed along the length of a longitudinally compressed fiber, and damage becomes more and more extensive as the level of compressive strain is increased.

Two principal mechanisms have been considered responsible for changes in mechanical properties of individual fibers in discussions by other workers (20,82). These mechanisms are: (1) changes in fibril orientation, and (2) redistribution of stress among the fibrils by internal slippage. Fibers dried under longitudinal compression may be considered to show extremes of these two structural changes. Such fibers consist of many fairly intact segments interspaced with zones in which the fiber wall is drastically disoriented.

It is hypothesized that the mechanical properties of the relatively intact segments are more like those of the original fiber than those of the buckled zones. The decrease in tensile strength and initial modulus may be attributed primarily to stress concentrations in the buckled zones. The increase in ultimate elongation can also be attributed primarily to the buckled zones since the small changes in the fibril orientation of the intact segments can account for only about one fourth of the total increase in ultimate elongation in summerwood fibers and even less in springwood fibers. Increases in the work-to-rupture values are not so readily assigned to the buckled zones and it is

felt, after an examination of the average load-elongation plots, that the increases in this quantity may be due as much to the relatively intact segments as they are to the buckled zones.

Responsibility for the changes in tensile strength properties has been placed upon stress concentrations for several reasons. Longitudinally compressed fibers have been interpreted to consist of two different types of microfibrils. The first type exists in the relatively intact segments and is oriented around the fiber axis having an average orientation only a few degrees different from the original fiber. The second type exists within the buckled zones and shows no preferred orientation at all. It is in this second group that stress concentrations would be expected, since the mechanism for redistribution of an applied stress between a number of parallel elements would no longer be possible in this case.

The disoriented buckled zones are relatively easy to pull out as evidenced by the large permanent set observed during load-unload cycling. Even after the buckled zones have been pulled out under tensile load, however, the internal order of the fiber is still disturbed and microscopic stress concentrations will still exist. The relative permanence of the damage caused by longitudinal compression is further demonstrated by the fact that rewetting of compression-dried fibers causes no recovery in strength properties.

Springwood and summerwood fibers show significant differences in the manner in which they undergo longitudinal compressive strains. Springwood fibers show a far more pliable behavior and the compression is easily accomplished with buckled zones being very uniformly distributed over the length of the fiber. Summerwood fibers, on the other hand, are more difficult to compress uniformly and often show marked resistance to longitudinal compression in comparison

with springwood fibers. Several observations help to explain this behavior: (1) Summerwood fibers are known to have somewhat larger proportions of S_2 layer; (2) The summerwood fibers had a somewhat higher average cellulose content; (3) They had a larger average cross-sectional area; and (4) They had a higher relative crystallinity. As the changes in crystallite orientation were greater for the summerwood than for the springwood and as the summerwood showed significant changes in relative crystallinity while the springwood did not, it is felt that the differences in behavior of these fibers are significant. Although the effect which longitudinal compression has on the mechanical properties of the two fiber types is essentially the same and probably occurs by the same mechanisms, it may be that the role of the relatively intact segments is somewhat different in the two cases.

When reaching conclusions regarding the general behavior of individual pulp fibers on the basis of a study such as this, it must be kept in mind that the experimental work is limited in scope. In this case, the entire study is based on a single bolt of longleaf pine, although it was carefully selected and in no way atypical.

Considering the number of commercial processes in which fibers are likely to be longitudinally compressed in the wet state, it seems probable that the phenomena described in this study are of considerable importance in many types of paper. Consequently, it will be necessary for any description of the mechanical properties of paper to take into account the fact that fibers which have been so compressed are likely to be weaker and more extensible, on the average, than those which have not been compressed. In the case of the so-called extensible paper, it seems likely that the effects observed in this study are of predominant importance.

GLOSSARY

Negative strain	Longitudinal compressive strain
Applied negative strain	Longitudinal compressive strain as measured from fiducial marks on the rubber blankets
Actual negative strain	Longitudinal compressive strain as measured from photographically determined decreases in fiber length
IPC	The Institute of Paper Chemistry
FLER	The IPC Fiber Load-Elongation Recorder
CFDA	The IPC Compacted Fiber Dimension Apparatus
Layer	Designates the major cell wall divisions (e.g., the S_2 is the middle secondary layer)
Lamella	Cylindrical subdivision of a layer
Fibril	Primary cellulosic structural elements of the fiber. Can represent any of the levels of organization described when used in a general sense
Equator	Line defined by the centers of the 002 and the $10\bar{1}$-$10\bar{1}$ maxima of Laue x-ray diffraction patterns

ACKNOWLEDGMENTS

The author wishes to express a special note of gratitude to Dr. J. A. Van den Akker for his continual help and encouragement during the course of this work. The critical discussions with Dr. J. P. Brezinski, Dr. N. S. Thompson, and Dr. D. G. Williams are gratefully acknowledged. Recognition is also due to Mrs. B. Spang for her meticulous testing work.

The author is indebted to Mr. P. K. Dumbleton for his design help and to Mr. P. F. Van Rossum and Mr. M. C. Filz, Jr. for the construction of the experimental apparatus. The large quantity of photographic work would not have been possible without the help of Mr. D. E. Beyer and Mr. F. R. Sweeney. Thanks also go to Miss O. Smith for her painstaking work and help with the electron microscope.

Special thanks are extended to all the members of the IPC faculty and staff and to the students who have extended their knowledge and help in order to make this work possible. The author wishes to thank The Institute of Paper Chemistry for granting this opportunity to learn and for its generous financial support.

Finally, my most sincere thanks are extended to my wife, Susan, for her continual support throughout this work and for her help in preparing and typing the manuscript.

LITERATURE CITED

1. Van den Akker, J. A., Lathrop, A. L., Voelker, M. H., and Dearth, L. R., Tappi 41, no. 8:416-25(Aug., 1958).

2. Helle, A. T., Norsk Skogind. 18, no. 3:92-7(1964); 19, no. 3:107-11, no. 9:357-63(1965); Sevensk Papperstid. 66, no. 24:1015-30(Dec., 1963).

3. Bergman, J., and Rennel, J., Svensk Papperstid. 70, no. 22:757-71(Nov. 30, 1967).

4. Duncker, B., and Nordman, L., Svensk Papperstid. 71, no. 5:165-77(March, 1968).

5. Ott, E., Spurlin, H. M., and Grafflin, M. W., ed. Cellulose and cellulose derivatives. 2nd ed. New York, Interscience, 1954. 1601 p.

6. Dunning, C. E. Longleaf pine cell-wall morphology. Doctor's Dissertation. Appleton, Wis., The Institute of Paper Chemistry, 1968. 409 p.

7. Ebeling, K. Distribution of energy consumption during straining of paper. Doctor's Dissertation. Appleton, Wis., The Institute of Paper Chemistry, 1970. 737 p.

8. Rånby, B. G. The fine structure of cellulose fibrils. In Bolam's Fundamentals of papermaking fibers. p. 55-82. Kenley, Surrey, England, Tech. Sect. Brit. Paper & Board Makers' Assocn., Inc., 1958.

9. Meyer, K. H., and Misch, L., Helv. Chim. Acta. 20, no. 2:232-44(1937).

10. Naegli, C. Micellartheorie, neudruck der originalveröffentlichung. In Oswald's Klassicker. no. 227. Leipzig, A. Frey, 1928.

11. Hearle, J. Development of ideas of fine structure. In Hearle and Peter's Fiber structure. p. 209-32. Manchester, Butterworth's, 1963.

12. Côté, W. A., Jr., ed. Cellular ultrastructure of woody plants. Syracuse, N.Y., Syracuse University Press, 1965. 603 p.

13. Frey-Wyssling, A., and Mühlethaler, K. Ultrastructural plant cytology. New York, Elsevier Publ. Co., 1965. 377 p.

14. Mann, J., Pure Appl. Chem. 5, no. 1:91-105(1962).

15. Zhbankov, R. G. Infrared spectra of cellulose and its derivatives. New York, Consultants Bureau, 1966. 333 p.

16. Panshin, A. J., De Zeeuw, C., and Brown, H. P. Textbook of wood technology. Vol. 1, 2nd ed. p. 71, 202-21. New York, McGraw-Hill, 1964.

17. Liang, C. Y., Basset, K. H., McGinnes, E. A., and Marchessault, R. H., Tappi 43, no. 12:1017-24(1960).

18. Marchessault, R. H., Settineri, W., and Winter, W., Tappi 50, no. 2:55-9 (1967).

19. Fengel, D., Papier. 21, no. 10A:635-45(1967).

20. Spiegelberg, H. L. The effect of hemicelluloses on the mechanical properties of individual pulp fibers. Doctor's Dissertation. Appleton, Wis., The Institute of Paper Chemistry, 1966. 115 p.

21. Frey-Wyssling, A. The general structure of fibers. In Bolam's Fundamentals of papermaking fibers. p. 1-6. Kenley, Surrey, England, Tech. Sect. Brit. Paper & Board Makers' Assocn., Inc., 1958.

22. Dolmetsch, H. H., and Dolmetsch, H., Text. Res. J. 39, no. 6:564-84(1969).

23. McIntosh, D. C., Tappi 50, no. 10:482-8(1967).

24. Page, D. H., and DeGrace, J. H., Tappi 50, no. 10:489-95(1967).

25. Emerton, H. W. The outer secondary wall. Its structure. In Bolam's Fundamentals of papermaking fibers. p. 35-54. Kenley, Surrey, England, Tech. Sect. Brit. Paper & Board Makers' Assocn., Inc., 1958.

26. Bucher, H. Discontinuities in the microscopic structure of wood fibers. In Bolam's Fundamentals of papermaking fibers. p. 7-26. Kenley, Surrey, England, Tech. Sect. Brit. Paper & Board Makers' Assocn., Inc., 1958.

27. Jayme, G., and Hunger, G. Electron microscope 2- and 3-dimensional classification of fiber bonding. In Bolam's The formation and structure of paper. Vol. I. p. 135-70. London, Tech. Sect. Brit. Paper & Board Makers' Assocn., Inc., 1962.

28. Schniewind, A. P., Holz als Roh- und Werkstoff. 24, no. 10:502-6(1966).

29. Preston, R. D. Observed fine structure in plant fibers. In Hearle and Peter's Fiber structure. p. 251-68. Manchester and London, The Textile Institute and Butterworth's, 1963.

30. Hiller, C. H., Tappi 47, no. 2:125-8(1964).

31. Robinson, W., Phil. Trans. Roy. Soc. London 210, no. B373:49-82(1921).

32. Wardrop, A. B., and Dadswell, H. E., Council Sci. Ind. Res. Bull. no. 221:14-32(1947).

33. Ambronn, H., Kolloid Z. 36:Zsigmondy Fest, p. 119(1925). Quoted by Wardrop and Dadswell (32) but not seen by this author.

34. Bienfait, J. L., J. Agric. Res. 33:183-94(1926). Quoted by Wardrop and Dadswell (32) but not seen by this author.

35. Frey-Wyssling, A. Schweizerische Verband für die Material-prüfung der Technik. Eidgen. tech. Hochsch., Zurich, Bericht no. 36. Quoted by Wardrop and Dadswell (32) but not seen by this author.

36. Green, H., and Yorston, F. H., Pulp Paper Mag. Can. 40, no. 3:244-50(March, 1939).

37. Kisser, J., and Steininger, A., Holz als Roh- und Werkstoff. 10, no. 11: 415-21(1952).

38. Dinwoodie, J. M., J. Inst. Wood Sci. 4, no. 3:37-53(1969).

39. Frey-Wyssling, A., Holz als Roh- und Werkstoff. 11, no. 7:283-7(1953).

40. Hartler, N., Norsk Skogind. 23, no. 4:1-7(1969).

41. Frey-Wyssling, A. Die pflanzliche zellwand. p. 311-14. Berlin, Springer Verlag, 1959.

41A. Frey-Wyssling, A. Contribution to discussion. In Bolam's Fundamentals of papermaking fibers. p. 33-4. Kenley, Surrey, and London, England, Tech. Sect. Brit. Paper & Board Makers' Assocn., Inc., 1958.

42. Hartler, N., and Le Mon, S., Norsk Skogind. 23, no. 5:1-8(1969).

43. Dinwoodie, J. M., Nature 212, no. 15061:525-7(1966).

44. Stone, J. E., and Nickerson, L. F., Pulp Paper Mag. Can. 59, no. 6:165-73 (June, 1958).

45. Stone, J. E., and Nickerson, L. F., Pulp Paper Mag. Can. 62, no. 6:T317-26 (June, 1961).

46. Hartler, N., and Sundberg, O., Svensk Papperstid. 63, no. 8:263-71(1960).

47. Hartler, N., Das Papier 18, no. 12:633(1964).

48. Rånby, B. G. Contribution to discussion. Symposium on wood preparation. Tappi 44, no. 8:186-7A(1961).

49. Hartler, N., Svensk Papperstid. 66, no. 11:443-53(1963).

50. Green, H. V., Pulp Paper Mag. Can. 63, no. 3:T155-68(1962).

51. Green, H., and Yorston, F. H., Pulp Paper Mag. Can. 41, no. 2:123-6(1940).

52. Bausch, H., and Hartler, N., Svensk Papperstid. 63, no. 9:279-85(May, 1960).

53. Stone, J. E., Tappi 44, no. 8:166-75A(1961).

54. Forgacs, O. L., Tappi 44, no. 2:112-19(1961).

55. Forgacs, O. L., and Mason, S. G., Tappi 41, no. 11:695-704(1958).

56. Alexander, S. D., Marton, R., and McGovern, S. D., Tappi 51, no. 6:277-83 (1968).

57. Emerton, H. W. Fundamentals of the beating process. p. 124. Kenley, England, Brit. Paper and Board Makers' Assocn., 1958.

58. Iwasaki, T., Lindberg, B., and Meier, H., Svensk Papperstid. 65, no. 20:795-816(Oct., 1962).

59. Samuelsson, L., Svensk Papperstid. 67, no. 23:943-8(1964).

60. Page, D. H., Pulp Paper Mag. Can. 67, no. 1:T2-12(Jan., 1966).

61. Van den Akker, J. A. Some theoretical considerations on the mechanical properties of fibrous structures. In Bolam's Formation and structure of paper. Transactions of the Symposium held at Oxford, Sept., 1961. Vol. I. p. 205-41. London, Tech. Sect. Brit. Paper and Board Makers' Assocn., Inc., 1962.

62. Page, D. H., and Tydeman, P. A. Physical processes occurring during the drying phase. In Bolam's Consideration of the paper web. Transactions of the Symposium held at Cambridge, Sept., 1965. Vol. I. p. 371-92. London, Tech. Sect. Brit. Paper and Board Makers' Assocn., Inc., 1966.

63. Page, D. H., and Tydeman, P. A. A new theory of the shrinkage, structure, and properties of paper. In Bolam's Formation and structure of paper. Proceedings of the Symposium held at Oxford, Sept., 1961. Vol. I. p. 397-413. London, Tech. Sect. Brit. Paper and Board Makers' Assocn., Inc., 1962.

64. Hartler, N., Svensk Papperstid. 66, no. 11:443-53(1963).

65. McIntosh, D. C., and Leopold, B. Bonding strength of individual fibers. In Bolam's Formation and structure of paper. Proceedings of the Symposium held at Oxford, Sept., 1961. Vol. I. p. 265-70. London, Tech. Sect. Brit. Paper and Board Makers' Assocn., Inc., 1962.

66. Diaz, R. J., Special Tech. Publ. no. 241, Am. Soc. for Testing Materials, p. 51, 1958.

67. Schoudy, C. A., Southern Pulp Paper Mfr. 21, no. 12:60(Dec. 10, 1958).

68. Welsh, H. S. Fundamental properties of high stretch paper. In Bolam's Consolidation of the paper web. Vol. I. p. 397-409. London, Brit. Paper and Board Makers' Assocn., Inc., 1966.

69. Ihrman, C. B., and Öhrn, O. E. Extensible paper by the double-roll compacting process. In Bolam's Consolidation of the paper web. Vol. I. p. 410-33. London, Brit. Paper and Board Makers' Assocn., Inc., 1966.

70. Schneider, R. L. Unpublished work, The Institute of Paper Chemistry, 1959.

71. Stone, J. E., and Scallan, A. W., Pulp Paper Mag. Can. 66, no. 8:T407-14 (1965).

72. Dinwoodie, J. M. Structural changes in the cell wall associated with longitudinal compression. In TAPPI Special Technical Publication no. 8. Chap. 18. p. 233. New York, TAPPI, 1970.

73. Dolmetsch, H., Cell. Chem. Technol. 3, no. 3:237-53(1969).

74. Wakeham, H. Mechanical properties of cellulose and its derivatives. In Ott and Spurlin's Cellulose and cellulose derivatives. 2nd ed. Part III. p. 1247-1356. New York, Interscience, 1954.

75. Morton, W. E., and Hearle, J. W. S. Physical properties of textile fibers. Manchester and London, Butterworth and Co., Ltd. and the Textile Institute, 1962. 609 p.

76. Meredith, R., ed. The mechanical properties of textile fibers. New York, Interscience, 1956. 333 p.

77. Pierce, F. T., J. Textile Inst. 17:T355(1926).

78. Hartler, N., Kull, G., and Stockman, L., Svensk Papperstid. 66, no. 8:309-11 (1963).

79. Hardacker, K. W. Measurements of tensile strength. In TAPPI Special Technical Publication no. 8. Chap. 15. p. 201. New York, TAPPI, 1970.

80. Howsmon, J. A., and Sisson, W. A., Submicroscopic structure. In Ott and Spurlin's Cellulose and cellulose derivatives. 2nd ed. Part I. p. 231-346. New York, Interscience, 1954.

81. Page, D. H., J. Microscopy 90, no. 2:137-43(1969).

82. Jentzen, C. A. Effect of stress applied during drying on properties of individual pulp fibers. Doctor's Dissertation. Appleton, Wis., The Institute of Paper Chemistry, 1964. 129 p.

83. Hearle, J. W. S., J. Appl. Polymer Sci. 7:1207-23(1963).

84. Cowdrey, D. R., and Preston, R. D. The mechanical properties of cell walls. In Côté's Cellular ultrastructure of woody plants. p. 473-92. Syracuse, N.Y. Syracuse University Press, 1965.

85. Mark, R. Tensile stress analysis of the cell walls of coniferous tracheids. In Côté's Cellular ultrastructure of woody plants. p. 493-533. Syracuse, N.Y. Syracuse University Press, 1965.

86. Thompson, N. S., and Kaustinen, O., Tappi 47, no. 3:157-62(March, 1964).

87. Hardacker, K. W. Unpublished work, 1967.

88. Hardacker, K. W., Tappi 45, no. 3:237-46(1962).

89. Hardacker, K. W., Tappi 52, no. 9:1742-6(1969).

90. Klug, H. P., and Alexander, L. E. X-ray diffraction procedures. New York, John Wiley and Sons, Inc., 1954. 716 p.

91. Hermans, P. H., and Weidinger, A., J. Appl. Phys.19, no. 5:491-506(1948).

92. Hermans, P. H., and Weidinger, A., J. Polymer Sci. 4, no. 2:135-44(1949).

93. Hermans, P. H., and Weidinger, A., Textile Res. J. 31, no. 6:558-71(1961).

94. Jayme, G., and Knolle, H., Das Papier 18, no. 6:249-55(1964).

95. Segal, L., Creely, J. J., Martin, A. E., Jr., and Conrad, C. M., Textile Res. J. 29, no. 10:786-94(1959).

96. Ant-Wuorinen, O., and Vispää, A., Paperi ja Puu 47, no. 5:311-22(1965).

97. Gjonnes, J., Norman, N., and Viervoll, H., Acta Chem. Scand. 12, no. 3:489-94(1958).

98. Gjonnes, J., and Norman, N., Acta Chem. Scand. 12, no. 10:2028-33(1958).

99. Ellefsen, O., Wang Lund, E., Tonnesen, B. A., and Oien, K., Norsk Skogind. 11, no. 9:284-93, 349-55(1957).

100. Sisson, W. A., Textile Res. J. 7, no. 11:425-31(1937).

101. Hermans, P. H. Contribution to the physics of cellulose fibers. New York, Elsevier, 1946. 222 p.

102. Hermans, P. H. Physics and chemistry of cellulose fibers. New York, Elsevier, 1949. 534 p.

103. Meylan, B. A., Forest Prod. J. 17, no. 5:51-8(1967).

104. Wellon, J. D. Cell wall polysaccharides in southern pine wood. Paper presented at the Symposium on Utilization of Southern Pines, Alexandria, La., Nov. 6-8, 1968.

105. Thompson, N. S. Personal communication, 1971.

106. Schulz, J. H. The effect of strain applied during drying on the mechanical behavior of paper. Doctor's Dissertation. Appleton, Wisconsin, The Institute of Paper Chemistry, 1961. 161 p.

107. Brezinski, J. P., and Hardacker, K. W. Unpublished work, 1968.

APPENDIX I

pH CHANGES DURING PREPARATION OF HOLOCELLULOSE PULPS

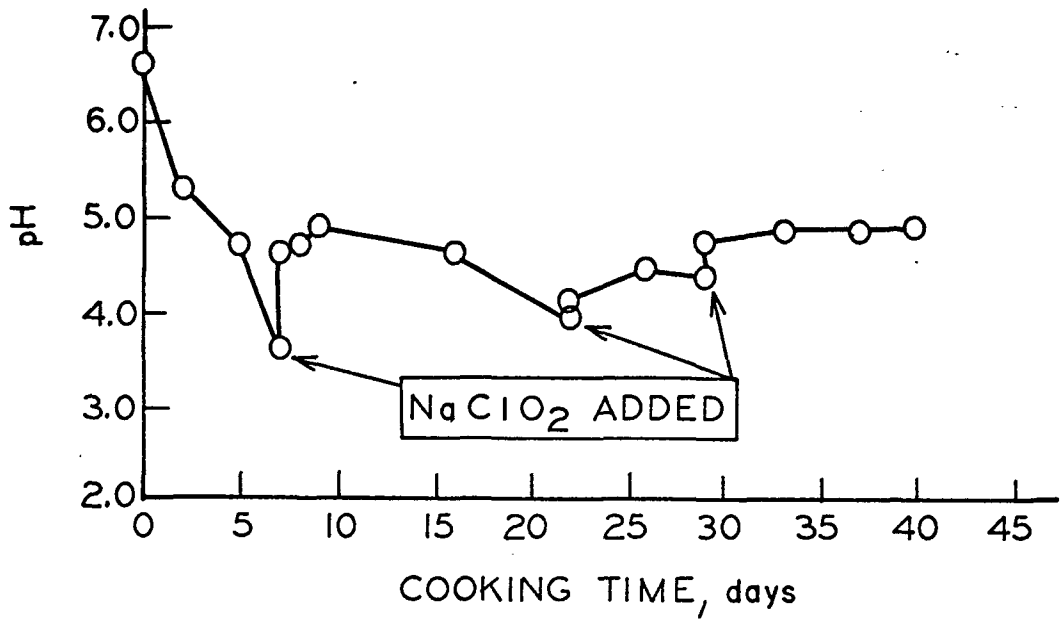

Figure 62. Changes in pH During Room Temperature Acid Chlorite Cooking of Springwood Chips

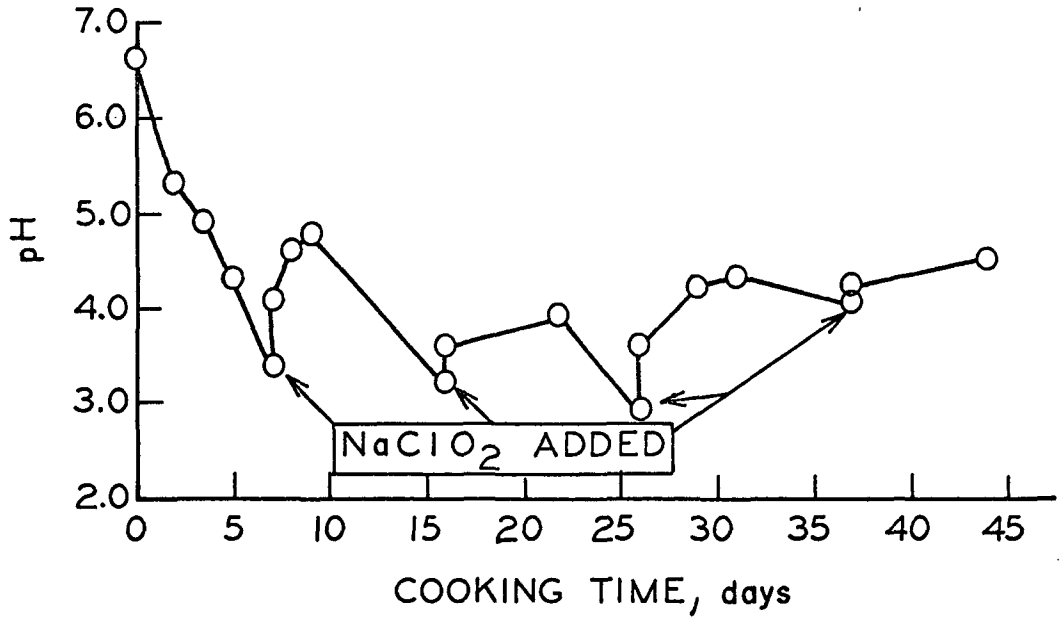

Figure 63. Changes in pH During Room Temperature Acid Chlorite Cooking of Summerwood Chips

APPENDIX II

DETERMINATION OF LATERAL AIR PRESSURE REQUIREMENT OF EXPERIMENTAL APPARATUS

Assume that a total longitudinal compression force of 2.0 g. is to be applied to a fiber which is a flat ribbon. Assume that the entire force is due to friction along the two planar faces of the fiber. Each surface measures approximately 100 μm. x 5.0 mm. and assume that across each surface a frictional force of 1.0 g. must be transmitted.

If F is the friction force required along each face, N is the force required to induce friction, and c is the coefficient of friction, the variables are related by

$$N = F/c$$

If it is assumed that

$$F = 1.0 \text{ g.}$$

and $c = 0.05$, a very conservative estimate,

then $N = 20$ g.

A force of 20 g. must therefore be applied normal to the fiber surface. If P represents the pressure required, and A is the surface area of the fiber, the

$$P = N/A$$

If $N = 20$ g.

and $A = 100 \text{ μm.} \times 5000 \text{ μm.} = 5 \times 10^5 \text{ μm.}^2 = 0.5 \text{ mm.}^2$

then $P = 20 \text{ g.}/0.5 \text{ mm.}^2 = 40 \text{ g./mm.}^2 = 57 \text{ lb./in.}^2$

APPENDIX III

ELECTRON MICROGRAPHS OF HOLOCELLULOSE FIBER CROSS SECTIONS

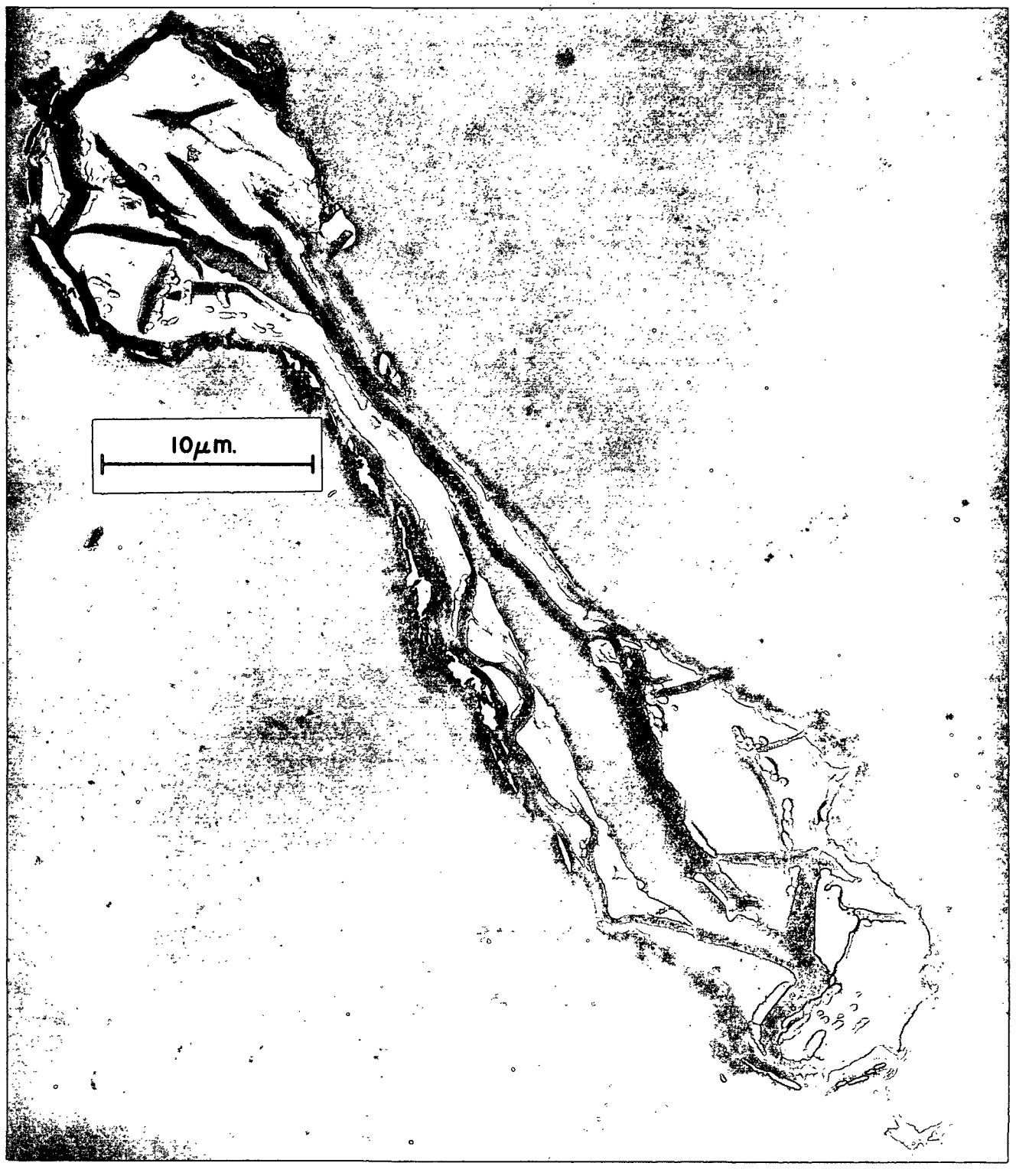

Figure 64. Springwood Fiber Dried Under 20% Negative Strain.
Plate No. 8046 F

Figure 65. Springwood Fibers Dried Under 0% Negative Strain.
Plate No. 8605 F

Figure 66. Summerwood Fibers Dried Under 20% Negative Strain.
Plate No. 8603 F

APPENDIX IV

ELECTRON MICROGRAPHS OF HOLOCELLULOSE FIBER LONGITUDINAL SECTIONS

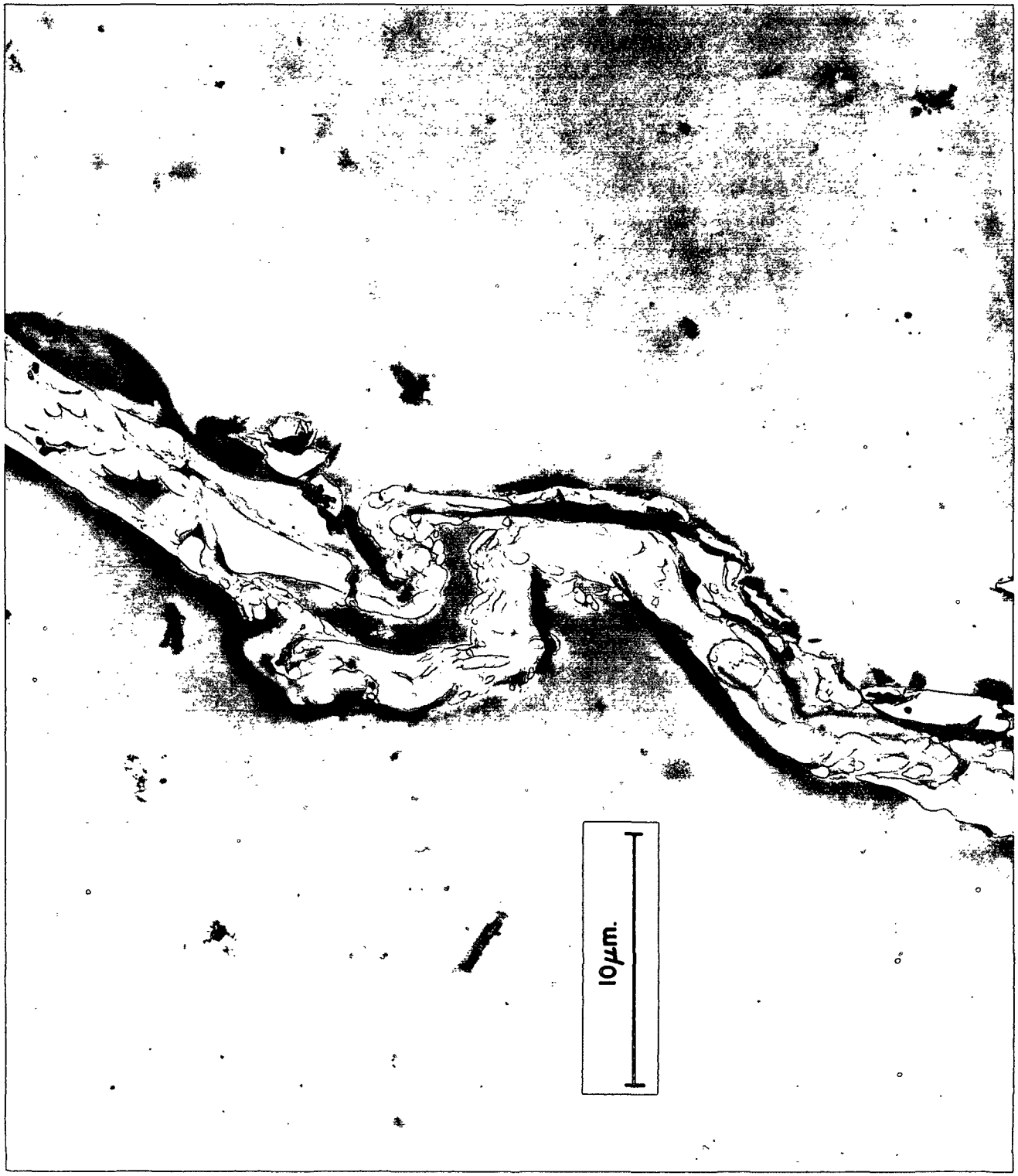

Figure 67. Springwood Fiber Dried Under 20% Negative Strain.
Plate No. 8231 F

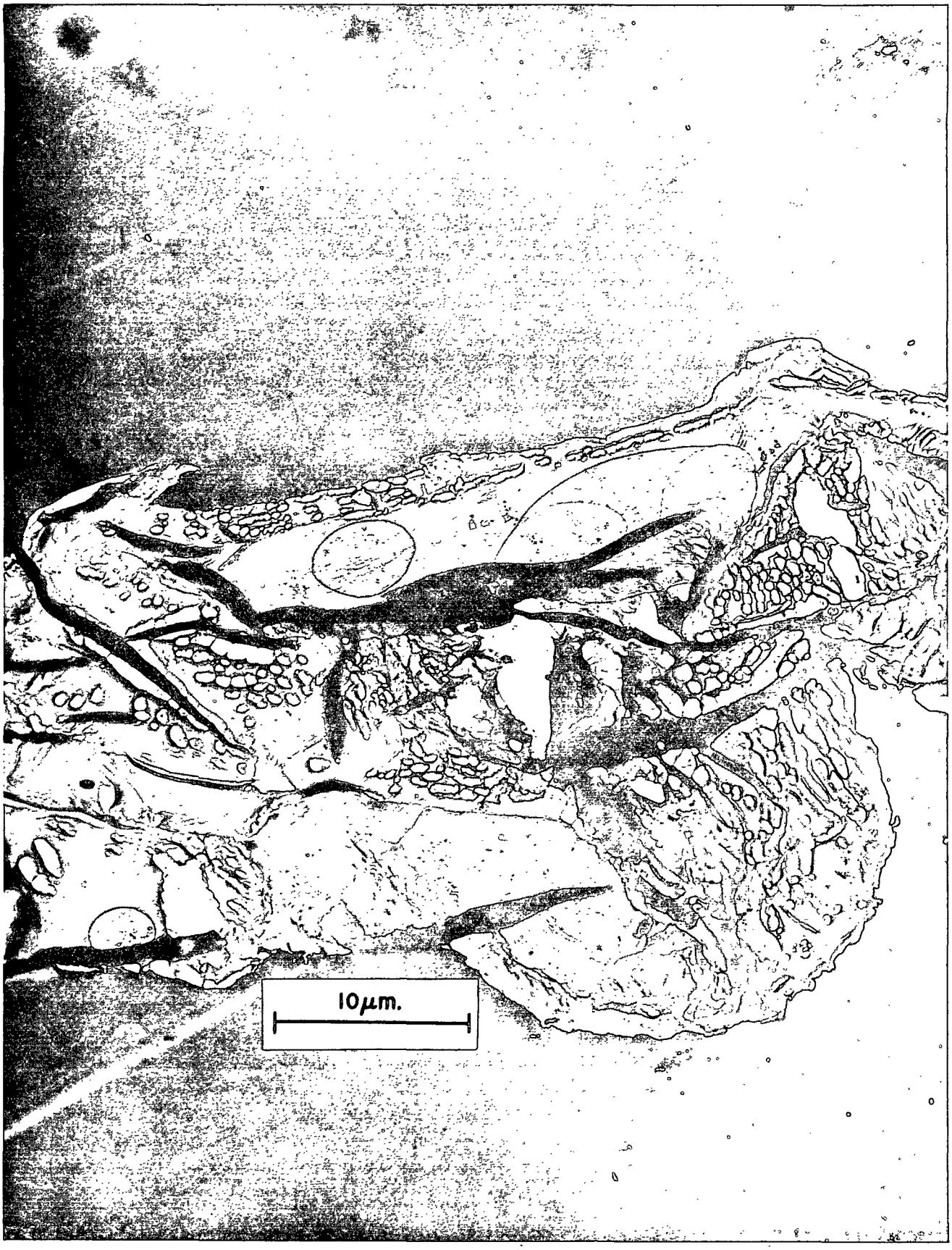

Figure 68. Summerwood Fiber Dried Under 20% Negative Strain.
Plate No. 8558 F

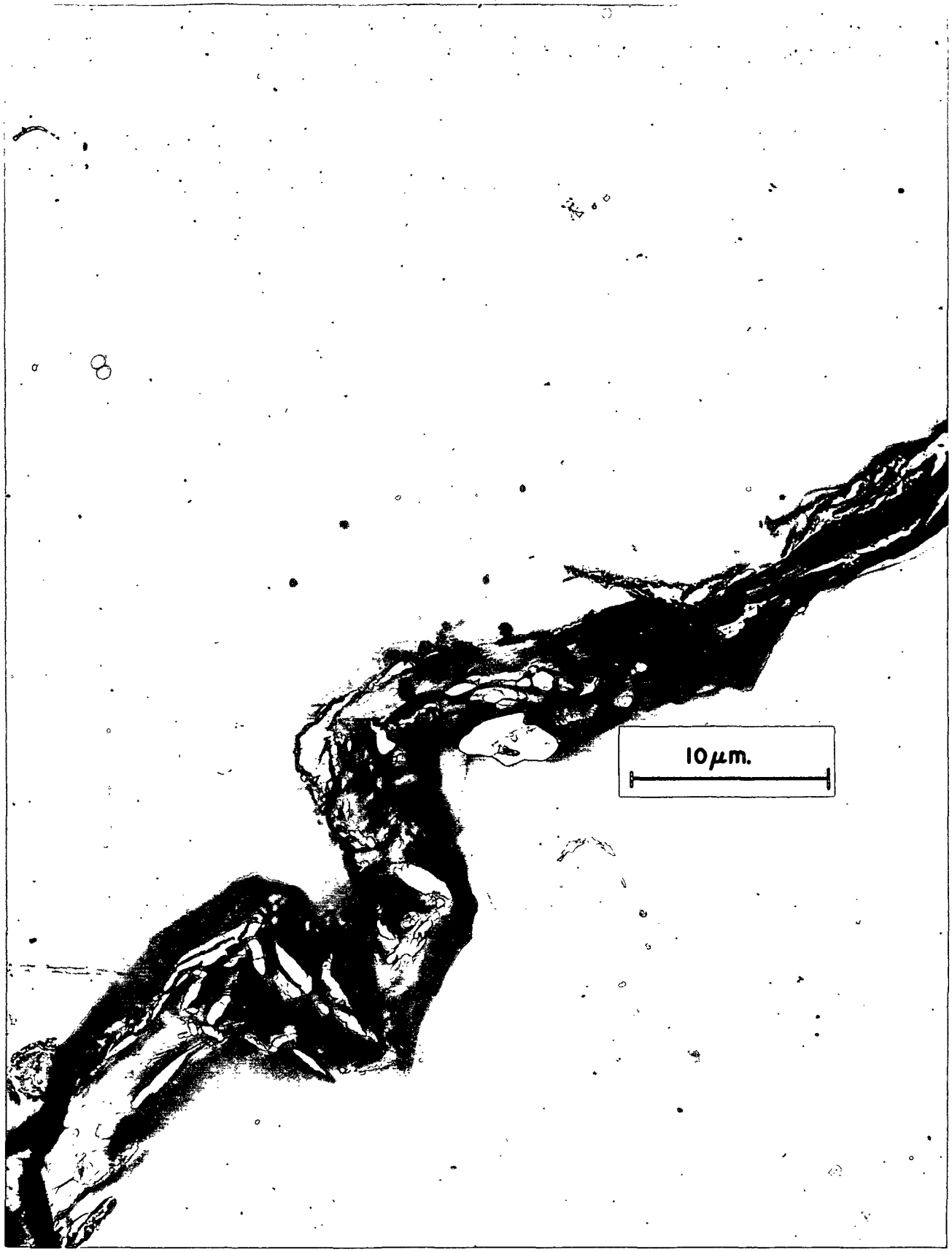

Figure 69. Springwood Fiber Dried Under 20% Negative Strain.
Plate No. 8304 F

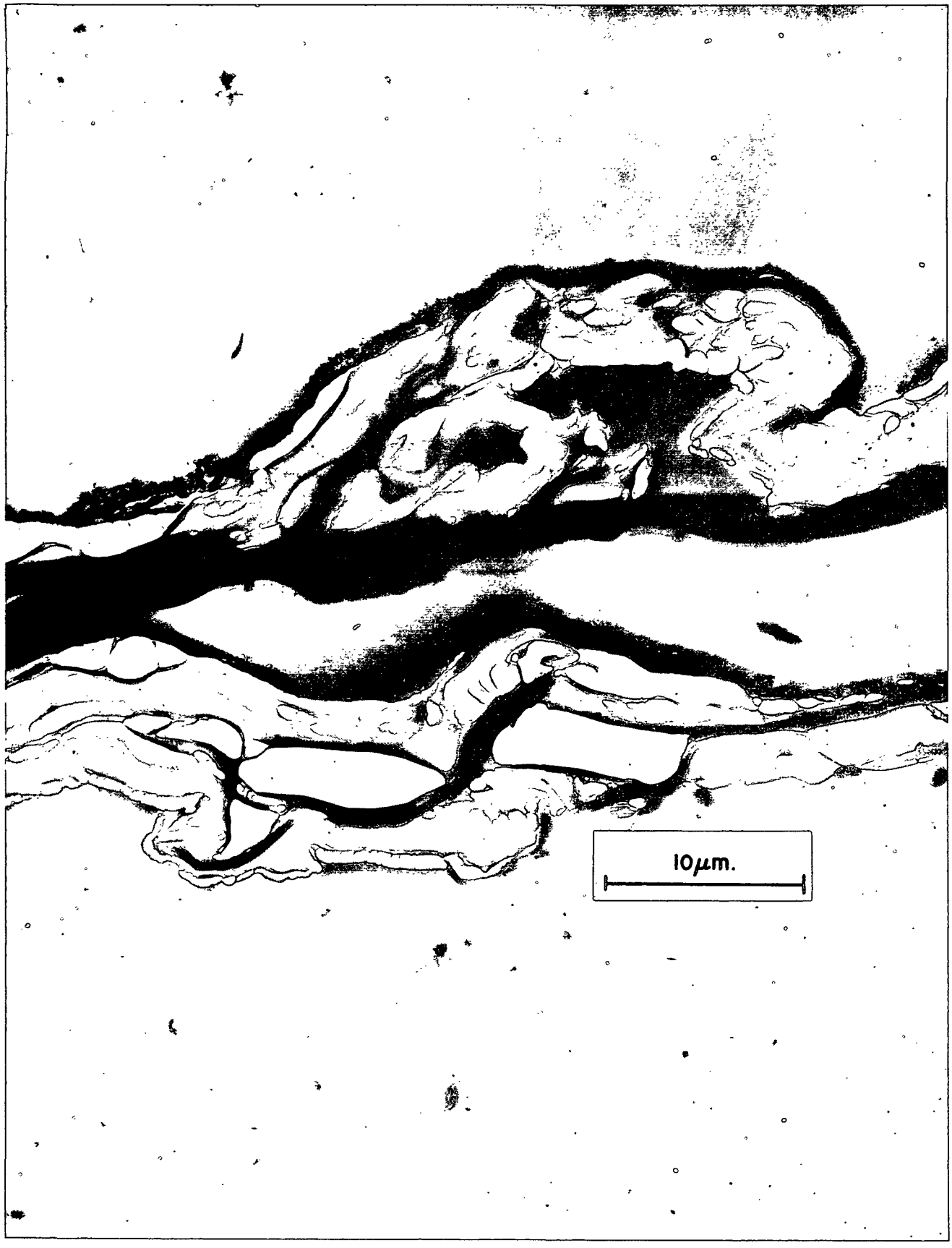

Figure 70. Springwood Fibers Dried Under 20% Negative Strain.
Plate No. 8229 F

Figure 71. Summerwood Fiber Dried Under 20% Negative Strain.
Plate No. 8315 F

APPENDIX V

POLARIZED LIGHT MICROGRAPHS OF BLEACHED SOUTHERN PINE KRAFT FIBERS